

TECHNOLOGIES FOR SUSTAINABLE LIFE CONCISE  
MONOGRAPHS SERIES

# Advanced Energy Efficient Building Envelope Systems

Moncef Krarti  
Zhiqiang (John) Zhai  
Benjamin Park  
Kathleen Menyhart  
Vinay Shekar  
Jenna L. Testa  
Saleh Nasser AL Saadi  
Mohamed El Mankibi  
Robert Slowinski

@Seismicisolation

© 2017, The American Society of Mechanical Engineers (ASME), 2 Park Avenue, New York, NY 10016, USA ([www.asme.org](http://www.asme.org))

All rights reserved. Printed in the United States of America. Except as permitted under the United States Copyright Act of 1976, no part of this publication may be reproduced or distributed in any form or by any means, or stored in a database or retrieval system, without the prior written permission of the publisher.

INFORMATION CONTAINED IN THIS WORK HAS BEEN OBTAINED BY THE AMERICAN SOCIETY OF MECHANICAL ENGINEERS FROM SOURCES BELIEVED TO BE RELIABLE. HOWEVER, NEITHER ASME NOR ITS AUTHORS OR EDITORS GUARANTEE THE ACCURACY OR COMPLETENESS OF ANY INFORMATION PUBLISHED IN THIS WORK. NEITHER ASME NOR ITS AUTHORS AND EDITORS SHALL BE RESPONSIBLE FOR ANY ERRORS, OMISSIONS, OR DAMAGES ARISING OUT OF THE USE OF THIS INFORMATION. THE WORK IS PUBLISHED WITH THE UNDERSTANDING THAT ASME AND ITS AUTHORS AND EDITORS ARE SUPPLYING INFORMATION BUT ARE NOT ATTEMPTING TO RENDER ENGINEERING OR OTHER PROFESSIONAL SERVICES. IF SUCH ENGINEERING OR PROFESSIONAL SERVICES ARE REQUIRED, THE ASSISTANCE OF AN APPROPRIATE PROFESSIONAL SHOULD BE SOUGHT.

ASME shall not be responsible for statements or opinions advanced in papers or . . . printed in its publications (B7.1.3). Statement from the Bylaws.

For authorization to photocopy material for internal or personal use under those circumstances not falling within the fair use provisions of the Copyright Act, contact the Copyright Clearance Center (CCC), 222 Rosewood Drive, Danvers, MA 01923, tel: 978-750-8400, [www.copyright.com](http://www.copyright.com).

Requests for special permission or bulk reproduction should be addressed to the ASME Publishing Department, or submitted online at <https://www.asme.org/shop/books/book-proposals/permissions>

ASME Press books are available at special quantity discounts to use as premiums or for use in corporate training programs. For more information, contact Special Sales at [CustomerCare@asme.org](mailto:CustomerCare@asme.org)

*Library of Congress Cataloging-in-Publication Data*

Names: Krarti, Moncef, editor, author.

Title: Advanced energy efficient building envelope systems / [compiled by] Moncef Krarti, Zhiqiang (John) Zhai, Benjamin Park, Kathleen Menyhart, Vinay Shekar, Jenna L. Testa, Saleh Nasser AL Saadi, Mohamed El Mankibi, and Robert Slowinski.

Description: New York : ASME Press, [2017] | Includes bibliographical references and index.

Identifiers: LCCN 2017002517 | ISBN 9780791861370 (alk. paper)

Subjects: LCSH: Insulation (Heat) | Exterior walls. | Roofs. | Buildings--Energy conservation.

Classification: LCC TH1715 .A38 2017 | DDC 693.8/32--dc23

LC record available at <https://lccn.loc.gov/2017002517>



# Table of Contents

Preface	v
Abstract	vii
<b>1. Dynamic Insulation Systems</b>	<b>1</b>
1.1 Introduction	1
1.2 Description of DIM Technology	4
1.3 Model for DIM Systems	6
1.4 Optimal Control Strategies for DIM Systems	12
1.5 Comparative Analysis of Control Strategies	21
1.6 Sensitivity Analysis	22
1.7 Impact of Climate	26
1.8 Economic Analysis	26
1.9 Summary and Conclusions	31
References	35
<b>2. Dynamic Cool Roofing Systems</b>	<b>39</b>
2.1 Introduction	39
2.2 Cool Roof Properties	40
2.3 Performance of Static Cool Roofs	43
2.4 Current Cool Roof Energy Standards	53
2.5 Other Benefits and Challenges	55
2.6 Advances in Switchable Roof Coatings	56
2.7 Evaluation of Dynamic Cool Roofs Performance	59
2.8 Economic Analysis of Dynamic Cool Roofs	63
2.9 Summary and Conclusions	65
References	70
<b>3. Breathing and Living Walls</b>	<b>75</b>
3.1 "Breathing Wall" Concept	75
3.2 "Living Wall" Concept	77
3.3 State of the Art	78
3.4 Prototypes and Products	80
3.5 Modeling Advanced Façade Systems	82
3.6 Testing Advanced Façade Systems	85
3.7 Thermal Performance of Single-Layer Breathing Wall	89
3.8 Thermal Performance of Advanced Multi-Layer Walls	94
3.9 Thermal Performance of Buildings with PCM-Enhanced Walls	101
3.10 Thermal Performance of Buildings with Advanced Multi-Layer Walls	115
3.11 Summary on Single-Layer Breathing Wall	121
3.12 Summary on Advanced Multi-Layer Living Wall	122
References	127
<b>Authors Biography</b>	<b>131</b>

@Seismicisolation

## Preface

Building heating and cooling energy use accounts for up to 40% of the total energy consumption in developed countries. Heat losses and gains through the building envelope greatly contribute to thermal heating and cooling loads and subsequently to the overall energy performance of buildings. Several advances in building technology have been made that continue to transform building energy performance and promote new and innovative construction techniques and challenges traditional practices. In fact, some of the existing systems that are often required by energy efficiency codes and standards may not provide the optimal energy performance and indoor air quality (IAQ). For instance, leaky buildings traditionally perform very poorly in terms of energy consumption, but in general, their IAQ—as a result of the incoming outside air—is fairly good. For the sake of energy efficiency, the trend has been tighter, more effectively sealed buildings, which in turn has led to more IAQ, mold, and sick building syndrome problems. As the push for improved energy performance points designers and builders towards tighter construction, the very principle that reduces the building's energy consumption—reduced infiltration—is a net loser for indoor air quality.

In this monograph, some advanced technologies of building envelope are presented to challenge the existing paradigms for high performance buildings. Specifically, four building envelope systems are described in three chapters to showcase their ability to enhance the energy efficiency and optimize the IAQ of buildings. These advanced building envelope systems include:

- *Dynamic Insulation Materials:* These materials are assemblies that can change their thermal resistance through for instance, a controlled exchange of liquid or gaseous media, and are applied to the exterior walls and roofs of buildings. When applied and optimally controlled, these materials can save significant annual heating and cooling energy use for both residential and commercial buildings (Chapter 1).
- *Variable Reflectivity Cool roofs:* These systems are associated with coatings that can change their reflective properties over time depending on desired controlled strategies. It is well known that

static cool roofs can save energy use during cooling periods but may increase energy consumption during swing or heating seasons due to lower solar heat gains. The variable reflectivity coatings allow the reduction in heating penalty associated with conventional cool roofs (Chapter 2).

- *One-Layer Breathing Walls:* These systems provide air ventilation through the walls while recovering thermal energy. Essentially using heat exchanging mechanism, filtrated fresh air is introduced through the walls from outside to inside and is heated or cooled by the thermal energy wasted by conduction and convection with the walls (Chapter 3).
- *Multi-Layer Living Walls:* These walls utilize basic biomimetic principles to adapt to the change in climatic conditions. In particular, these climate-adaptive intelligent walls have embedded systems of air, water, and phase change material and can be controlled to maintain acceptable indoor environment under changing outdoor conditions (Chapter 3).

In all three chapters, an overview of the basic operating concepts of these advanced envelope systems is first provided. Then, their energy performance is summarized based on reported results using either experimental or modeling analyses.

It should be noted that the main goal of this monograph is to promote innovative ideas and disseminate the ongoing research and development related to the theme of sustainable buildings. It is a small contribution to the ASME initiative on Integrated and Sustainable Building Equipment and Systems (ISBES).

Moncef Krarti, PhD, PE, LEED-PE, ASME Fellow  
Guest Editor

## **Abstract**

This monograph presents the latest research developments of innovative building envelope systems. These systems have the ability to allow building structures to be responsive to changes in outdoor conditions to ensure comfortable indoor environment and acceptable indoor air quality at higher energy efficiency compared to conventional systems. In particular, the monograph overviews the basic operation principles and thermal performance of four technologies described in three chapters: (i) dynamic insulation materials that can change its thermal properties in order to better adapt the building envelope with its outdoor environment and reduce building heating and cooling thermal loads, (ii) variable reflectance coatings for application on roofs to lower and even eliminate the energy penalties associated with reduced solar heat gains during heating operation of buildings, (iii) single layer breathing walls to recover energy wasted from heat transmission inside the walls and provide air ventilation to indoor spaces, and (iv) multi-layer living walls to apply biomimetic principles and phase-change materials to adapt building envelope properties with the changing outdoor conditions.

*Guest Editor:*  
*Moncef Krarti, PhD, PE, LEED-AP*

@Seismicisolation

---

# 1. Dynamic insulation systems

---

*Moncef Krarti, Kathleen Menyhart, Vinay Shekar, and Benjamin Park,  
Building Systems Program, University of Colorado, Boulder, CO 80309 – USA*

**Abstract:** This chapter overviews the latest reported analysis results of dynamic insulation materials allowing building envelope to vary its thermal resistance properties. In particular, the chapter presents a summary of the results obtained from a set of analyses to evaluate the potential energy savings associated with replacing traditional, static insulation with dynamic insulation materials (DIMs) for both residential and commercial buildings. In order to determine the effectiveness of DIMs to reduce heating and cooling energy use, two different control schemes are investigated including simplified 2-step control with low-high insulation settings and optimal control strategy based on genetic algorithm (GA) search technique. It is generally found that the performance of DIMs varied significantly by climate, with total heating and cooling energy use savings that can reach up to 40% especially in locations with mild weather conditions.

---

## 1.1 Introduction

Dynamic Insulation Materials (DIMs) are emerging as promising new technology to reduce energy consumption required to maintain thermal comfort in buildings [1]. Space heating and cooling of buildings represents a significant portion of the total energy consumption in the United States and other developed countries. In the US, 48% of total residential energy use and 35% of total commercial energy use are attributed to both space heating and cooling [2].

A traditional building envelope system uses insulation materials with a static R-value, which is often selected based on the requirements of local building and energy codes. In contrast, DIM panels are designed so that the rate of heat transfer through a wall can be varied over time. The variation in wall thermal properties can be achieved with the introduction of various inert gases, each with a different thermal conductivity [3] or by mechanically sliding or compressing the wall, as proposed by Clark et al. in a 2016 patent application [4].

## **2 TECHNOLOGIES FOR SUSTAINABLE LIFE**

Typically, it is best to minimize heat transfer through the building envelope by selecting walls and roofs with high thermal resistances (i.e., with high R-values and low U-values). Several advanced materials and systems with low thermal conductivity values have been developed and tested such as vacuum insulation panels, gas filled panels and aerogels, and reflective insulations [5–9]. However, as demonstrated by Masoso and Grobler, it is not always beneficial to impose highly insulated building envelope components [10]. In some instances, it is more advantageous to lower the thermal resistance of the building shell. For instance, on a typical summer day, a well-insulated building would effectively limit heat gain due to conduction. However, internal heat gains (due to occupants, equipment, and lighting) and solar heat gain heat (from glazed windows) could remain trapped indoors. To release this unwanted heat, passive strategies, such as stack ventilation or night flushing can be used. Although effective, opening windows is a strategy that is not always available or desirable to utilize for a variety of reasons. In some climates, even during the cooling season, nighttime temperatures may be too low to keep windows open overnight. Hayashi, et al, studied the window-opening behavior of dwellers in nine different detached homes in Japan (both cold and hot-humid climates). Using sensors to monitor and record the opening width and comparing it to the ambient air temperature variation, these researchers found that in general, dwellers do not open windows enough to realize the energy savings that is possible with passive cooling [11]. Windows are generally closed at night and when occupants leave during the day. Survey respondents indicated the following reasons for closing windows: outdoor noise and air pollution, crime prevention, and privacy, as well as keeping mosquitos and other insects out [11]. In a commercial setting, such as an office building, automated strategies have been shown to be significantly more effective than relying on individual control [12–13].

Using walls and/or roofs with switchable insulation would allow for the building envelope to be well insulated (i.e., having a high R-value) when heat transfer between indoors and outdoors is not desirable and to have higher thermal conductance (i.e., having a low R-value) when enhanced heat transfer is desirable. Although this technology is still being developed, the idea is not new. In a report published by Los Alamos National Laboratory in 1982, it was noted that future building efficiency research should focus on control strategies for the transfer and

storage of thermal energy [14]. In a 2011 review of building insulation materials, Jelle indicates that DIMs show promise as a future technology [1]. In a recently reported study on the potential energy savings of DIMs in three different U.S. climates, switchable insulation layers with two different R-value settings were considered [3]. In one case, the DIM resistance was altered from a low value of RSI-0.5 to a high value of RSI-2.5 (RSI-0.5/RSI-2.5). In the second case, a low value of RSI-1.0 was combined with a high value of RSI-2.5 (RSI-1.0/RSI-2.5). In all three US climates, it was found that a two-step variable resistance envelope of RSI-0.5/RSI-2.5, was more effective than RSI-1.0/RSI-2.5, and could reduce cooling energy use by an average of 15% and up to 39% in heating-dominated climates, when compared to static insulation layers [3].

Although very little research has been published on the topic of DIMs, similar technologies exist for other components of the building envelope. For instance, electrochromic windows employ a switching mechanism to vary the transmittance of visible and infrared solar energy [15]. In the reported study, using windows that could be switched from 62% visible transmittance (0.47 SHGC) to fully tinted (with less than 2% visible transmittance/0.09 SHGC), potential energy savings were found to be higher than 45% when compared to single pane static glazing and about 20% when compared to ASHRAE 90.1-2007 code-compliant glazing [15]. Jonsson and Roos used computer simulations to evaluate the effectiveness of various control strategies for smart (electrochromic) windows [16]. Although the most energy efficient solution would be to keep windows in their tinted state (low visible transmittance and low SHGC) when there is a need for cooling, and switch to a clear state when there is a need for heating, this solution does not take into account daylight and occupant preference. The same study showed the benefits of adding occupancy sensors so that when people are present the windows are optimized for daylighting; and when the space is empty, the windows are optimized for energy savings. Other studies have considered coupling ventilation airflow within building envelope using the concept of breathing walls [17–20]. A typical breathing wall, referred to sometimes as a dynamic wall, draw a steady stream of filtered air through the wall cavity and into the building to provide clean ventilation and partially conditioned air to the occupants. Several studies indicated that the airflow can effectively vary the thermal resistance



## **4 TECHNOLOGIES FOR SUSTAINABLE LIFE**

of breathing walls depending on the indoor-outdoor temperature difference and the ventilation rate [20–21]. As extension of breathing walls, recent studies have considered living walls by integrating air and/or water flows as well as phase-change materials (PCMs) within building envelope [22–24]. Preliminary analysis results indicate that the performance of the living walls is very sensitive to the PCM melting range. With optimal melting temperature close to the heating and cooling set-points, living walls can achieve savings in annual and peak heating and cooling loads of up to 30% [23–24]. As detailed in [3–4], the DIM technology evaluated in this chapter does not require any PCM integration or any fluid flow from the outside to the inside of the building. A more detailed overview of both breathing and living walls is provided in Chapter 3.

The aim of this chapter is to overview the DIM technology and the potential benefits of its deployment in reducing both the heating and cooling requirements for residential and commercial buildings. Moreover, the chapter outlines the best control strategies for DIM during various seasons and for various climatic conditions. Most of the results outlined in this chapter are based on published studies by the authors.

### **1.2 Description of DIM Technology**

Traditional thermal insulation materials, including mineral wool, polyurethane, and both expanded and extruded polystyrene (EPS, XPS), exhibit low thermal conductivities in the range of 0.02-0.04 W/mK. Recently developed high-performance envelope technologies include vacuum insulation panels (VIPs), gas insulation panels (GIPs), and nanoinsulation materials (NIMs). While these state-of-the-art (high-performance) thermal insulation assemblies have initial conductivities that range between 0.003-0.02 W/(m·K), concerns exist regarding the long-term reliability of these insulation material technologies. For example, VIP conductivities are known to rise to 0.008-0.03 W/(m·K) due to water vapor diffusion and other potential mechanisms (e.g., puncturing) [25]. Similarly, it is well known that high-performance XPS loses its thermal resistance over time due to high vapor diffusivity [1].

High thermal resistance materials and assemblies are effective in reducing heat transfer through the building envelope when there is a significant indoor-outdoor temperature difference. As noted earlier, building envelopes with high R-value can be beneficial for one season of the year but are not necessarily beneficial for the other seasons. For

example, in cold climates, high thermal insulation can actually increase building thermal loads – especially during mild periods when it may be beneficial to let heat that is trapped indoors to escape outdoors. A number of strategies exist to release stored heat, such as opening windows, night ventilation, or lower conductivity building envelopes.

Some studies have theorized on dynamic insulation materials (DIMs) and systems in which the thermal conductivities of wall assemblies are controllable and tunable, either due to applied electrical voltage to conducting polymers or other electrochromic materials (ECMs) [26–27]. While some prototypes of ECMs are available, these technologies have only been applied to smart windows rather than opaque building envelope systems.

The basic operating principle of DIM technologies is depicted in Figure 1-1. In lieu of traditional, static insulation assemblies (e.g., XPS, VIPs, GIPs), a DIM is a rigid, cellular panel that is placed within the external wall cavities of a building. The DIM panel is designed with either an open cavity or an interconnected system of conduits. Once installed, the bulk thermal diffusivity of the assembly is tailored by the introduction of inert gases with variable conductivities (e.g., carbon dioxide, nitrogen, helium), thereby affecting the rate of heat transfer through the envelope. It is envisioned that the insulation media can be regulated via

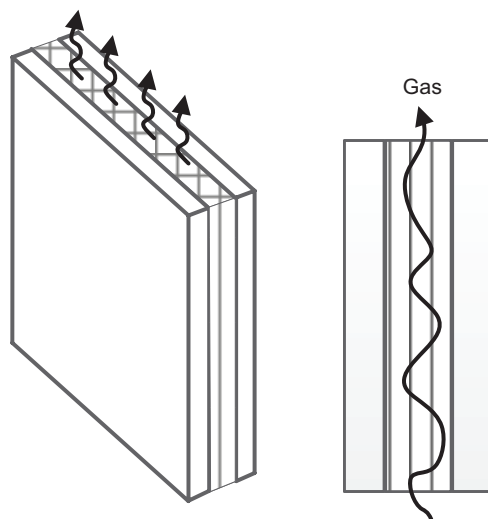


**Figure 1-1** Operating principle of dynamic insulation materials (DIMs).

## 6 TECHNOLOGIES FOR SUSTAINABLE LIFE

control strategies based on indoor-outdoor temperature differences and exchanged daily, monthly, or seasonally, depending on the climate and necessary heating and cooling demands.

### 1.3 Model for DIM Systems

One approach to evaluate the DIM performance is to use RC modeling approach. Specifically, DIM system has been modeled using a 3R2C thermal network model modified to have a virtual node at wall surface exposed to surroundings [3]. The virtual node has no thermal capacitance so that the surface temperature can react quickly to the surrounding conditions. Figure 1-2 depicts a thermal network of exterior wall connecting the indoor space to the outdoor environment. All resistances and capacitances are assumed to be time invariant.

Convection and long-wave radiation exchanges occur at both sides while short-wave solar radiation is considered only at the outer surface of an exterior wall. The transient heat balance analysis for both nodes yields the following differential equations as:

$$\frac{T_{ext} - T_1}{R} A + h_o A (T_o - T_{ext}) + Q_{LWR} + Q_{solar} = 0 \quad (1.1)$$

$$\frac{T_{ext} - T_1}{R} A + \frac{T_1 - T_2}{R} A = C_1 \frac{dT_1}{dt} \quad (1.2)$$

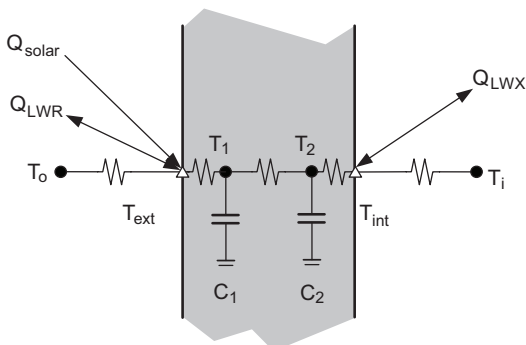


**Figure 1-2** Description of RC thermal network for a single layer exterior wall.

$$\frac{T_1 - T_2}{R} A + \frac{T_2 - T_{int}}{R} A = C_2 \frac{dT_2}{dt} \quad (1.3)$$

$$\frac{T_2 - T_{int}}{R} A + h_i A (T_{int} - T_i) + Q_{LWX} = 0 \quad (1.4)$$

where,

$R$  = thermal resistance of materials ( $m^2\text{-K/W}$ ),

$C$  = thermal capacitance of materials ( $\text{W/K}$ ),

$A$  = area of the surfaces ( $m^2$ ),

$T_{out}$  = outdoor air temperature ( $^\circ\text{C}$ ),

$T_{zone}$  = indoor air temperature ( $^\circ\text{C}$ ),

$T$  = the surface temperature of the exterior walls ( $^\circ\text{C}$ ),

$h_o$  = the convective coefficient at outer surface of the exterior walls ( $\text{W/m}^2\text{-K}$ ),

$h_i$  = the convective coefficient at inner surface of the exterior walls ( $\text{W/m}^2\text{-K}$ ),

$Q_{LWR}$  = net longwave radiation ( $\text{W}$ ),

$Q_{solar}$  = exterior solar radiation incident ( $\text{W}$ ),

$Q_{LWX}$  = longwave radiant heat exchange between surfaces ( $\text{W}$ )

Figure 1-3 illustrates the RC thermal network used to model a DIM layer in a multi-layer exterior wall separating a thermal zone characterized by its indoor temperature,  $T_i$ . The material in the middle of the exterior wall (M2) is considered as a dynamic insulation material (DIM). The thermal resistance of M2 is controlled based on the heating or cooling requirement of the thermal zone [3].

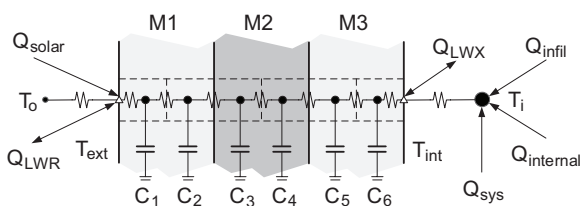


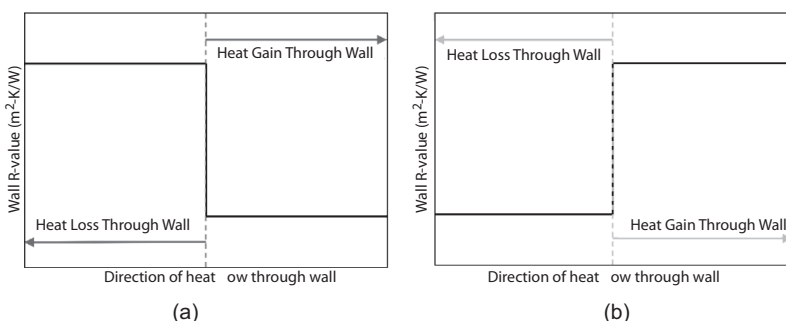
**Figure 1-3** Thermal network for the multi-layer exterior walls and a thermal zone.

## 8 TECHNOLOGIES FOR SUSTAINABLE LIFE

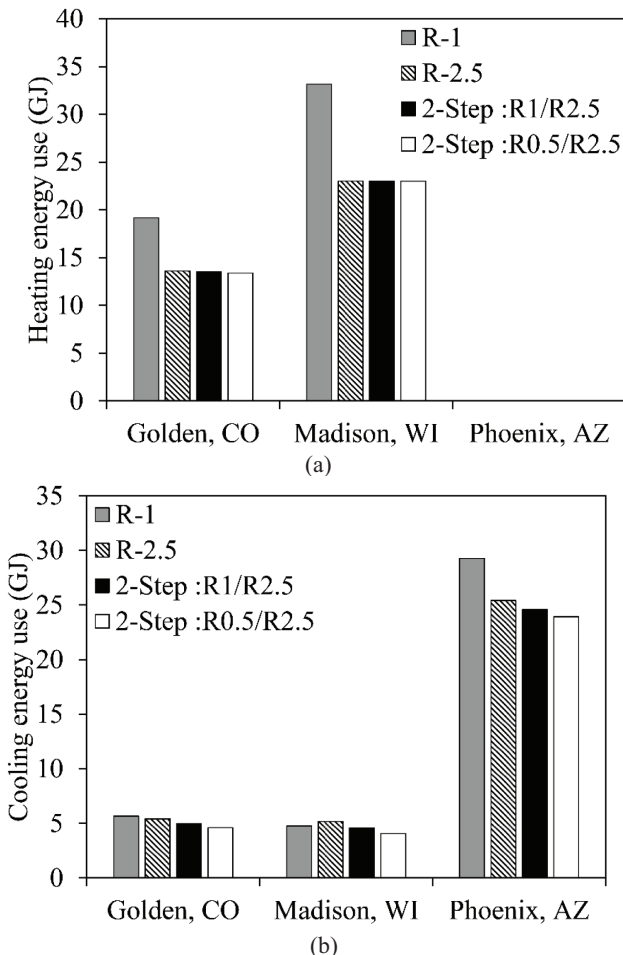
In order to control the thermal resistance of M2, the direction of heat flow through the exterior wall has been considered as a control parameter [3]. Then, heat flow direction can be determined by monitoring the inside, middle, and outside surface temperatures of the exterior wall.

Figure 1-4 depicts the control strategy to vary the thermal resistance for the DIM layer and ultimately the exterior wall. Firstly, the controller determines the direction of heat flow through the building envelope. Then, the controller examines the temperature distribution inside the exterior wall to determine the appropriate RSI-value (R-value in SI unit) of the DIM in the middle layer of the exterior walls. For example, when the outside surface temperature is higher than the inside surface temperature in cooling season, M2 increases its thermal resistance so that it reduces the heat gains through the exterior walls. Whereas when the outside surface temperature is lower than the inside surface temperature during the cooling season, the thermal resistance of M2 is reduced to release heat from indoors to outdoors through the exterior wall.

The performance of the DIMs has been initially explored using the RC model described by Figures 1-2 and 1-3 and the two-step control strategy outlined in Figure 1-4 for a residential building [3]. Figure 1-5 summarizes the analysis results and indicates that potential heating energy savings associated with deploying of DIMs instead of static insulation layers. The solar heat gains transmitted through the windows assist in heating indoor space air, and thus reduce heating thermal loads. However, the addition of heat gains from transmitted solar radiation results in an increase in building cooling thermal loads. The low RSI-value walls are more effective to release the heat trapped indoors during



**Figure 1-4** A two-step R-value control strategy for DIM layer during (M2): (a) heating operation and (b) cooling operation.



**Figure 1-5** (a) Annual heating energy use and (b) annual cooling energy use for four DIM control strategy when the building has windows and internal gains in three US locations: Golden, CO; Madison, WI; and Phoenix, AZ.

cooler nighttime periods than the high RSI-value walls. The 2-step control strategies take advantage of the DIM low RSI-value during nighttime, and minimize heat gains through the exterior walls during daytime by increasing their thermal resistance. Specifically, it has been found as noted in Table 1-1 that a 2-step-RSI-1/ RSI-2.5 control strategy can reduce the cooling energy use by up to 8% compared to static

**Table 1-1** Heating and cooling energy use savings compared to CASE 1 (RSI-1.0 exterior walls) in three US locations: Golden, CO; Madison, WI; and Phoenix, AZ.

Heating energy use savings (GJ)		% savings		
		2-Step RSI-0.5/ RSI-2.5	R-2.5	2-Step RSI-0.5/ RSI-2.5
Golden, CO	-5.55	-5.65	-5.77	-29.0
Madison, WI	-10.14	-10.14	-10.15	-30.6
Phoenix, AZ	n/a	n/a	n/a	n/a
Cooling energy use savings (GJ)		% savings		
		2-Step RSI-0.5/ RSI-2.5	R-2.5	2-Step RSI-0.5/ RSI-2.5
Golden, CO	-0.24	-0.67	-1.05	-4.3
Madison, WI	0.40	-0.18	-0.69	8.5
Phoenix, AZ	-3.86	-4.70	-5.34	-13.2

RSI-2.5 wall option in Golden, CO [3]. While, the 2-step-RSI-0.5/RSI-2.5 control strategy can reduce the cooling energy use by up to 15% compared to the RSI-2.5 wall option in Golden, CO. Moreover, cooling energy use can be decreased by 11% and 21%, respectively, with 2-step-RSI-1/RSI-2.5 and 2-step-RSI-0.5/RSI-2.5 control strategy in

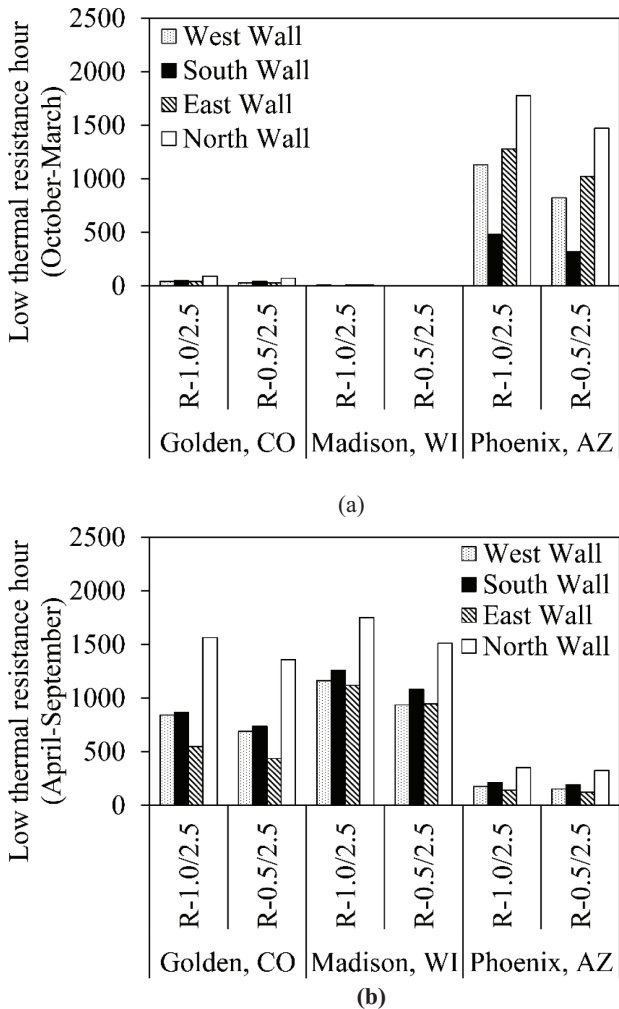


**Figure 1-6** Number of hours for maintaining low R-value for the exterior walls in the building with windows and internal load in three US locations: Golden, CO; Madison, WI; and Phoenix, AZ.

## 12 TECHNOLOGIES FOR SUSTAINABLE LIFE

Madison, WI. However, the 2-step control can achieve only 6% cooling energy savings and has little impact on heating energy use in Phoenix, AZ [3].

The number of hours when each DIM exterior wall is set at the low thermal resistance over a year has been found to vary depending on the orientation as shown in Figure 1-6 for three US climates [3]. In particular, the results of Figure 1-6 indicate that the North DIM wall is most actively controlled especially when high internal loads are considered.

### 1.4 Optimal Control Strategies for DIM Systems

To explore different control options for DIMs, a Genetic Algorithm (GA) optimization technique has been considered to determine the best schedule for DIM settings associated to each of the building walls [28]. GA-based optimization techniques have been successfully used to select building shapes [29], envelope features [30], and HVAC systems [31]. For instance, Bichiou and Krarti [32] have applied GA-based optimization to select energy efficiency measures for both envelope and HVAC systems to minimize life-cycle costs for operating commercial buildings. For the control of DIM systems, the following objective function and constraints for the GA-based optimization analysis has been proposed [28]:

$$f = \min \left( \sum_0^{24\text{hrs}} E_{cooling} * \text{rate}_{cooling} + E_{heating} * \text{rate}_{heating} \right) \quad (1.5)$$

for :  $kl \leq k \leq ku$

Where,

- $k$ - thermal conductivity values to be set for the DIM for all the building walls
- $kl, ku$ - lower bound and upper bounds of thermal conductivity values
- $\text{rate}_{cooling, heating}$  - utility rates for electricity and natural gas, respectively
- $E_{cooling}$ - Energy use associated with the cooling system
- $E_{heating}$ - Energy use associated with the heating system

The optimization objective function of Eq. (1.5) is set to minimize the total building heating and cooling energy cost during one day by varying the thermal conductivity value (and thus R-value) settings the DIM for each building wall separately. The thermal conductivity values of each wall have an upper and lower bounds which have been set

to be 2.0 W/m.K and 0.032 W/m.K, respectively [28]. For a fixed thickness of 0.075 m (3-in) insulation, the upper and lower bounds of thermal conductivity correspond to the DIM layer having a low resistance of 0.04 m<sup>2</sup>K/W to a high resistance of 2.37 m<sup>2</sup>K/W. The GA-based optimizer can evaluate all potential DIM layer R-values between 0.04 m<sup>2</sup>K/W and 2.37 m<sup>2</sup>K/W to identify the best hourly DIM settings for 24-hour period for all the building walls. The optimal selection would result in the least combined heating and cooling energy costs as noted by Eq. (1.5). For simplicity, energy and energy demand penalties have been excluded in the reported study from the objective function [28]. However, the GA-optimization framework can handle any energy and demand charges and additional constraints (such as desired thermal comfort levels).

Other important parameters required for the GA-based optimization implementation include the number of variables to optimize ( $n_{vars}$ ) and the population size. In particular, the number of variables can affect significantly the search effort and thus the computational time needed to identify the optimal DIM settings. It should be noted that the parameter  $n_{vars}$  defines the number of daily periods during which the DIM settings are to be switched. For instance, specifying  $n_{vars}$  as 6 implies that the DIM settings are optimized for every 4-hr periods during one day (24hrs/6 = 4hrs). The population size specifies the number of options the GA-based optimizer utilizes during each iteration to reach the optimum solution. A population size of 50 implies that the GA analysis involves 50 sets of DIM settings during each iteration. Based on a sensitivity analysis of the GA optimization performance, it was found that a population size of 200 is sufficient for determining the optimal DIM settings [28]. However, the analysis has indicated that the optimization is very sensitive to change in the parameter  $n_{vars}$ .

Since GA-based optimization over an entire year is computationally time consuming, the analysis considers representative days for each season to evaluate the impact of optimal DIM control for all the building walls. Representative days are selected from the application of the 2-step control strategy. In particular, three representative days have been selected for Golden, CO include one for the swing season (one day in May), one for the heating season (one day in December), and one for cooling season (one day in July). To assess the benefits of GA-based optimal controls, the total heating and cooling energy use and cost

savings using DIM walls are estimated relative to statically but highly insulated office building. For the cost analysis, average US energy prices of \$0.10/kWh electricity and \$8.9/1000 ft<sup>3</sup> natural gas are considered based EIA average energy costs for commercial buildings [33–34].

In the following sections, the optimal controls obtained for DIM walls for an office building are described for representative days [28].

#### 1.4.1 Swing Season Analysis

Figure 1-7 shows optimized R-value settings obtained for the DIM layers applied to the South, West, North, and East walls for three days in May including 6th, 16th, and 24th [28]. The optimization results show that DIM R-value settings change significantly for each wall orientation during May 16th and 26th but only slightly during May 6th. Specifically, DIMs for all walls are set to switch to a low R-value for the entire daytime period between 8:00 and 16:00 on May 16th. Similarly, the low R-value settings are selected for all the walls during the 8:00–12:00 period on May 24th but only for the East and North walls during the 4-hour periods 12:00–16:00 and 16:00–20:00 periods. It should be noted that the period of 8:00–16:00 coincides with the time of the day when the building is occupied and has high internal gains. Indeed, heat gains associated with equipment, lighting, and people are at their maximum during this period. Due to these high internal heat gains, GA-based optimizer opts to set the DIM layers at their lowest thermal resistance value in order to allow the excess heat gains trapped indoors to be released outdoors through the building envelope. For May 6th, unlike the case during May 16th and 24th, the DIM layers for all the walls are set at the high thermal resistance R-value during all the periods. To better understand this selection by the GA-based optimization, sol-air temperature hourly variations for the three days in May are also included in Figure 1-7. It should be noted that sol-air temperature combines the effects of both the ambient temperature and the incident solar radiation on the walls. Since during May 16th and 24th, the sol-air temperature remains low during the occupied hours (8:00 to 16:00), the GA-based optimizer decides to set the DIM layers at their lowest R-value in order for the outdoors to act as a sink for indoor heat gains. When the sol-air temperature is high, the DIM layers are set at their high R-value to prevent additional heat gains from outdoors as is the case for May 6th during the occupied period. Therefore, and even though the internal heat

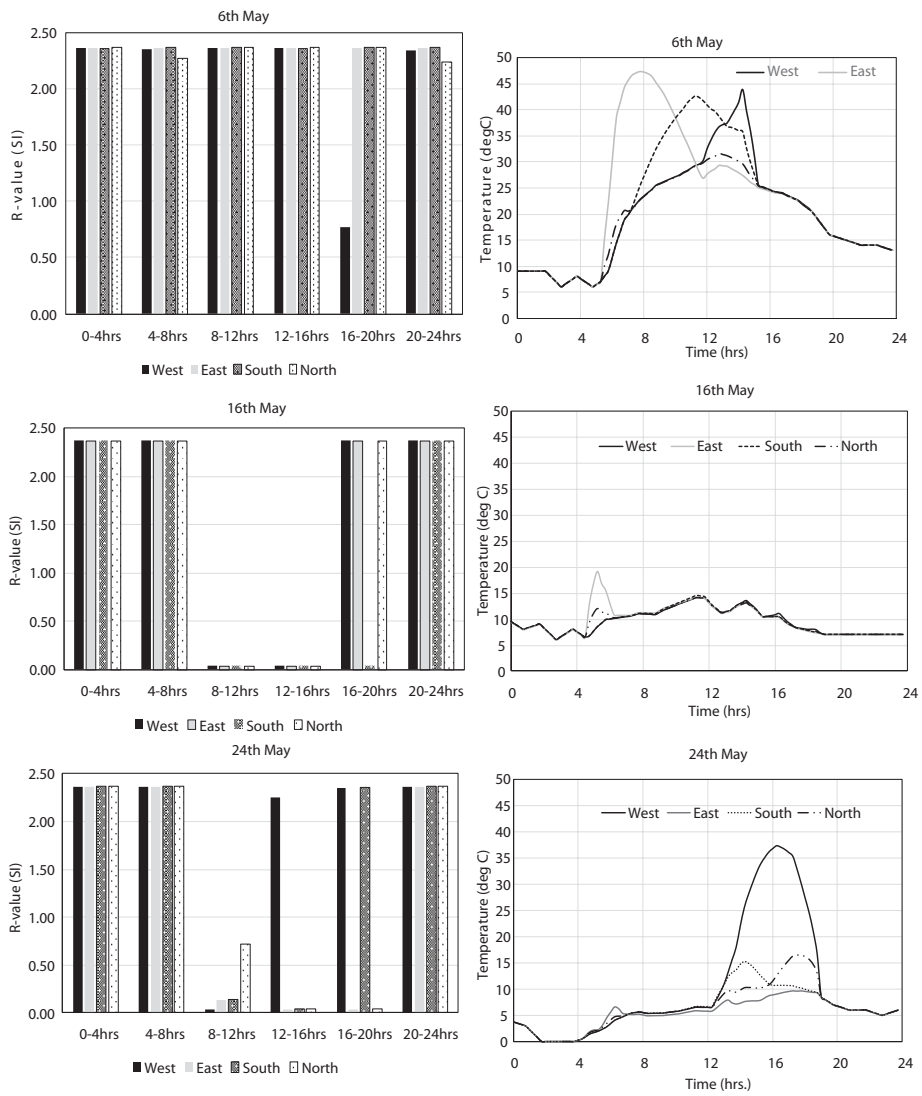


**Figure 1-7** GA-based optimized DIM insulation R-value settings obtained using 4-hr periods and Sol-air temperatures during May 6th, 16th, and 24th for an office building in Golden, CO.

gains in the building are high, the walls with DIM layers are not able to release this excess heat as the sol-air temperature during the same time is also high. During these periods, the GA-based optimization determines that the best option is to have highly insulated building envelope to ensure that the cooling thermal load is not increased further by the

high sol-air temperatures. This same behavior can also be noted for the West wall on May 24th. Indeed, the increase in the sol-air temperature on the West facing wall after 12:00 prevents the optimizer to set the DIM layer for that wall to a low R-value while the DIM layers in the other walls have been switched to lower R-value settings.

As noted in the results shown in Figure 1-7, DIMs have the ability to vary the thermal resistance of the walls in response to mainly building internal loads and external ambient conditions. This feature can allow DIMs to be utilized to lower the building indoor temperatures during unoccupied periods and thus freely pre-cool the building thermal mass. The advantage of this free pre-cooling is to maintain lower cooling thermal loads during the daytime and hence lower energy use and cost. To investigate this additional benefit of DIMs, the office building has been passively pre-cooled by allowing its indoor temperature to float during unoccupied periods. The impact of this pre-cooling strategy associated with the flexible settings of DIMs is illustrated in Figure 1-7. In particular, the time variation of total building thermal cooling load and the indoor mean air temperature (MAT) are shown during May 16th. It is evident that the MAT variation obtained by the GA-based optimization during unoccupied periods is lower when compared to that obtained when the building walls are statically insulated with a high R-value. Moreover, the DIM-based pre-cooling strategy lowers the total building thermal cooling load during the occupied daytime period.

The same pre-cooling strategy analysis has been carried out during May 6th which is characterized by high sol-air temperature during the daytime [28]. The optimal R-value settings for the DIM layers for May 6th are summarized in Figure 1-8 for all four wall orientations. Based on the GA-based optimization results, the DIM layers have to be set at the low R-value during the unoccupied periods but need to have the high R-value during the daytime period since the sol-air temperatures for all walls are high as depicted in Figure 1.9. As a result, the building is pre-cooled during the unoccupied period lowering its daytime thermal cooling load.

### 1.4.2 Heating Season Analysis

The impact of optimal settings for DIM layers has been evaluated during the heating season for an office building located in Golden, CO [28]. Specifically, two days from December have been selected to

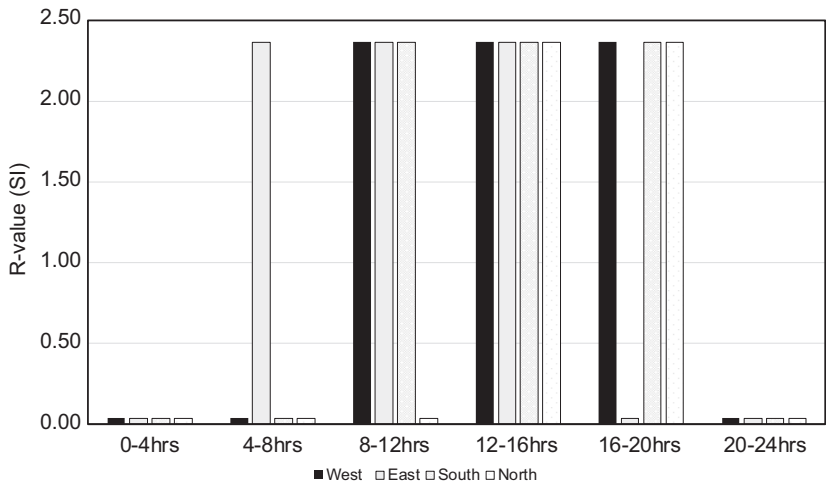


**Figure 1-8** R-value settings obtained by GA-based optimization for May 6th May when the office building is located in Golden, CO.

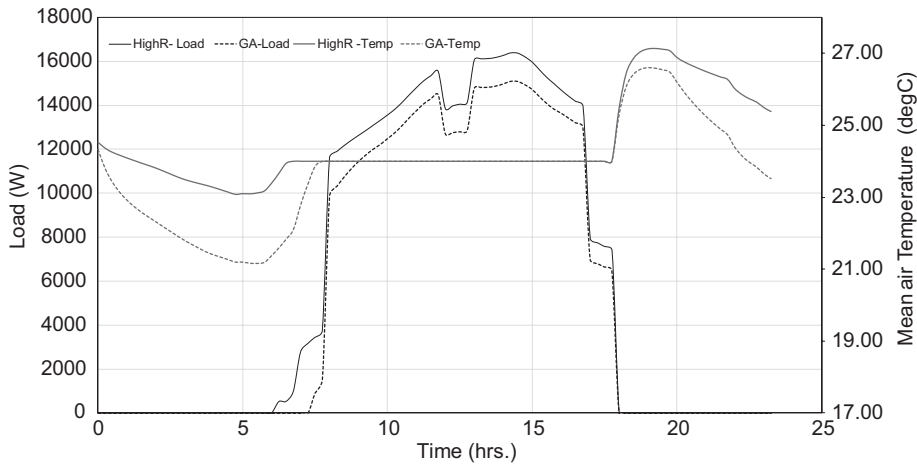


**Figure 1.9** Thermal loads and temperature settings obtained by GA-based optimization during May 6th when the office building is located in Golden, CO.

assess the performance of optimally controlled DIM layers applied to all the exterior walls of the small office building. In particular, December 3rd and 16th used for the GA-based optimization analysis include one mild day (December 3rd) and one extremely cold day (December 16th). The use of highly insulated walls is typically considered the most effective approach during the entire heating season of Golden, CO to reduce heat loss from both residential and commercial buildings. But the results of GA-based optimization indicate that when the external conditions (i.e. sol-air temperatures) are mild as is the case on December 3rd, DIM layers with low R-value settings can be utilized to release internal heat gains from the office building during the occupied period. Passive pre-cooling ability has not been considered in the optimization analysis as it would not be practical to use this feature in a heating month. The thermal resistance R-value settings for DIMs obtained for December 3rd by the GA-based optimization are shown in Figure 1-10. It can be seen that the R-value

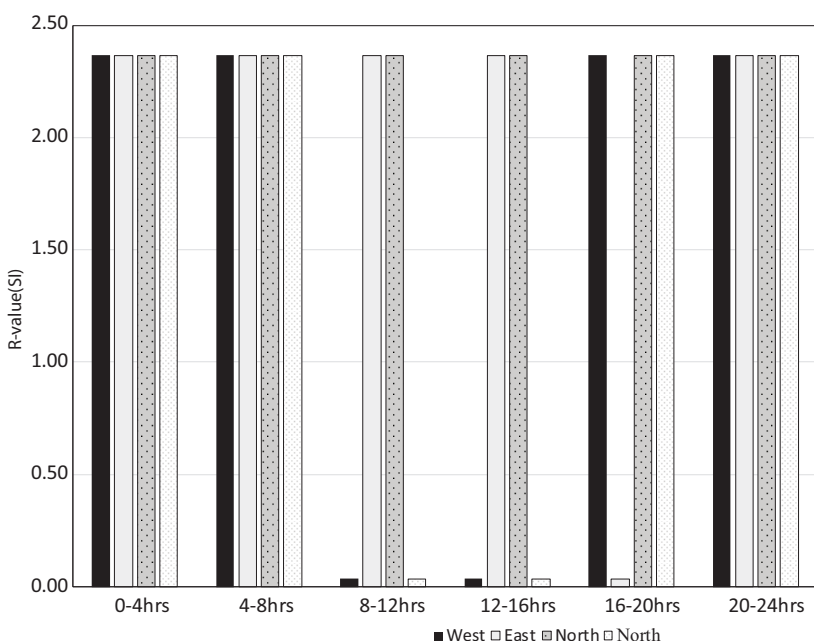


**Figure 1-10** R-value settings obtained by GA-based optimization for December 3rd when the office building is located in Golden, CO.

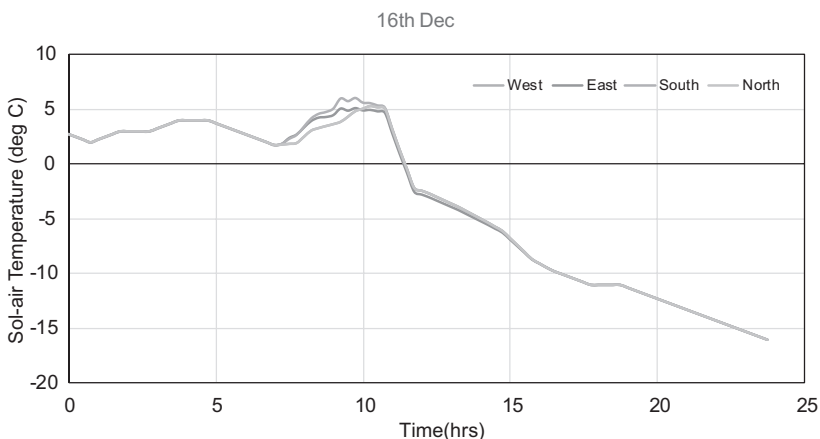


**Figure 1-11** Hourly variation of sol-air temperatures (Dec 16th Golden, CO).

is lowered for the DIM layers of the West and North walls during the occupied period. For December 3rd, the GA-based optimization has saved as much as 16% of total office building heating and cooling energy costs.

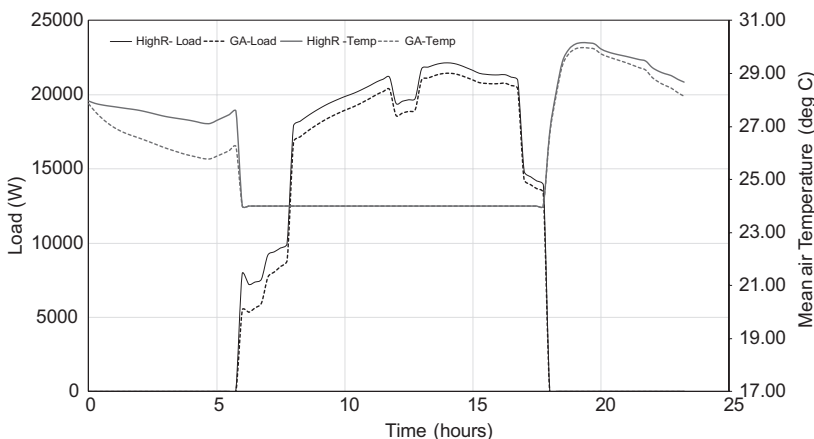
But for a heating dominated climate such as that of Golden, CO, mild weather conditions are seldom experienced during the winter season. A more representative day for Golden, CO winter weather conditions is December 16th which has extreme cold temperatures.

Figure 1-11 represents the time-variation of the sol-air temperature experienced by each building wall during December 16th in Golden, CO. It can be seen that all the walls are subject to very low sol-air temperatures ranging from 5°C to -15°C throughout the day. For these extreme outdoor conditions, the GA-based optimization maintains high R-values for all the walls with DIM layers during the entire day of December 16th.

#### 1.4.3 Cooling Season Analysis

Moreover, the effectiveness of DIMs has been assessed during the cooling season for an office building located in Golden, CO [28]. First, the analysis is carried out for the entire month of July using the 2-step simplified control strategy. It was found that, the potential for energy use cost savings due to the application of DIMs is rather limited to very few days in July. The DIM energy saving potential is further evaluated

using the GA-based optimization for two days in July: a hot day represented by July 8th and a mild day represented by July 24th. The percent energy cost savings for both days are estimated to be 5% July 8th and 18% for July 24th. It should be noted that the passive pre-cooling ability of the DIM layers has been considered for the optimization analysis



**Figure 1-12** Thermal loads and temperature settings obtained by GA-based optimization during July 8th when the office building is located in Golden, CO.

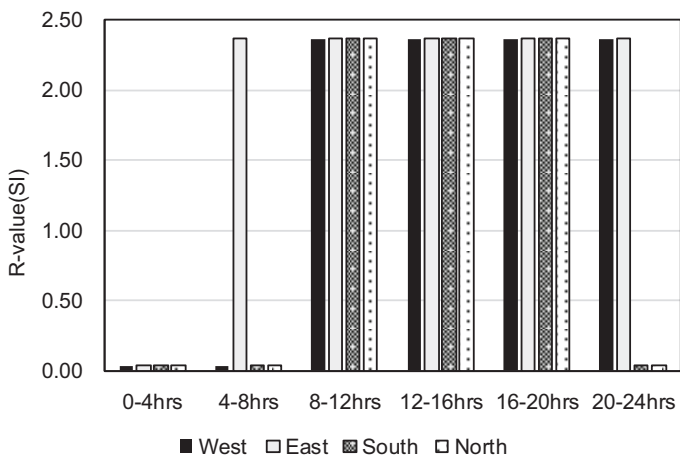


**Figure 1-13** R-value settings obtained by GA-based optimization for July 8th when the office building is located in Golden, CO.

performed for the two days in July. While July 8th represents a typical hot day in July, the 5% energy cost saving potential associated with the use of DIMs are actually due to the ability of the building to passively and freely pre-cool during the unoccupied periods. The DIM operation settings and their impact during July 8th are better illustrated by the time-variation of thermal cooling load and mean air temperature as well as optimal R-value settings as shown in Figures 1-12 and 1-13, respectively.

### 1.5 Comparative Analysis of Control Strategies

While the opportunity of energy use and cost savings associated with the application of DIMs is evident from the results obtained using GA-based optimization, it is important to compare these results to those obtained from the simplified 2-Step control [3]. Figure 1-14 provides a summary of the comparative analysis results for five representative days (i.e., two days for the swing season, one day for the heating season, and two days for the cooling season) [28]. The comparative analysis is carried out using 4-hr periods for the GA-based optimization with the

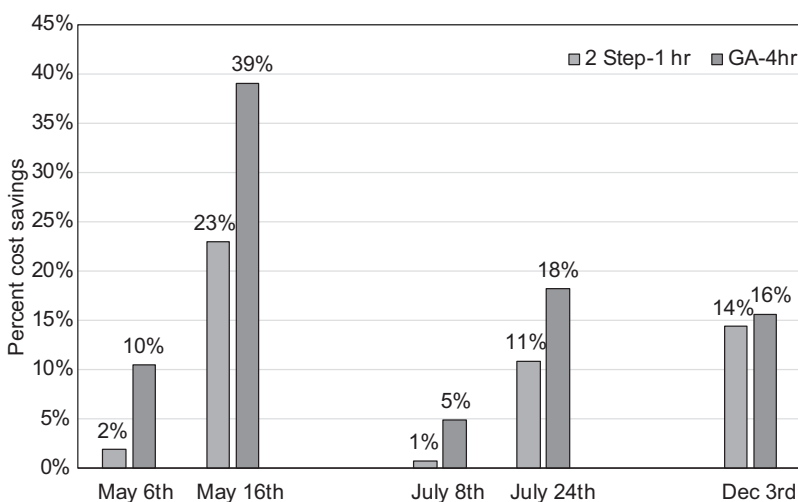


**Figure 1-14** Percent energy cost savings from DIMs obtained using GA-based optimization and those achieved by 2-Step controls for five representative days when the office building is located in Golden, CO.

ability to passively pre-cool the building and 1-hr periods for the 2-Step control. It should be noted that the GA-based optimization results using 1-hr and 4-hr periods were found to provide the same energy use and cost savings associated with the application of DIM layers for all the exterior building walls.

It is clear from the results outlined in Figure 1-14 that the GA-based optimization outperforms the 2-Step controls for all the five days considered in the analysis. This finding is expected since the GA-based optimization algorithm actually searches for the best DIM settings to reduce the total building energy use costs as defined by Eq. (1.5). The significant differences in the potential energy cost savings clearly indicate that the 2-Step approach while simple to implement, is not the most effective control technique to operate the DIM layers. It should also be noted, however, that during the heating season, both techniques provide similar performance and lead to almost identical energy cost savings. Further analysis shows that the main difference in the performance between the two control options during both the swing and cooling seasons is the ability of the GA-based optimization to take advantage of cool outdoor temperatures to adjust the DIM settings in order to freely pre-cool the building thermal mass during unoccupied hours.

## 1.6 Sensitivity Analysis

It has been shown that the performance of DIMs applied to the exterior building walls can be affected by several design and operating parameters including but not limited to utility rates (i.e., energy and demand charges), floor aspect ratios, climates, and wall constructions [3]. A series of sensitivity analyses is carried out using the office building model to assess the performance of DIMs under various design and operating conditions as briefly described in the following sections.

### 1.6.1 Impact of the Utility Rates

The energy prices used in the reported analyses are based on EIA average rates obtained for the US commercial buildings [33–34]. In order to evaluate the impact of the energy prices on the behavior of the DIMs, both the electricity rates and natural gas rates are varied from the considered baseline values. The analysis to assess the impact of energy prices is performed for December 3rd when the office building located in Golden, CO, experiences both heating and cooling thermal

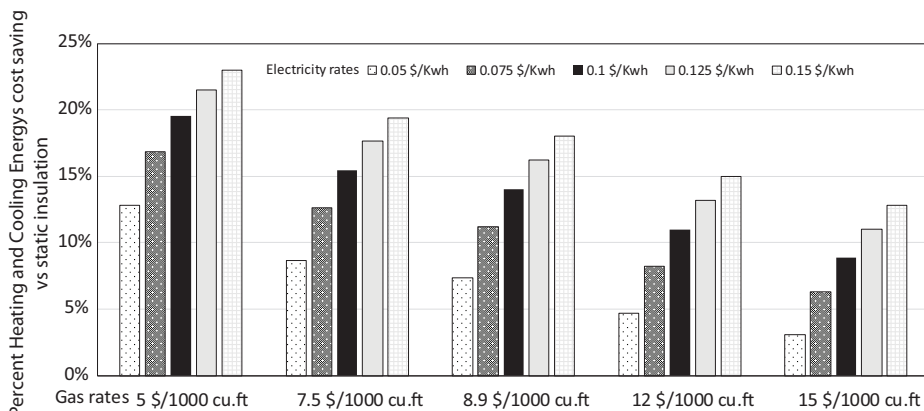


**Figure 1-15** Impact of electricity and natural gas prices on the energy cost savings that DIMs can achieve for an office building located in Golden, CO.

loads. The results of the sensitivity analysis are summarized in Figure 1-15.

Since electricity is mostly consumed during the daytime by the cooling system, the DIM settings are adjusted in order to release the internal heat gains to the outdoors to lower the required cooling energy. Hence as the electricity price increases, the controller increasingly activates the DIMs regardless of the natural gas prices as can be noted from the results shown in Figure 1-15. Similarly, the heating requirements for the office building occur mainly during the unoccupied period on December 3rd, the DIM layers are generally set at high R-value. Thus, while any increase in gas prices increases the heating energy costs, it forces the controller to maintain high R-value for the walls for longer periods and thus reduce the overall energy cost saving potential for the DIMs for any given electricity price as is apparent in Figure 1-15.

### 1.6.2 Impact of the Building Shape

The effect on DIM performance of changing the building shape has also been evaluated for an office building. In particular, the shape is varied by changing the building floor aspect ratio defined as the ratio of the length to the width of the building footprint. By keeping the building orientation and floor area fixed, the floor aspect ratio is varied from a wide floor to a long floor. The sensitivity results obtained for December

3rd are illustrated in Figures 1-16 and 1-17 when the office building is located in Golden, CO. In particular, Figure 1-16 shows the variation of the combined heating and cooling energy costs as a function of the floor aspect ratio. Figure 1-17 represents the percent energy cost savings due to DIMs as a function of the building floor aspect ratio. Both Figures clearly indicate that the percent energy cost saving which can be achieved by DIMs compared to statically insulated walls is the highest when the building floor aspect ratio is close to 1 which corresponds to the most compact building form (i.e., a square).

Figure 1-18 shows the frequency (in terms of the number of hours) when a low R-value is set for the DIM layers as a function of the building floor aspect ratio for all wall orientations. Figure 1-18 clearly indicates that DIMs are most active for a compact building with a floor aspect ratio close to unity for the four wall orientations. It should be noted that the DIM layers are set differently depending on the wall orientation DIMs facing North and West are the most active. This high activity for both walls is associated to their low sol-air temperature experienced during the day.

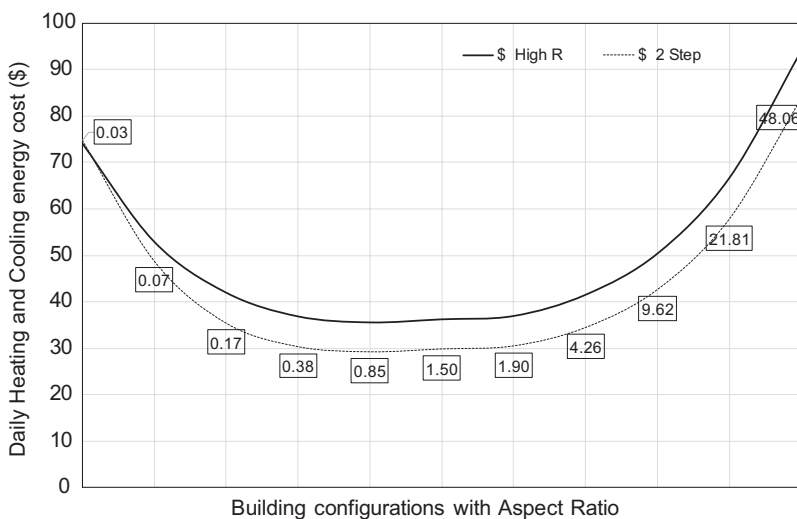


**Figure 1-16** Variation of heating and cooling energy costs as a function of the office building floor aspect ratio (indicated in the boxes) during December 3rd in Golden, CO.

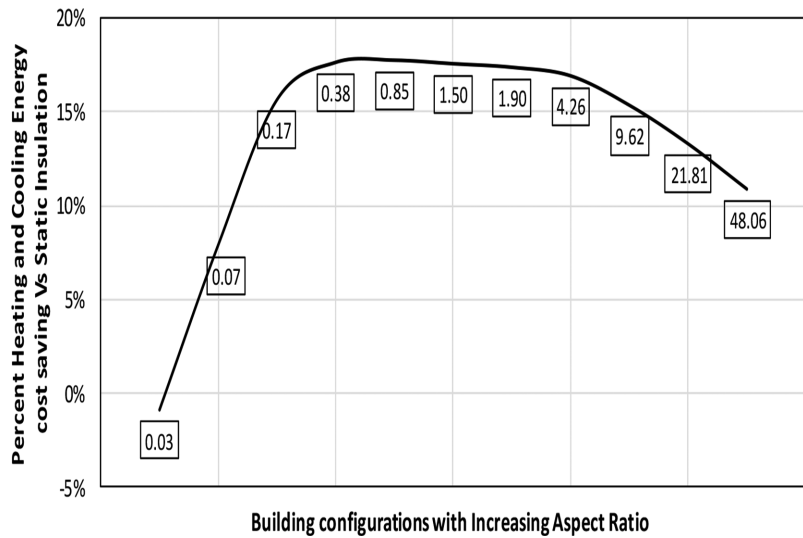


**Figure 1-17** Variation of % energy cost saving as a function of the office building aspect ratio (indicated in the boxes) during December 3rd in Golden, CO.

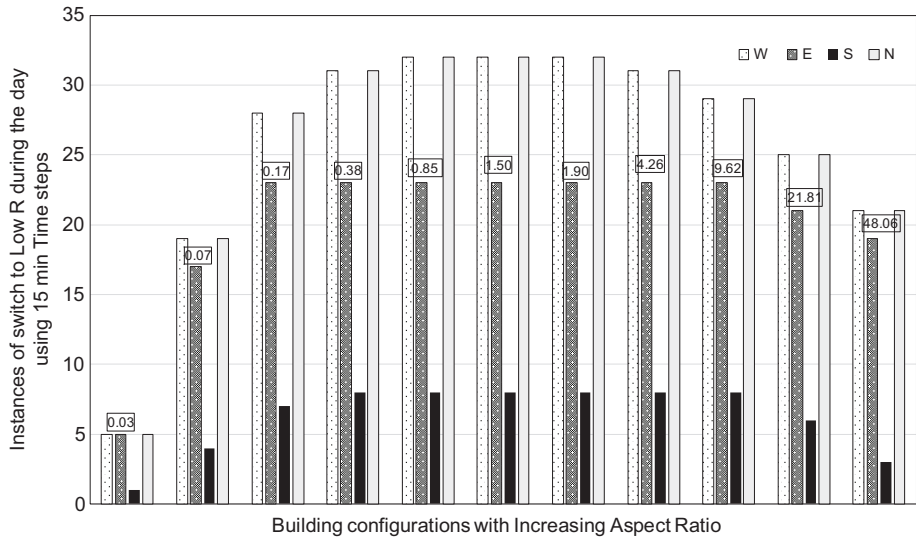


**Figure 1-18** Frequency of DIM settings to low R-value as a function of the office building aspect ratio.

## 1.7 Impact of Climate

To determine whether or not these results could be generalized across cities within the same climate zone, a broader analysis was completed with 44 different cities (2 or 3 cities in each of the 15 climate zones that are found in the U.S.). Table 1-2 summarizes the overall wall R-values for both static and variable insulation considered for all 44 cities [35].

Heating and cooling degree-days are often used to characterize climate conditions for building energy analysis. Since degree-days vary by the weather data that is used, all heating and cooling degree days used in this project were calculated from weather data that was used in the simulation (TMY3) with a base temperature of 65°F (18°C).

### 1.7.1 Heating Degree Days

When comparing the simulated heating savings to heating degree days (HDDs) for each location, it is found that there is greater potential for heating energy savings with the deployment of DIMs in colder climates (with high HDD values) as shown in Figure 1-19 [35].

Although there is variation among cities within each climate zone, heating degree-days is found to be a fairly good indicator of the savings that could be realized with the deployment of DIMs for a given location.

### 1.7.2 Cooling Degree Days

When comparing the cooling energy savings (the difference between 2-Step: None/High and Code-R) with cooling degree-days (CDDs), as shown in Figure 1-20, the potential for DIMs is found to depend on the baseline case used for the comparative analysis to estimate annual energy savings [35]. Specifically, for warmer climates (high CDD values), 2-Step DIMs save energy when compared to code-required insulation. However, this energy savings could also be achieved by using static insulation with a higher R-value. For colder climates, the opposite behavior is found. Switching to static insulation with a higher R-value does not decrease the cooling load, but a dynamic insulation system would.

## 1.8 Economic Analysis

One important consideration when determining the potential of a new technology is its cost-effectiveness. As part of a cost analysis for the deployment of DIMs, their potential in annual energy cost savings has been estimated [35]. These annual energy cost savings are found to be typically proportional to the reduction in source energy use by a

**Table 1-2** Summary of insulation levels tested by climate zone.

Climate zone	Static insulation			2-Step variable insulation		
	None	Code	High	Med/Code	None/Code	None/High
1,2	RSI-0.4 (R-2.5)	RSI-1.9 (R-11)	RSI-3.0 (R-17)	RSI-1.4/1.9 (R-8.0/11)	RSI-0.4/1.9 (R-2.5/11)	RSI-0.4/3.0 (R-2.5/17)
	RSI-0.4 (R-2.5)	RSI-3.0 (R-17)	RSI-3.9 (R-22)	RSI-1.4/3.0 (R-8.0/17)	RSI-0.4/3.0 (R-2.5/17)	RSI-0.4/3.9 (R-2.5/22)
3,4,5	RSI-0.4 (R-2.5)	RSI-3.9 (R-22)	RSI-5.3 (R-30)	RSI-1.4/3.9 (R-8.0/22)	RSI-0.4/3.9 (R-2.5/22)	RSI-0.4/5.3 (R-2.5/30)
	RSI-0.4 (R-2.5)	RSI-3.9 (R-22)	RSI-5.3 (R-30)	RSI-1.4/3.9 (R-8.0/22)	RSI-0.4/3.9 (R-2.5/22)	RSI-0.4/5.3 (R-2.5/30)

### Potential Heating Energy Savings with DIMS (by replacing constant with variable insulation)

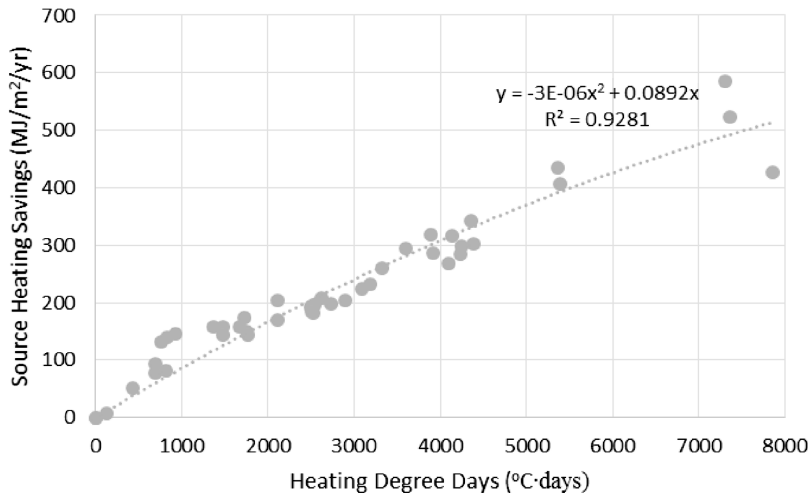


**Figure 1-19** Net Heating Energy Savings with DIMs by HDD.

### Potential Cooling Energy Savings with DIMs

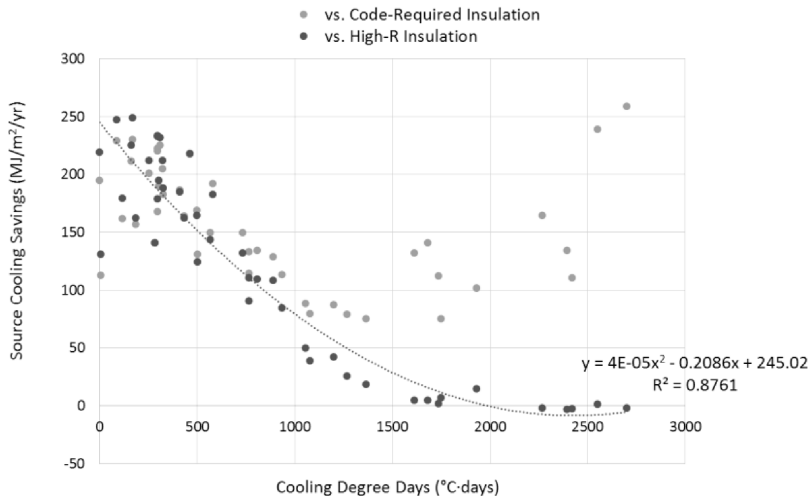


**Figure 1-20** Net Cooling Energy Savings as a function of CDD (vs. High-R).

@Seismicisolation

building. Indeed, source energy takes into account the raw fuel used in the production of energy that is delivered by the utility company. Since most cooling equipment in U.S. buildings is served by electricity which is generated by burning fossil fuels, reducing source energy consumption is essential in reversing the effects of climate change. In 2014, it was estimated that 30% greenhouse gas emissions in the U.S. were from electricity production [36].

In all locations considered in the analysis, it is found that there is potential energy savings with DIMs, when compared with code-required static insulation. However, in several of these locations, similar savings could be realized by investing in a higher level of static insulation, which would be more cost effective than a dynamic insulation system. For DIM technology to be viable in the market place, it would need to outperform static insulation with a higher R-value. For this reason, the potential source energy savings were calculated as the difference between using above-code static insulation (i.e., High-R) and dynamic 2-step insulation (i.e., 2-Step: None/High-R). The US map in Figure 1-21 shows contours for the percent energy savings

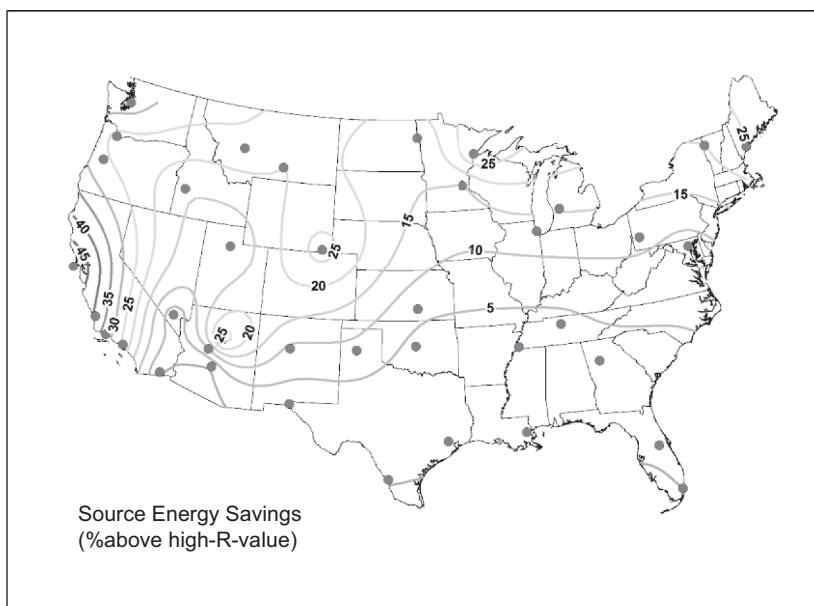


**Figure 1-21** Source Energy Savings contour map associated with DIMs applied to US residential buildings.

associated with the deployment of DIMs on residential buildings by geographical location [35]. The largest potential for total source energy savings (above High-R) was 51.2% in San Francisco (57.4% for cooling and 12.9% for heating). For the cities in climate zone 1a (Hilo, Honolulu, and Miami), 2a (Houston, New Orleans, and Orlando), and 2b (Imperial, Laredo, and Phoenix) there was only a negligible difference between 2-Step: None/High and High-R (ranging from -0.2% to 1.3% savings). Mostly likely, this is because the diurnal temperature swing during the summer months is not large enough to take advantage of the free cooling that is possible with DIMs.

Another approach to measure the cost effectiveness of deploying DIMs was estimated in terms of site energy cost savings, which directly correlates with a reduction in utility bills for the homeowners. Often cost-effectiveness is the primary factor considered by a homeowner when deciding whether or not to invest in energy efficiency measures. It is also used to calculate the return on investment (ROI) or payback period. The map in Figure 1-22 shows the potential savings per square

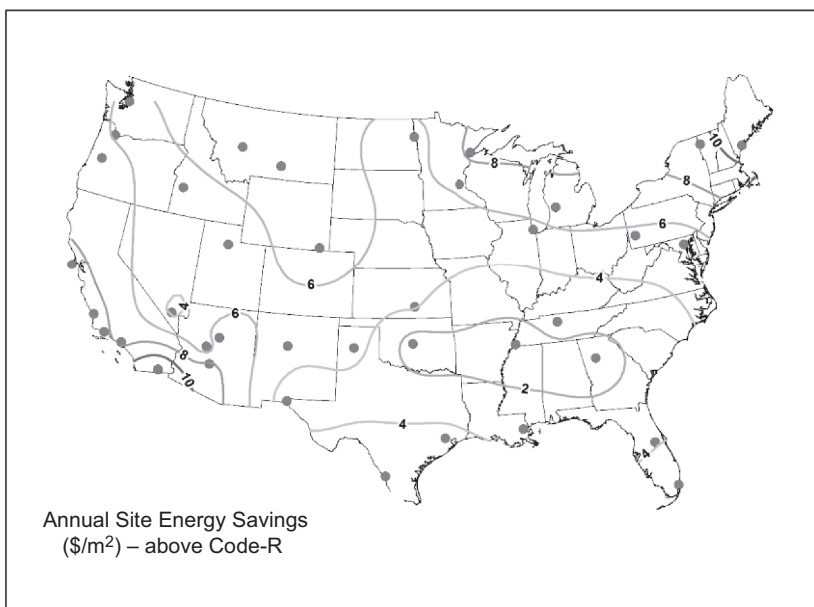


**Figure 1-22** Energy Cost Savings contour map associated with DIMs applied to US residential buildings.

meter of dynamic insulation systems, in comparison to code-required static insulation, and takes into consideration the current electricity and natural gas rates [2]. For electricity, these rates range from a low of \$0.0833/kWh in Oklahoma to high of \$0.2692/kWh in Hawaii. For natural gas, these rates range from a low of \$0.54/therm in North Dakota to a high of \$3.25/therm in Hawaii.

When considering site energy cost savings, it is found that utility rates have a large impact [35]. In states with high utility rates such as Alaska, California, Maine, and Vermont, DIMs can achieve significant energy cost savings for homes as reflected in the percent cost savings map shown in Figure 1-22. The largest overall cost savings was \$13.62/m<sup>2</sup> in Fairbanks, AK (\$13.25 from cooling savings and \$0.37 from heating savings). The lowest cost savings tend to be clustered in the Southeast and South Central states – especially Memphis, Atlanta, Oklahoma City, which are all in climate zone 3a. The cost of electricity also tends to be relatively low in these states, with Oklahoma currently being the lowest of the 50 states.

As noted earlier, the best application for DIMs would be in climates where simply adding more insulation is not effective. The additional costs for DIMs would depend primarily on the specific dynamic insulation system adopted and installed. Table 1-3 illustrates the payback period of DIMs applied to residential buildings for various US climates using two scenarios for their additional installation cost relative to the static insulation. For US residential buildings, the average costs of adding wall static insulation is \$1.75 per square foot (\$18.84/m<sup>2</sup>). If DIMs could be manufactured for 50% more (\$28.26/m<sup>2</sup>), the payback period would be less than 3.5 years in all of the cities where it would be recommended (climate zones 3b-8). Even if the cost was double that of static insulation (\$37.68/m<sup>2</sup>), the payback period would be less than 5 years in all but three of the cities listed in Table 1-3.

## 1.9 Summary and Conclusions

In this chapter, the potential of deploying DIMs to replace static insulation layers in exterior walls of residential buildings has been investigated for all US climates. The analysis includes annual simulation to assess heating and cooling energy savings associated with DIMs. The results of the analysis indicate that although heating energy can be saved through the use of DIMs, especially in warm to mild climates,

**Table 1-3** Evaluation for payback periods for DIMs applied to US homes

Climate zone	City	Site energy cost savings (\$/m <sup>2</sup> )	Payback period (years)	
			DIMs cost is 150% of static insulation	DIMs cost is 200% of static insulation
3b	El Paso, TX	\$2.84	3.3	6.6
	Las Vegas, NV	\$3.60	2.6	5.2
	Los Angeles, CA	\$7.50	1.3	2.5
3c	San Francisco, CA	\$8.63	1.1	2.2
	Santa Barbara, CA	\$8.38	1.1	2.2
	San Luis Obispo, CA	\$8.96	1.1	2.1
4a	Baltimore, MD	\$4.97	1.9	3.8
	Nashville, TN	\$2.77	3.4	6.8
	Wichita, KS	\$4.21	2.2	4.5
4b	Albuquerque, NM	\$4.73	2.0	4.0
	Amarillo, TX	\$4.66	2.0	4.0
	Prescott, AZ	\$4.55	2.1	4.1
4c	Eugene, OR	\$6.40	1.5	2.9
	Portland, OR	\$5.92	1.6	3.2
	Seattle, WA	\$5.84	1.6	3.2
5a	Chicago, IL	\$5.33	1.8	3.5
	Grand Rapids, MI	\$7.31	1.3	2.6
	Pittsburgh, PA	\$5.65	1.7	3.3
5b	Boise, ID	\$5.59	1.7	3.4
	Flagstaff, AZ	\$7.55	1.2	2.5
6a	Salt Lake City, UT	\$4.83	2.0	3.9
	Burlington, VT	\$9.40	1.0	2.0
	Minneapolis, MN	\$6.26	1.5	3.0
	Portland, ME	\$10.89	0.9	1.7

(Continued)

**Table 1-3** Evaluation for payback periods for DIMs applied to US homes (Continued)

Climate zone	City	Site energy cost savings (\$/m <sup>2</sup> )	Payback period (years)	
			DIMs cost is 150% of static insulation	DIMs cost is 200% of static insulation
6b	Billings, MT	\$6.78	1.4	2.8
	Cheyenne, WY	\$7.07	1.3	2.7
	Helena, MT	\$7.02	1.3	2.7
7	Anchorage, AK	\$11.52	0.8	1.6
	Duluth, MN	\$8.49	1.1	2.2
	Grand Forks, ND	\$5.25	1.8	3.6
8	Fairbanks, AK	\$13.62	0.7	1.4
	Nome, AK	\$6.84	1.4	2.8

cooling energy savings are more significant. This is particularly true when accounting for equipment inefficiencies and source energy losses.

The results of the reported analyses outlined in this chapter have indicated that orientation affects the frequency with which an exterior wall is switched to a lower R-value. In colder climates, where DIMs are used to release trapped heat, it is found that the north wall is one that is most frequently switched to a low R-value. On the other hand, when the wall R-value is lowered to allow heat to enter a building, the south wall is found to be the most active.

When comparing DIMs to code-required static insulation, energy and cost savings can be achieved in buildings located in all 44 US cities studied. And, in virtually all of these cities, the largest energy savings were achieved by using the 2-Step insulation with the lowest possible low R-value and the highest possible high R-value. Although seasonal control was only evaluated in select cities, in all cases it was less effective than an hourly controlled DIM system. The analysis results indicate that when using dynamic insulation, the greatest energy savings would be achieved by using an automated optimized control system, which responds to actual input

from temperature sensors and can take advantage of diurnal temperature swings, rather than relying on seasonal settings and manual control.

The potential energy savings that can be achieved when DIMs are optimally controlled. In particular, Genetic Algorithm (GA) optimization is utilized in order to determine the optimal DIM settings during representative days to minimize the heating and cooling energy costs associated with a prototypical office building for 3 climate zones, different building shapes, and various energy prices. The reported results indicate that DIMs can potentially save as much as 17% in annual heating and cooling energy costs. Moreover, the optimally controlled DIMs can have several benefits including:

- DIMs can be used to enhance passive pre-cooling control strategies of buildings. This benefit of DIMs presents a significant opportunity to reduce cooling thermal loads during the daytime.
- The operation of DIMs mainly depends upon the interactions of internal gain loads and the external ambient conditions. When the internal heat gains are high and the ambient temperatures are mild, DIMs provide a good opportunity for energy use saving.
- The optimal settings for DIMs and consequently their performance is highly dependent on the energy prices and climate conditions. It has been shown that DIMs are more effective for higher electricity prices and milder climate conditions.

In summary, DIMs can be used for enhancing passive cooling capabilities of buildings especially in mild climates and weather conditions. Moreover, it is expected that DIMs could achieve even more energy savings if intermediate thermal resistance settings are allowed in addition to only high and low R-values considered in the analysis reported in this chapter.

Heating degree-days (HDDs) and cooling degree-days (CDDs) were found to be good indicators of potential energy savings. As expected, HDDs correlate well with the potential of heating energy savings associated with DIMs. However, only for the warmest climates, where allowing heat to enter the building during the winter to offset the heating load, DIMs would provide some energy savings relative to adding static insulation. For cities with high CDDs, DIMs can achieve higher cooling savings when compared to code-required insulation

levels. For cities with low CDDs, DIMs could provide higher cooling savings when compared to above-code insulation levels.

In the overview outlined in this chapter, DIMs were only applied for building exterior walls. In climate zones where DIMs have been shown to be effective, future research could be conducted to determine the effect of using variable insulation systems in building roofs. Moreover, DIMs also need to be developed for seamless integration with building envelope systems. To be practical, DIMs must be robust enough to handle the demands of construction sites. To be a viable alternative to static insulation systems, DIM's installation and operation costs must also be comparable with the potential energy cost savings discussed in this chapter.

## References

- [1] B.P. Jelle, Traditional, state-of-the-art and future thermal building insulation materials and solutions – Properties, requirements and possibilities, *Energy and Buildings*, 43, 2549–2563, 2011.
- [2] EIA, U.S. Energy Information Administration (EIA) – Independent Statistics and Analysis, 2016. [Online].
- [3] B. Park, W.V. Srubar, and M. Krarti, Energy performance analysis of variable thermal resistance envelopes in residential buildings, *Energy and Buildings*, 103, 317–325, 2015.
- [4] W.W. Clark, L.A. Schaefer, W.A. Knotts, C. Mo, and M. Kimber, Patent US20130081786 – variable thermal insulation. *Google Books*, 2013. [Online]. Available: <https://www.google.com/patents/US20130081786>.
- [5] R. Baetens, B.P. Jelle, J.V. Thue, M.J. Tenpierik, S. Grynning, and S. Uvsløkk, Vacuum insulation panels for building applications: A review and beyond, *Energy and Buildings*, 42, 147–172, 2010.
- [6] R. Baetens, B.P. Jelle, A. Gustavsen, and S. Grynninga, Gas-filled panels for building applications: A state-of-the-art review, *Energy and Buildings*, 42, 1969–1975, 2010.
- [7] R. Baetens, B.P. Jelle, and A. Gustavsen, Aerogel insulation for building applications: A state-of-the-art review, *Energy and Buildings*, 43, 761–769, 2011.
- [8] S. Schiavoni, F. D'Alessandro, F. Bianchi, and F. Asdrubali, Insulation materials for the building sector: A review and comparative analysis, *Renewable and Sustainable Energy Reviews*, 62, 988–1011, 2016.

- [9] S.W. Lee, C.H. Lim, and E. Bin Salleh, Reflective thermal insulation systems in building: A review on radiant barrier and reflective insulation, *Renewable and Sustainable Energy Reviews*, 65, 643–661, 2016.
- [10] O.T. Masoso and L.J. Grobler, “A new and innovative look at anti-insulation behaviour in building energy consumption,” *Energy and Buildings*, 1889–1894, 2008.
- [11] M. Hayashi, H. Yoshinori, and M. Sugawara, Dwellers’ Habit of Opening Windows in Detached Houses in Cold and Hot-Humid Climate of Japan, *Journal of Environmental Protection*, 663–671, 2014.
- [12] K. Kapsis, A. Tzempelikos, A.K. Athienitis, and R.G. Zmeureanu, Daylight performance evaluation of a bottom-up motorized roller shade, *Solar Energy*, 84(12), 2120–2131, 2010.
- [13] D. Bourgeois, C. Reinhart, and I. MacDonald, Adding advanced behavioural models in whole building energy simulation: A study on the total energy impact of manual and automated lighting control, *Energy and Buildings*, 38(7), 814–823, 2006.
- [14] D.A. Neerer and R.D. McFarland, Some potential benefits of fundamental research for the passive solar heating and cooling of buildings, *Los Alamos National Laboratory*, Los Alamos, New Mexico, 1982.
- [15] N.L. Sbar, L. Podbelski, H.M. Yang, and B. Pease, Electrochromic dynamic windows for office buildings, *International Journal of Sustainable Built Environment*, 1.1, 123–139, 2012.
- [16] A. Jonosson and A. Roos, Evaluation of control strategies for different smart window combinations using computer simulations, *Solar Energy*, 84(1), 1–9, 2010.
- [17] M. Krarti, Effect of airflow on heat transfer in walls, *Journal of Solar Energy Engineering*, 116(1), 35–42, 1994.
- [18] B.J. Taylor, D.A. Cawthorne, and M.S. Imbabi, Analytical investigation of the steady-state behavior of dynamic and diffusive building envelopes, *Building and Environment*, 31(6), 519–525, 1996.
- [19] A. Dimoudi, A. Androutsopoloulus, and S. Lykouli, Experimental work on a linked, dynamic and ventilated wall component, *Energy and Buildings*, 36(5), 443–453, 2004.

- [20] K. Qiu and F. Haghigat, Modeling the combined conduction-air infiltration through diffusive building envelope, *Energy and Buildings*, 39, 1140–1150, 2007.
- [21] M. Solupe and M. Krarti, Assessment of Air Infiltration Heat Recovery and Its Impact on Energy Consumption for Residential Buildings, *Energy Conversion and Management*, 78, 316–323, 2014.
- [22] J. Kosny, E. Kossecka, A. Brzezinski, A. Tleoubaev, and D. Yarbrough, Dynamic thermal performance analysis of fiber insulations containing bio-based phase change materials (PCMs), *Energy and Buildings*, 52, 122–131, 2012.
- [23] M. EL Mankibi, Z. Zhai, S.N. Al-Saadi, and A. Zoubir, Numerical modeling of thermal behaviors of active multi-layer living wall, *Energy and Buildings*, 106, 96–110, 2015.
- [24] S.N. AL Saadi and Z. Zhai, Systematic evaluation of mathematical methods and numerical schemes for modeling PCM-enhanced building enclosure, *Energy and Buildings*, 92, 374–388, 2015.
- [25] S.E. Kalnæs and B.P. Jelle, Vacuum insulation panel products: A state-of-the-art review and future research pathways, *Applied Energy*, 116, 355–375, 2014.
- [26] S.B. Sadineni, S. Madala and R.F. Boehm, Passive building energy savings: A review of building envelope components. *Renewable and Sustainable Energy Reviews*, 15(8), 3617–3631, 2011.
- [27] B.P. Jelle, A. Gustavsen, and R. Baetens, The path to the high performance thermal building insulation materials and solutions of tomorrow, *Journal of Building Physics*, 34(2), 99–123, 2010.
- [28] V. Shekar and M. Krarti, Control Strategies for Dynamic Insulation Materials Applied to Commercial Buildings, submitted to *Energy and Buildings*, 2016.
- [29] S. Wang and X. Xu, Parameter estimation of internal thermal mass of building dynamic models using genetic algorithm, *Energy Conversion and Management*, 47(13–14), 1927–1941, 2006.
- [30] J.A. Wright, H.A. Loosemore, and R. Farmani, Optimization of building thermal design and control by multi-criterion genetic algorithm, *Energy and Buildings*, 34(9), 959–972, 2002.

- [31] D. Tuhus-Dubrow and M. Krarti, Genetic-algorithm based approach to optimize building envelope design for residential buildings, *Building and Environment*, 45(7), 1574–1581, 2010.
- [32] Y. Bichiou and M. Krarti, Optimization of envelope and HVAC systems selection for residential buildings, *Energy Buildings*, 43(12), 3373–3382, 2011.
- [33] EIA, “U.S. Price of Natural Gas Sold to Commercial Consumers (Dollars per Thousand Cubic Feet).” [Online]. Available: <http://www.eia.gov>. [Accessed: 05-May-2016].
- [34] EIA, “Average Retail Price of Electricity,” 2013. [Accessed: 05-May-2016]. Available: <http://www.eia.gov/>.
- [35] K. Menyhart and M. Krarti, Potential energy savings from deployment of Dynamic Insulation Materials for US residential buildings, *Building and Environment*, 10.1016/j.buildenv.2016.12.009, 2016.
- [36] EPA, Sources of Greenhouse Gas Emissions, [Online]. Available: <https://www3.epa.gov/climatechange/ghgemissions/sources.html>.

---

## 2. Dynamic cool roofing systems

---

*Moncef Krarti, and Jenna Testa, Building Systems Program, University of Colorado, Boulder CO 80309–USA*

**Abstract:** Light colored roofs, known as cool roofs, have gained popularity as a strategy to reduce cooling energy use for both residential and commercial buildings. While static cool roofs (SCRs) with constant optical properties are effective in reducing cooling thermal loads, they can increase energy use due to heating. A solution to avoiding significant heating energy penalties is the adoption of dynamic cool roofs (DCRs) with variable reflective coatings. This chapter explores the potential energy savings of DCRs with seasonally variable reflective surfaces for various building prototypes when compared a static cool roofs. The analysis demonstrates that any additional energy savings from DCRs depend largely on the climate, insulation level, reflectance of the roof, and to a lesser extent on the building thermal mass. This chapter shows that older buildings, with low insulation levels, in colder climates are the best target for retrofit using DCRs. Specifically, reported results, discussed throughout the chapter, show that when a variable reflective costing is applied to low insulation buildings, source energy savings can be achieved and range from 4.33 to 19.44 MJ/m<sup>2</sup> (i.e., 1.6 to 4.9%) for residential units and from 1.17 to 18.00 MJ/m<sup>2</sup> (i.e., 0.3 to 3.9%) for offices. Based on an economic analysis, it is found that the break-even cost for a variable reflectance coating system with a 22-year life span ranges from 0.80 to 4.84 \$/m<sup>2</sup> for residential buildings, and from 0.86 to 4.92 \$/m<sup>2</sup> for commercial buildings.

---

### 2.1 Introduction

A significant portion of the energy consumed in the United States (US) is attributed to buildings. According to the US Energy Information Administration, commercial and residential buildings consumed 40% of the nation's total end-use energy in 2015 [1]. In 2010, the residential building sector consumed 28% of its source energy in space heating, 15% in space cooling, and 13% in water heating. While the commercial building sector consumed 20% of its source energy in lighting, 16% in space heating, and 15% in space cooling [2]. A large portion of the

heating and cooling energy use is associated to building envelope systems such as windows, walls, and roofs.

Heat gain through a roof, specifically for a single-story building, can be a dominant component of a building's total cooling load since it is highly susceptible to solar radiation [3]. One common solution to reducing the cooling thermal loads due to heat gains through roofs is to increase the solar reflectance of the roof top surfaces by installing high reflective coatings or commonly referred to as cool roofs. Due to their low solar absorptivity and high thermal emissivity, cool roofs maintain lower surface temperatures and reduce the heat flow into buildings [4]. Indeed, the low solar absorption increases the solar reflectance and the high thermal emittance enhances the ability of the roof surface to radiate any absorbed solar energy [5, 6]. Based on the existing literature, an average standard roof reflectance ranges from 0.20 to 0.30, an average initial low-sloped cool roof white material ranges from 0.70 to 0.80, and an average aged low-sloped cool roof white material ranges from 0.55 to 0.70 [3, 5, 7, 9]. The typical thermal emittance of most roofing materials, regardless of color or reflectance is typically between 0.80 and 0.90 [4, 8, 6].

In addition to white cool roofing materials, there has been recent developments in colored cool roofing materials specifically for steep-sloped roofs. A cool colored surface absorbs the visible part of the spectrum in order to appear a specific color, but is highly reflecting in the near-infrared (NIR) part of the spectrum which accounts for nearly 50% of solar radiation [10]. Synnefa et al. [11] have developed prototypes of cool colored coatings using near infrared reflective pigments added to acryl-based coatings which can reduce solar reflectance by 0.06 (light blue) and 0.22 (black) [11]. Levinson et al. [12] have developed coating systems for various types of substrates and found that coated steel and glazed clay-tile roofing achieved NIR reflectance as high as 0.50 and 0.75, respectively, using a one-coat system [12]. Pisello et al. [13] have developed a new coating system for colored clay tiles which includes a white englobe above the substrate and a sodium silicate based binder with pigment added for color. The study found that the new coatings are able to reflect the NIR by 75% which is 10% more than traditional tiles with an equivalent visible appearance [13].

## 2.2 Cool Roof Properties

Cool roofs have exterior surfaces or coatings that minimize solar absorption and maximize thermal emittance. They maintain lower surface temperatures

and reduce heat flows into buildings [4–5]. In particular, solar absorption is minimized by increasing roof solar reflectance, defined as the fraction of the solar radiation that is diffusely reflected away by the surface. Lighter surfaces have higher reflectance values than dark surfaces. Specifically, solar reflectance for black surfaces is close to 0 and to 1 for white surfaces. In addition to color, surface roughness and presence of impurities can also effect roof solar reflectance [6]. Roof thermal emittance measures the surface's ability to radiate any absorbed solar energy. The higher their thermal emittance is, the more rapidly roofs can cool [7]. Cool roofs can also increase their thermal resistance since the thermal conductivity values of insulation layers typically increase with temperature [4, 8].

The majority of buildings in the US have relatively dark roofs. For instance, aerial photos of Chicago, Philadelphia, and Washington DC have indicated that buildings roofs in these cities have an average solar reflectance of 0.25 [3]. According to a survey conducted for ASHRAE in 1998, it is found that standard shingles have a solar reflectance ranging from 0.03 to 0.26, with most values between 0.10 and 0.15. Moreover, non-white roofing membranes, such as single-ply roofing materials, smooth bitumen, and granule-surface bitumen have solar reflectance values that range from 0.06 to 0.26. Similarly, gravel roofs have low solar reflectance values varying from 0.12 to 0.34.

Commercial roof products that qualify as cool roofs fall into three categories: single ply, liquid applied coating, and white finished metal panels [7]. Freshly applied white elastomeric coatings have solar reflectance values that range from 0.60 to 0.85. Solar reflectance of new white single-ply roofing membranes typically exceeds 0.70 [6, 9]. Thermal emittance values of non-metallic surfaces are generally between 0.80 and 0.90. Shiny metal roofs can have a relatively high solar reflectance, upwards of 0.60, but they tend to have low thermal emittances which can make them as hot as dark roofs. Therefore, they would not be good materials for cool roofs [9]. One method to quantify the properties of cool roofs is the estimation of their Solar Reflectance Index (SRI). SRI is calculated by using solar reflectance and thermal emittance values adjusted with wind coefficients. The higher the SRI value of a roof is, the lower is its surface temperature and thus the lower is the heat gains into the building. SRI is defined to be zero for a clean black roof (with a solar reflectance of 0.05 and a thermal emittance of 0.90) and 100 for a clean white roof (with a solar reflectance of 0.80 and a thermal emittance of

0.90) [10]. The SRI of a roof surface can be determined by the following equations:

$$SRI = 123.97 - 141.35(x) + 9.655(x^2) \quad (2.1)$$

With,

$$x = \frac{20.979 * \alpha - 0.603 * \varepsilon}{9.5205 * \varepsilon + 12.0} \quad (2.2)$$

Where,  $\alpha$  is the absorption and  $\varepsilon$  is the emissivity of the roof surface.

To be considered cool roofs, surfaces should have their initial SRI exceed 78 [7]. Table 2-1 shows typical roofing materials with their solar reflectance, infrared emittance, temperature rise, and SRI values.

The properties provided in Table 2-1 are specific for newly installed roofs. Over time, solar reflectance values of cool roofs are likely to decrease over time because of surface dirt accumulations and material degradations. The emittance, however, would not decrease significantly [11]. Indeed, soiling and accumulation of soot particles can reduce roof surface solar reflectance by about 0.15 with most of the degradation occurring during the first year [11–12]. Standard maintenance and washing of roof surfaces can restore some of their original solar reflectance properties depending on the washing method. Akbari et al. found in a

**Table 2-1** Typical roofing material properties.

Product	Solar reflectance	Infrared emittance	Temperature rise	SRI
Smooth bitumen	0.06	0.86	83	-1
Generic black shingle	0.05	0.91	82	1
Grey EPDM	0.23	0.87	68	21
Shasta white shingle	0.26	0.91	64	27
Light gravel	0.34	0.90	57	37
Aluminum	0.61	0.25	48	56
White EPDM	0.69	0.87	25	84
White coating on shingle	0.71	0.91	23	87
White PVC (Sarnafil)	0.83	0.92	11	104

study on aging that solar reflectance values of 5–8 year aged cool roofs dropped from 0.80 to 0.50. However, they found that simply washing the roof surfaces with water could restore their solar reflectance to 70%–100% of the original values [13].

### 2.3 Performance of Static Cool Roofs

Several field studies have monitored and documented cooling energy savings and cooling peak demand reductions from static cool roofs (SCRs) in warm climates including California, Florida, and Nevada. Early case studies focused on residential buildings, while the majority of recent studies has focused on commercial buildings. The reported studies have discussed the impact of cool roofs on air-conditioning electricity use, roof surface temperatures, plenum, indoor, and outdoor air temperatures, and insulation levels. In particular, Parker et al. [14] monitored peak power demand and cooling energy use of residential buildings with increased roof solar reflectance for 11 Florida homes during summer months. The daily electricity savings for individual homes were found to range from 5.4 to 138 Wh/m<sup>2</sup> (2% to 45%) and peak power demand were reduced from 1.5 to 7.8 W/m<sup>2</sup> (12% to 23%). The study indicated that energy use savings from SCRs are inversely correlated with the ceiling insulation level and the location of the duct system. Specifically, large energy savings were obtained for home with poor insulated levels and with duct systems located in the attic space [14]. Similarly, Akbari et al. [15] monitored peak power demand and cooling energy use savings from high reflective coatings installed on roofs for one house and two school bungalows in Sacramento, California. The measurements revealed that increasing roof solar reflectance for the house by 0.55 resulted in a daily cooling energy use reduction of 14 Wh/m<sup>2</sup> and a peak demand reduction of 3.55 W/m<sup>2</sup>. Seasonal cooling energy use savings and peak demand reductions were estimated to be 80% and 17%, respectively. Comparative analysis of measurements obtained from the two school bungalows revealed that a white roof bungalow used 52 Wh/m<sup>2</sup> less energy than a bungalow with a metal roof, and 42 Wh/m<sup>2</sup> less energy than a bungalow with a brown roof. The peak load was found to be 6.78 W/m<sup>2</sup> lower for the white roof. The seasonal cooling energy and peak demand savings for the school bungalow were estimated to be 35% and 32%, respectively [15].

Recently, several studies have been carried out to assess the performance of SCRs when applied to commercial buildings. Hildebrandt et al. [16] have measured that daily cooling energy use savings associated with SCRs for an office building, museum, and hospice in Sacramento, CA are 10, 20, and 11 Wh/m<sup>2</sup> (17%, 26%, and 39%), respectively. All three monitored buildings were retrofitted with high reflective roofs so the increase in the solar reflectance was approximately 0.40 [16]. Parker et al. [17] monitored seven retail stores within a strip mall in Cocoa Beach, Florida before and after applying high reflective coatings. The roofs were metal corrugated and had an initial value for the solar reflectance of 0.29 for the first half of the summer and a value of approximately 0.75 for the second half of the summer. The measurements showed an average reduction in daily cooling energy use of 62 Wh/m<sup>2</sup> (25% savings) with a range of 5 to 137 Wh/m<sup>2</sup> (2–43% savings). The average peak-demand savings were 5.9 W (40% savings) [17]. Konopacki et al. [18] measured summer daily cooling energy use savings from high reflective coatings of three commercial buildings in California: two medical office buildings in Gilroy and Davis and a retail store in San Jose. The average increase in roof solar reflectance for all three buildings was 0.40. The cooling electricity use was reduced by 67 Wh/m<sup>2</sup> (18% savings) in the Davis medical office, 39 Wh/m<sup>2</sup> (13% savings) in the Gilroy medical office, and 4 Wh/m<sup>2</sup> (2%) in the San Jose retail store. The roof temperature of all three buildings had dropped by an average of about 12°C [18]. Similarly, Konopacki and Akbari [19] have measured cooling energy use savings from retrofitting the roof of a retail store in Austin, Texas. The measurements showed a daily cooling energy use savings of 39 Wh/m<sup>2</sup> (11% savings), and a peak demand reduction of 3.77 W/m<sup>2</sup> (14% decrease). The increase in roof solar reflectance from the original roof to the retrofitted roof was 0.70 [19]. Akbari [20] monitored the cooling energy use of two small non-residential, regeneration, buildings in Nevada during the summer of 2000. The buildings were monitored first without any alterations for 1.5 months to establish baseline conditions. Then, the roofs of the buildings were painted with reflective white coatings. After the application of the reflective coatings, the roof solar reflectance value was increased on average from 0.26 to 0.72. The average monitored daily electricity savings were about 33 Wh/m<sup>2</sup> (1.5% savings) [20]. Akbari et al. [21] have also measured the cooling energy use savings from increasing roof solar

reflectance of three commercial buildings in California: a retail store in Sacramento, an elementary school in San Marcos, and a cold storage building in Reedley. The estimated average daily savings in cooling energy use for the retail store was estimated to be  $72 \text{ Wh/m}^2$  (52% savings), and the peak demand reduction was found to be  $10 \text{ W/m}^2$  (50% savings). The estimated daily savings in cooling energy use and peak demand for the school were about  $42\text{--}48 \text{ Wh/m}^2$  (17–18% savings), and  $5 \text{ W/m}^2$  (12% savings), respectively. The cold storage facility had daily cooling savings of  $69 \text{ Wh/m}^2$  (4% savings) and peak demand reduction of  $5\text{--}6 \text{ W/m}^2$  (6% savings) [21].

Table 2-2 shows a summary of reported performance of cool roofs based on field studies carried out for US buildings. The ability of a cool roof to reduce a building's energy use is primarily proportional to the conditioned roof area (CRA). Thus, a better approach to compare findings from various studies is to normalize reported SCRs energy use savings by CRA ( $\text{Wh/m}^2$  or  $\text{kWh/m}^2$ ) as listed in Table 2-2. In general, reported savings from applying high solar reflective coatings appear to be dependent on roof insulation, duct location, change in reflectance, and building type/loads.

In addition to experimental studies, several evaluations of SCRs based on modeling and simulation analyses have been reported in the literature [3, 22–27]. Unlike the field case studies, the simulation based analyses have explored the effects of SCRs on both cooling energy use savings and heating thermal penalties in various climates.

One of the first simulation based studies of SCRs was conducted by Konopacki et al. [3] and Akbari et al. [23]. This study has documented the potential energy use savings from increased roof solar reflectance for both residential and commercial buildings in 11 cities throughout the US including Atlanta, Chicago, Los Angeles, Dallas/Fort Worth, Houston, Miami/Fort Lauderdale, New Orleans, New York City, Philadelphia, Phoenix, and DC/Baltimore. The building prototypes modeled in each city consisted of a new/old residential building, new/old office building, new/old retail building, primary and secondary school, hospital, nursing home, and a grocery store. All building prototypes were single-story, since the energy use savings associated with SCRs are assumed to only effect the top floors. For all old vintage building prototypes, schools, health care buildings, and grocery stores, R-11 roofs and R-7 walls were considered. For all new vintage building

**Table 2-2** Summary of performance of SCRs based on field studies reported for US buildings.

Location	Roof system			Daily savings		Reduced demand	
	R-Val	Duct	$\Delta\rho$	Wh/m <sup>2</sup>	%	W/m <sup>2</sup>	%
California							
Davis [18]	1.4	Interior	0.36	68	18	3.34	12
Gilroy [18]	3.3	Plenum	0.35	39	13	2.37	8
San Jose [18]	RB	Plenum	0.44	4	2	1.61	9
Sacramento [15]	3.3	Ceiling	0.60	47	46	6.78	20
Sacramento [15]	1.9	Attic	0.59	14	63	3.55	25
Sacramento [16]	3.3	Plenum	0.40	10	17	n/a	n/a
Sacramento [16]	0	Interior	0.40	20	26	n/a	n/a
Sacramento [16]	1.9	Attic	0.40	11	39	n/a	n/a
Sacramento [21]	RB	None	0.61	72	52	10	50
San Marcus [21]	5.3	None	0.54	45	17	5	12
Reedley [21]	5.1	None	0.61	69	4	5	6
Florida							
Cocoa Beach [17]	1.9	Plenum	0.46	7.5	25	0.65	29
Cape Canaveral [14]	1.9	Attic	n/a	58	22	1.51	12
Cocoa Beach [14]	0	Attic	0.63	137	43	7.75	28
Cocoa Beach [14]	0	Attic	0.39	116	26	7.64	29
Cocoa Beach [14]	1.9	Attic	0.52	85	25	5.49	28
Cocoa Beach [14]	3.3	Attic	0.42	31	13	1.61	11
Merritt Island [14]	1.2	Attic	0.44	73	20	6.24	23
Merritt Island [14]	4.4	Attic	0.51	24	11	n/a	n/a
Miami [14]	1.9	Attic	0.30	64	15	3.44	16
Palm Bay [14]	3.3	Attic	0.44	23	10	2.58	16
Palm Bay [14]	3.3	Attic	0.42	5.4	2	1.83	12
West Florida [14]	0	Attic	0.53	68	25	5.92	30
Lakeland [14]	5.3	Attic	0.65	n/a	17	n/a	n/a

(Continued)

**Table 2-2** Summary of performance of SCRs based on field studies reported for US buildings. (*Continued*)

Location	Roof system			Daily savings		Reduced demand	
	R-Val	Duct	$\Delta\rho$	Wh/ m <sup>2</sup>	%	W/m <sup>2</sup>	%
Nevada							
Battle Mount. [20]	3.2	None	0.45	31	1.2	n/a	n/a
Carlin [20]	3.2	None	0.45	39	1.6	n/a	n/a
Texas							
Austin [19]	2.1	Plenum	0.70	39	11	3.77	14

prototypes, R-19 roofs and R-11 walls were used. Whole-building energy simulations were completed for each building type and location for two cases: standard roof reflectance and high roof reflectance. A standard roof reflectance of 0.25 was used for residential and commercial prototypes, and a high roof reflectance of 0.55 and 0.70 were used for residential and commercial prototypes, respectively. The roofs were modeled using a single-layered construction with a thermal emittance of 0.91. The study results indicated that SCRs achieved annual cooling electricity savings per m<sup>2</sup> of flat roof area ranging from 1.1 to 5.2 kWh (7–17%) for old residential buildings, 0.4 to 2.8 kWh (6–15%) for new residences, 1.8 to 6.0 kWh (5–9%) for old offices, 1.1 to 3.3 kWh (3–7%) for new offices, 2.6 to 7.8 kWh (5–10%) for old retail stores, and 1.4 to 4.5 kWh (3–7%) for new retail stores. However, SCRs resulted also in annual heating energy use penalties per m<sup>2</sup> of flat roof area ranging from 0.002 to 0.17 therm (2–5%) for old residences, 0 to 0.13 therm (0–5%) for new residences, 0 to 0.19 therm (0–14%) for old offices, 0 to 0.11 therm (0–12%) for new offices, 0 to 0.10 therm (0–12%) for old retail stores, and 0 to 0.04 therm (0–7%) for new retail stores. The relative energy use savings were found to be most significant for shell dominated residential building prototypes. Moreover, buildings with longer hours of occupancy or operation (such as hospitals and nursing homes) showed larger savings per roof area than those with shortened occupancy schedules. In addition, old residential, office, and retail store prototypes provided larger electricity savings and gas penalties than those of the new vintage. This result is associated to lower roof

R-values specific to the old vintage buildings. Additionally, prototypes with gas heating systems provided larger net cost savings than prototypes with electric heat pumps, because of the higher cost of electric heat compared to gas [23]. Building location was found to have a significant effect on both energy use savings and penalties associated with SCRs. For example, new offices with electric heat pumps in Chicago and Philadelphia, new residences with electric heat pumps in New York City, and new residences with gas furnaces in Philadelphia all displayed limited impact of SCRs with net energy deficits or savings very close to zero. Moreover, the results indicated that there is a general linear trend between cooling degree days and cooling energy use savings, as well as between heating degree days and heating energy use penalties. Exceptions include locations like Phoenix and Los Angeles which exhibit higher cooling energy use savings than the general trend due to higher solar radiation fractions [22]. The simulation results confirmed that both cooling energy use savings and heating energy use penalties were found to vary as linear functions of changes in roof albedo for each building type and location [22, 23]. Thus, to estimate heating energy use penalties and cooling energy use savings from other differences in roof solar reflectance values not considered in the study, the results of the analysis can be adjusted by the ratio of the reflectance differences. Using the results obtained for individual building prototypes, energy use savings associated with SCRs were scaled up using the building stock statistics for 11 US metropolitan areas. The total impact of using SCRs for all 11 metropolitan areas were estimated to include annual electricity savings of 2.6 TWh (average of  $2.15 \text{ kWh/m}^2$ ); natural gas deficit of 6.9 TBtu (average of  $0.05 \text{ therms/m}^2$ ), average energy bill net savings of \$194 M (average  $\$0.16/\text{m}^2$ ), and a peak demand savings of 1.7 GW (average of  $1.45 \text{ W/m}^2$ ) [23].

Moreover, Konopacki and Akbari [24] used simulation to further evaluate how roof surface solar reflectance values, attic and duct insulation levels, and duct locations affect cooling and heating energy use in new single-family buildings. The study considered both dark-roofs with a solar reflectance of 0.10 and cool-roofs with solar reflectance of 0.70 for 16 sun-belt locations across the U.S. For each location and roof reflectance, several design alternatives have been modeling including 11 different attic insulation levels ranging from 1–60, 5 attic duct insulation values, and one duct located in the conditioned space. The simulation results were

then regressed as a function of roof system conductance and roof solar absorptance for each heating system type, duct-insulation level/location, and climate. From the regression analysis, an equivalent change in attic insulation level was calculated for a given change in solar reflectance so annual energy costs obtained for both dark and cool roofs are equal. The study results revealed that residences with SCRs can utilize lower levels of attic insulation than those with dark roofs in order to achieve zero net changes in annual energy use. In general, the uninsulated attic duct case was shown to have the largest reduction in R-value, where the smallest reduction was found with the conditioned zone ducts. In heating dominated climates, however, the effect of duct insulation and location was found to be negligible. Climates with greater cooling degree days were also shown to have the highest reduction in R-value [24].

Using the results of their previous simulation studies [20–24], Akbari and Konopacki [25] further evaluated correlations between building location heating degree days (HDD) and cooling degree days (CDD) and energy use savings achieved by SCRs. The analysis considered 240 different locations across the United States and 6 building types: new/old residential, new/old office building, and new/old retail. These building types were chosen because they make up 93% of the building stock in the U.S. [3]. The prototypes were fairly similar to the previous study by Konopacki et al. [3], except the old vintage roof insulation and wall insulation values were changed to R-11 and R-4.6, respectively, and the new vintage roof insulation and wall insulation values were changed to R-30 and R-13, respectively. The standard roof reflectance was changed to 0.2 for all prototypes, and the high roof reflectance was changed to 0.5 and 0.6 for the residential buildings and commercial buildings, respectively. The simulation analysis results indicated that [25]:

- For old-vintage gas heated residential buildings, annual cooling energy use savings from increasing roof solar reflectance ranged from 0.5 kWh/m<sup>2</sup> (for CDD<200) to 8.6 kWh/m<sup>2</sup> (for CDD>5000) (4–11%), and that annual heating energy use increases ranged from 0 therm/m<sup>2</sup> (for HDD<500) to 0.22 therm/m<sup>2</sup> (for HDD>8000) (0–2%). Similarly, annual cooling energy use savings are estimated for new-vintage residential buildings to range from 0.1 kWh/m<sup>2</sup> (for CDD<200) to 3.6 kWh/m<sup>2</sup> (for CDD>5000) (1–8%) while annual heating energy use increases

are determined to vary from 0 therm/m<sup>2</sup> (for HDD<500) to 0.07 therm/m<sup>2</sup> (for HDD>8000) (0–2%).

- For old-vintage gas-heated office buildings, the annual cooling energy use savings from increasing roof solar reflectance ranged from 4.8 kWh/m<sup>2</sup> (for CDD<200) to 8.2 kWh/m<sup>2</sup> (for CDD>5000) (4–8%), and the annual heating energy use penalties ranged from 0 therm/m<sup>2</sup> (for HDD<500) to 0.13 therm/m<sup>2</sup> (for HDD>8000) (0–3%). Moreover, the estimated annual cooling energy use savings for new-vintage office buildings varied from 1.2 kWh/m<sup>2</sup> (for CDD<200) to 2.8 kWh/m<sup>2</sup> (for CDD>5000) (2–4%) while annual heating energy use penalties ranged from 0 therm/m<sup>2</sup> (for HDD<500) to 0.05 therm/m<sup>2</sup> (for HDD>8000) (0–6%).
- For old-vintage gas-heated retail stores, annual cooling energy use savings from increasing the roof reflectance varied from 6.8 kWh/m<sup>2</sup> (for CDD<200) to 10.9 kWh/m<sup>2</sup> (for CDD>5000) (6–11%), and annual heating energy use penalties ranged from 0 therm/m<sup>2</sup> (for HDD<500) to 0.10 therm/m<sup>2</sup> (for HDD>8000) (0–6%). Meanwhile, annual cooling energy use savings potential for new-vintage retail stores ranged from 1.6 kWh/m<sup>2</sup> (for CDD<200) to 3.8 kWh/m<sup>2</sup> (for CDD>5000) (4–7%), and the annual heating penalties ranged from 0 therm/m<sup>2</sup> (for HDD<500) to 0.06 therm/m<sup>2</sup> (for HDD>8000) (0–10%).

As noted from the reported results listed above, SCRs can provide cooling energy use savings that increase with CDDs but can lead to heating energy use penalties that increase with HDDs. Moreover, SCRs achieve higher cooling energy use savings for residential compared to commercial buildings for locations with CDD over 5000, but result in lower savings for locations with CDD below 200. Typically, the application of SCRs can result in higher heating energy use increases for residences than for commercial buildings due to higher contributions of envelope components to space heating thermal loads. Similar trends were found by Konopacki et al. [23].

Levinson and Akbari [26] conducted a simulation based analysis of SCRs applied to four commercial building prototypes: new/old office buildings and new/old retail stores. The prototypes used for the simulation analysis were the same as those used by Akbari and Konopacki [24] with some minor changes. Specifically, roof insulation values for

old and new prototypes were changed to 19 and 7, respectively, and high roof solar reflectance was set to 0.55. In addition to energy use savings and penalties, the analysis evaluated SCRs energy cost savings and air pollutant savings for 236 US locations. The savings for all evaluated locations and prototypes were then scaled up to a national level using information about US building stock and building density. The simulation analysis results indicated that substituting weathered cool white roofs (with a solar reflectance 0.55) for weathered conventional gray roofs (with a solar reflectance 0.20) yielded the following annual impacts:

- Cooling energy use savings per unit conditioned roof area that varied from  $3.30 \text{ kWh/m}^2$  in Alaska to  $7.69 \text{ kWh/m}^2$  in Arizona with an average of  $5.02 \text{ kWh/m}^2$  nationwide;
- Heating energy use increases ranging from  $0.003 \text{ therm/m}^2$  in Hawaii to  $0.14 \text{ therm/m}^2$  in Wyoming with an average of  $0.065 \text{ therm/m}^2$  nationwide;
- Energy cost savings from a low of  $\$0.126/\text{m}^2$  in West Virginia to a high of  $\$1.14/\text{m}^2$  in Arizona with an average of  $\$0.356/\text{m}^2$  nationwide.
- Carbon emissions reductions from  $1.07 \text{ kg/m}^2$  in Alaska to  $4.97 \text{ kg/m}^2$  in Hawaii with an average  $3.02 \text{ kg/m}^2$  nationwide.

The analysis had indicated that retrofitting 80% of the 2.58 billion square meters of the existing commercial building conditioned roof area in the US would yield an annual electricity savings of 10.4 TWh; an annual heating fuel increases of 133 million therms; and an annual energy cost savings of \$735 million. It would also offer an annual  $\text{CO}_2$  reductions of 6.23 Mt, offsetting the annual  $\text{CO}_2$  emissions of 1.20 million typical cars or 25.4 typical peak power plants [3, 26].

Synnefa et al. [27] conducted a simulation analysis of SCRs by varying their solar reflectance values for several locations around the world. Specifically, the reported analysis has focused on single-family residential buildings located in 27 cities around the world representing different climatic conditions, including Mediterranean, humid continental, subtropical arid, and desert conditions. TRNSYS thermal simulation software was used for the simulations [27]. A building prototype energy model has been utilized with R-7 roof insulation and R-3 wall insulation.

A standard roof reflectance of 0.20 was used for benchmarking, and two high roof reflectance values were used for modeling SCRs: 0.60 and 0.85. The thermal emittance of the roof for all considered cases was set to 0.90. The results of the simulation analysis revealed that increasing roof reflectance by 0.65 reduced annual home cooling thermal load by 9–48 kWh/m<sup>2</sup> (18–93%), and increased annual heating thermal load use by 0.007–0.58 therm/m<sup>2</sup>. Additionally, the analysis showed that three main factors affect the potential thermal load reduction from SCRs include climate, roof U-value, and roof solar reflectance. In particular, the results of the analysis confirmed warmer climates can benefit more from high reflectance roofs than colder climates. Moreover, poorly insulated buildings would benefit more from SCRs than well insulated buildings. However, energy use savings are not directly proportional to the R-values of SCRs. Furthermore, larger increases in roof reflectance correspond to larger reductions in cooling energy use but also to higher increases in heating thermal loads [27].

A summary of the reported energy use savings results associated with the application of SCRs to residential and office buildings is provided in Table 2-3.

In summary, the reported literature demonstrates that several factors including building location, building construction, building type, and roof solar reflectance impact the potential energy use savings and peak demand reductions that SCRs can achieve. In warmer climates with abundant sunshine, cooling energy use and cost savings greatly outweigh heating energy use and cost penalties. In colder climates, or climates with equal heating and cooling seasons, SCRs may cause significant heating need increases. Thus, the best climates for cool roofs would have a long cooling season and a short heating season. In addition to outdoor temperature variations, global horizontal solar irradiance that the building can experience also affect cooling energy savings and heating thermal penalties. Building construction also can impact significantly the benefits and the penalties of SCRs. Older vintage buildings with low insulation levels would have higher cooling energy use savings and higher heating thermal penalties. Solar roof reflectance has a direct effect on the performance of SCRs. When roof solar reflectance is doubled, cooling energy use savings and heating thermal penalty would roughly double. Finally, building type and occupant levels can impact the potential savings from SCRs. Residential buildings

**Table 2-3** Summary of simulation results for the performance of SCRs applied to residential and office buildings.

Study	Wall R	Roof R	$\Delta\rho$	Annual savings kWh/m <sup>2</sup> (%)	Annual penalty therm/m <sup>2</sup> (%)
[23]	R-7	R-11	0.30	1.1–5.2 (7–17)	0–0.17 (2–5)
	R-11	R-19	0.30	0.4–2.8 (6–15)	0–0.13 (0–5)
	R-7	R-11	0.45	1.8–6.0 (5–9)	0–0.19 (0–14)
	R-11	R-19	0.45	1.1–3.3 (3–7)	0–0.11 (0–12)
[25]	R-5	R-11	0.30	0.5–8.6 (4–11)	0–0.22 (0–2)
	R-13	R-30	0.30	0.1–3.6 (1–8)	0–0.07 (0–2)
	R-6	R-11	0.40	4.8–8.2 (4–8)	0–0.13 (0–3)
	R-13	R-30	0.40	1.2–2.8 (2–4)	0–0.05 (0–6)
[26]	R-6	R-7	0.35	0.5–11.5 (n/a)	0–0.24 (n/a)
	R-13	R-19	0.35	0.1–4.1 (n/a)	0–0.10 (n/a)
[27]	R-3	R-7	0.40	8–29 (11–35)*	n/a
	R-3	R-7	0.65	9–48 (18–54)*	0–0.58 (n/a)*

tend to exhibit more relative cooling energy use savings and heating thermal penalty than commercial buildings. Commercial buildings, however, provide more relative cooling energy use savings when compared to heating thermal penalties. Moreover, buildings with longer operation schedules provide larger savings per roof area than those with shorter schedules.

## 2.4 Current Cool Roof Energy Standards

Over the last two decades, several national and state energy standards have added cool roof requirements or credits for specific climate zones. Some standards require the use of cool roofs by prescribing a specific roof reflectance and emittance to save energy consumption, reduce peak power demand, and improve air quality. Cool roof credits in standards do not require the use of cool roofs, but promote their use by allowing more flexibility in the design approach and permitting the use of less energy-efficient systems for buildings that integrate cool roofs. Such credits for cool roofs can be energy neutral, but may still reduce peak

power demand and improve air quality. They may also reduce the initial cost of buildings [29].

Current energy standards which incorporate cool roofs within the US include ASHRAE 90.1, ASHRAE 90.2, and California Title 24. In particular, ASHRAE 90.1-2013 prescribes the use of cool materials for low-sloped roofs on non-residential buildings in climate zones 1, 2, and 3. The cool roofs must have a minimum 3-year aged reflectance of 0.55 and a thermal emittance of at least 0.75, or a minimum aged SRI of 64 [30]. If cool roofs are not specified, then roof insulation levels must be increased to a value set by ASHRAE. ASHRAE 90.2 2007 uses a credit method which allows the reduction of the roof insulation level for residential buildings if cool roofs are prescribed in climate zones 1, 2, or 3. The standard 90.2 requires cool roofs to have a minimum initial solar reflectance of 0.65 and a minimum thermal emittance of 0.75, or have a minimum SRI of 75 [31].

California Title 24-2013 also prescribes the use of cool roofs within the state of California for both low and steep-sloped roofs for non-residential buildings in all California climate zones. A minimum aged reflectance of 0.63 and thermal emittance of 0.75 or an aged SRI of 75 is required for low-sloped roofs, and a minimum aged reflectance of 0.20 and thermal emittance of 0.75 of an aged SRI of 16 is required for steep-sloped roofs. In addition, Title 24 prescribes cool roofs for high-rise residential buildings with low-sloped roofs in climate zones 9–15, and for high-rise residential buildings with steep-sloped roofs in California climate zones 2–15. A minimum aged reflectance of 0.55 and thermal emittance of 0.75 or a minimum aged SRI of 64 is required for low-sloped roofs, and a minimum aged reflectance of 0.20 and thermal emittance of 0.75 of an aged SRI of 16 is required for steep-sloped roofs [32]. The roof U-factor is then prescribed according to aged solar reflectance.

In addition to energy standards, there are also voluntary energy credit programs which have adopted cool roof credits. US EPA Energy Star rewards points for the use of cool roofs. It requires that low-sloped roofs have an initial and aged reflectance of at least 0.65 and 0.50, respectively, and that steep-sloped roofs have an initial and aged reflectance of at least 0.25 and 0.15, respectively [29]. LEED also rewards 2 points for the use of cool roofs that has an initial and aged SRI of 82 and 64, respectively, for low-sloped roofs, and an initial and aged SRI of 39 and 32, respectively, for steep-sloped roofs [33].

## 2.5 Other Benefits and Challenges

### 2.5.1 Reduction of Heat Island Effect and Global Warming

An additional benefit to cool roofs is their potential to reduce heat island effect and global warming in urban cities. By increasing the solar reflectance of surfaces (including roofs and pavements) in urban centers, the outflow of short-wave solar radiation increases, less solar heat energy is then absorbed leading to lower surface temperatures and reduced outflow of thermal radiation into the atmosphere. This process of “negative radiative forcing” effectively counters global warming [34]. Akbari et al. [34] estimated that increasing the albedo of urban roofs and pavement surfaces worldwide would induce a negative radiative forcing equivalent to offsetting at least 40–160 Gt of emitted CO<sub>2</sub>.

### 2.5.2 Snow Accumulation and Ice Buildup

Based on the previously reviewed simulation analyses, it is evident SCRs can lead to large heating thermal penalties in colder climates. One factor that may reduce the penalties of SCRs compared to the estimates from reported studies is the accumulation of snow on roofs during winter seasons. Indeed, Hosseini and Akbari [35, 36] have demonstrated through whole-building simulation analyses that modeling snow accumulation on SCRs during the winter periods can lower the heating penalty to acceptable levels. Snow accumulation provides an additional layer of insulation and increases the solar reflectance of the roof regardless of their actual properties. Specifically, the study showed that the annual heating energy use penalty from implementing a SCR on an office building in Anchorage, AK is 3 GJ/100-m<sup>2</sup> when neglecting snow accumulation and is only 1 GJ/100-m<sup>2</sup> when considering the snow. Similarly, it was found that the heating energy penalty from implementing a SCR on a retail building in Anchorage, AK without considering snow is 2.3 GJ/100-m<sup>2</sup> and considering snow it drops to 1.3 GJ/100-m<sup>2</sup>. The same study shows that heating penalties in cold locations with a significant snow accumulation are most likely lower in reality compared to reported results obtained through simulation analyses that do not account for snow effects [35, 36]. It should be noted, however, that while normal snow accumulation may lead to lower heating penalties, SCRs may also increase snow collection and ice buildup. Indeed, lower surface temperatures of reflective roofs slow the melting process of snow and ice, and make cool roofs more susceptible to deeper snow, ice, and icicle formations [37, 38].

### **2.5.3 Roof Condensation**

Another potential negative impact of lower surface temperatures from SCRs is the susceptibility to condensation within the roof assembly. In cold climates with short summers, lower surface temperatures of SCRs may lead to accumulation of moisture in the roofing assembly by reducing the drying potential and increasing risk of interstitial condensation [39]. Ahrab et al. [39] analyzed the risk of accumulation and mold growth for various roof assemblies and locations within the US. The study found that moisture performance of standard and SCRs for office buildings was similar in hot climates, and moisture accumulation problems were never experienced during the 5-year analysis period. However, the analysis found that residential buildings with white roofs and conventional vapor retarders experienced risk of moisture accumulation and mold growth in very cold cities such as Anchorage, AK, US; Edmonton, AB, Canada; and St. John's, NL, Canada. The study also found that using smart vapor retarders or self-drying roofs helped to decrease the risk of moisture accumulation. Additionally, adding ventilated air spaces and using smart vapor retarders were found to have eliminated the condensation risks [39].

### **2.5.4 Aesthetics and Light Pollution**

One major drawback to SCRs reported from the perspective of building owners is aesthetics. White roofs are not as aesthetically pleasing as those with a more neutral or darker color. For this reason, cool roof applications have typically been limited to flat or low-sloped roofs since the color of the roof cannot be seen from the ground level. Additionally, SCRs do not only reflect solar radiation during daytime, but also visible light from artificial illumination during nighttime causing undesired light pollution as well as stray and obtrusive lights [37].

## **2.6 Advances in Switchable Roof Coatings**

It is clear from the reported literature that while SCRs have several benefits, they have some limitations and disadvantages. The largest disadvantage being higher potential heating energy use which may reduce the cost-effectiveness of SCRs to building owners and to utilities. Indeed, buildings with SCRs experience energy penalties as they transition from cooling to heating modes due to the increase in reflected solar energy that is no longer transferred into heat gains at the roof surfaces

[40]. An ideal alternative of SCRs would be roofing systems that can be highly reflective when buildings are in a cooling mode and highly absorptive when buildings transition to a heating mode [40]. In other terms, switchable cool roofs with coatings that have the ability to change reflectance throughout the year. These types of cool roofs are referred to as dynamic cool roofs or DCRs throughout this chapter.

For building applications, two types of switchable materials have been used for windows: thermochromic (TC) coatings, and electrochromic (EC) coatings. Both materials contain a specific category of polymers known as chromogenic polymers which react to external stimuli by changing their visible optical properties [41–46]. TC coatings contain a chromogenic polymer which reacts to temperature while EC glass contains a chromogenic polymer which reacts to an electric field [40]. Both switchable coating types have advantages and disadvantages. The major difference is that EC coatings can be manually controlled or potentially linked to a thermostat, while TC coatings are only controlled based on the temperature of the material itself from a low reflectance value at low temperatures to a high reflectance value at high temperatures [47–48]. TC coatings are currently less expensive and require less maintenance than EC coatings [48–49]. Currently, very limited literature exists on applying switchable coatings to building roofs. There has been no reported research to date on the application of EC coatings or any other manually controlled switchable roofing systems, but Azari et al. [50] discussed the potential for applying these coatings to be used for roofs and be linked to a thermostat without any specific analysis and quantification of the benefits of such controls. Recently, Gray [40] has applied TC coatings to cool roofs so that their color changes from black to clear in order to reveal the actual light color of the roofs. It was found that the low temperature reflectance potential by applying a TC coating to a cool roof is 0.3 and the high temperature reflectance potential is about 0.55. The difference between the low and high temperatures when the coating changes its optical properties was found to be 11°C. The emissivity of the switchable system was found to be about 0.95. However, Gray [40] found that there were several challenges encountered with the application of the TC coatings as switchable materials including adhesion to non-metallic surfaces, non-uniformity, and the need for higher and lower transparency temperatures to further increase cool roofs potential of heating and cooling energy savings. Furthermore,

the applied TC coating needed a long and unpractical time period to completely shift from the low reflectance to the high reflectance values requiring an 11°C temperature difference to occur [40]. Ideally, a more instantaneous shift in reflectance would be needed for energy use savings of DCRs to materialize [40]. A recent simulation based analysis evaluated the impacts of ideal switchable reflectance coatings on the potential energy use savings associated with DCRs for office buildings located in 4 US climates [51]. The benefits of DCRs compared to conventional SCRs with constant optical properties have been quantified using ideal coatings that can instantaneously switch reflectance between a low value of 0.30 to high value of 0.55 low [51–52].

As alternative to switchable reflectance roofs, Hooshangi [53] explores the performance of heterogenous directional reflective materials (DRMs) with corrugated tilted surfaces with reflective sides facing towards the sky and absorptive sides facing towards the ground. The tilt angle of the corrugation surfaces can be set depending on sun location in the summer and winter. The reflective sides reflect sunlight during the summer season when the sun is high in the sky and the absorptive sides absorb sunlight during the winter season when the sun is low in the sky [53]. Recently, Akbari and Touchaei [54] have developed a model to calculate the hourly reflectance of DRMs as a function of zenith and azimuth angles of the sun's position [28]. No analysis has been reported to compare potential energy use savings from DRM roofs compared to static cool roofs.

The main challenge for the application of DCRs is identifying the best control strategies to optimize their reflectance settings. Indeed, heat transfer through building roofs is quite complex with several different mechanisms contributing to the transient heat transfer including solar radiation at the interior and exterior, net longwave radiation at the exterior and interior, surface convection at the interior and exterior, and heat conduction within the roof assembly [40, 46]. Therefore, it is difficult to draw a direct relationship between roof reflectance and a control setting. Any change in roof reflectance can, of course, affect solar heat gains from the roof. However, building thermal loads are not only dependent on solar heat gains. In a very cold but sunny climate, a building may still require heating even if solar heat gains are high; thus, a lower reflectance roof would be desirable to increase heat gains. The opposite may be true in a warm climate that temporarily experiences low

solar heat gains; a high reflectance roof would still be desirable to reduce further any solar heat gains a building may experience from the roof. The building insulation level and thermal mass can also have important effects on the magnitude of the heat gains transferred from the roof to the conditioned building. There is currently very little research on optimizing control strategies for DCRs. An ideal control system would lead to a DCR that consumes the same amount of cooling energy as a SCR and the same amount of heating energy as a standard roof without a highly reflective coating. Some evaluation of potential controls strategies for switchable roofing systems have been reported using simulation analyses [40, 46–47]. It was found that several parameters should be accounted to determine the best strategies to change the reflectance levels of roofs including climate, building type, occupancy schedule, insulation level, and thermal mass [40].

## 2.7 Evaluation of Dynamic Cool Roofs Performance

As noted earlier, limited reported studies have been carried out to determine the benefits of DCRs compared to SCRs [40, 51–52]. In particular, Gray has used a whole-building simulation to estimate energy consumption from select US southeastern prototypical commercial buildings having SCRs and TC coated roofs. The reflectance of the TC coated roofs was changed based on a transition start temperature obtained from an experimental testing [40]. In particular, a low temperature reflectance of 0.30 and a high temperature reflectance of 0.55 were used in the analysis. The reflectance values considered for the SCRs were between 0.73 and 0.76 depending on the roof material [40]. The results from this analysis shows that there is less than 1% savings from TC coated roofs when compared to SCRs. Furthermore, in some cases, there is actually an overall increase in energy use [40]. Few reasons can be advanced to explain the poor performance of TC coatings including first the selected US southeastern region has a relatively hot climate with less potential for heating energy use savings. The second is the baseline SCR reflectance value used to compare the TC coatings. In almost all analyses of SCRs reported in the literature, the average reflectance value used for cool roofs is 0.55. If a more realistic cool roof reflectance value of 0.55 was used in the analysis, it is expected that the cooling energy use increases noted from the TC coated roofs would be significantly lower. Finally, the temperature based control strategy may

not be the optimal strategy for DCRs especially when the reflectance value shifts slowly with temperature and not instantaneously.

Moreover, two other recent studies have evaluated the benefits of ideal DCRs compared to SCRs [51–52]. Selected Results from these studies are briefly outlined in the following sections.

### 2.7.1 *Impact of Building Insulation level*

The performance of DCRs was found to be highly depending on the overall building insulation level [51–52]. The ranges of source energy savings reported for prototypical residential and commercial buildings for three insulation levels are summarized in Table 2-4.

The results of Table 2-4 show that the amount of insulation of the building is an important factor that affects the energy savings resulting from DCRs when compared to SCRs. In particular, it is found that annual energy use is lower for DCRs, regardless of the insulation level. However, when the R-value is large (the building is well insulated), heat transfer between the surface of the roof and the interior of the building is small and the impact on the energy use of using DCRs is not as significant compared to the case for buildings with low insulation levels [52].

### 2.7.2 *Impact of Building Mass*

The impact building mass level on the performance of DCRs was also evaluated with switchable roof reflectance of 0.30/0.55 and SCRs with a set reflectance value of 0.55 [52]. The ranges of source energy savings found for various building types and mass levels are summarized in Table 2-5.

Interestingly, Table 2-5 indicates that energy savings associated with DCRs relative to SCRs do not steadily increase with the thermal mass

**Table 2-4** Ranges of source annual energy savings from DCRs compared to SCRs for three roof insulation levels.

Insulation level (R-wall/R-roof)	Building prototype			
	Residential building		Office building	
m <sup>2</sup> .K/W	MJ/m <sup>2</sup>	%	MJ/m <sup>2</sup>	%
Low (0.9/1.85)	4.3–19.4	1.6–4.9	1.2–18.0	0.3–3.9
Medium (2.12/3.46)	2.3–10.2	1.3–4.1	0.4–9.4	0.1–2.6
High (3.42/4.85)	1.5–7.3	0.9–3.5	0.2–6.5	0.1–1.9

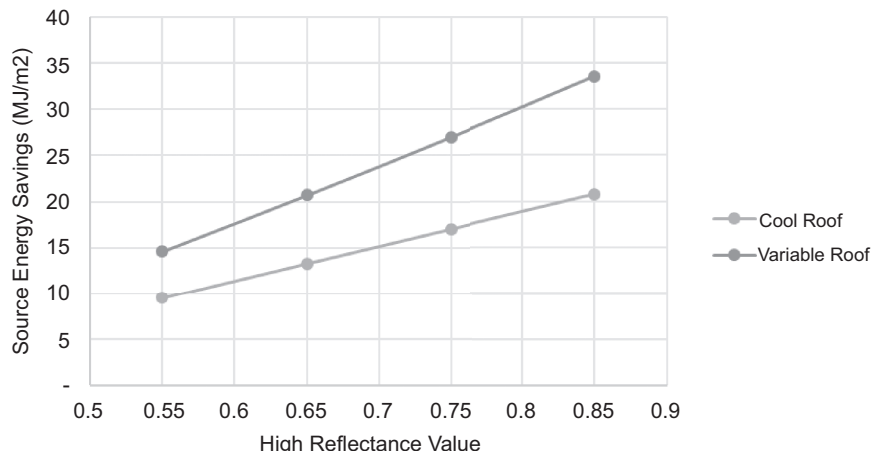
**Table 2-5** Ranges of source energy savings from DCRs compared to SCRS for of three roof mass levels.

Mass level (Wall/roof mass) kg/m <sup>2</sup>	Building prototype			
	Residential building		Office building	
	MJ/m <sup>2</sup>	%	MJ/m <sup>2</sup>	%
Light	1.5–16.9	0.9–3.9	0.2–15.6	0.1–3.2
Medium	1.7–19.4	1.1–4.9	0.3–18.0	0.1–3.9
Heavy	1.7–18.3	1.1–4.8	0.3–17.4	0.1–3.8

level. Rather the energy savings increase to a maximum level as mass increases, then start to decrease after a threshold roof mass level [52].

### 2.7.3 Impact of roof reflectance

The impact of roof reflectance settings has been evaluated on the performance of DCRs [51–52]. Indeed, this parameter is particularly of interest should the technology improves and allows large reflectance differential with lower low reflectance or higher high reflectance. Figures 2-1 and 2-2 summarize the analysis results obtained for an office located in Atlanta and Chicago, respectively [52]. Specifically, Figures 2-1 and 2-2 show source energy savings obtained from a static cool roof when compared to a standard roof and those obtained from a switchable

**Figure 2-1** Effect of high reflectance setting on annual energy use savings obtained from DCRs and SCRs compared to standard roofs with a low reflectance value in Atlanta, GA.

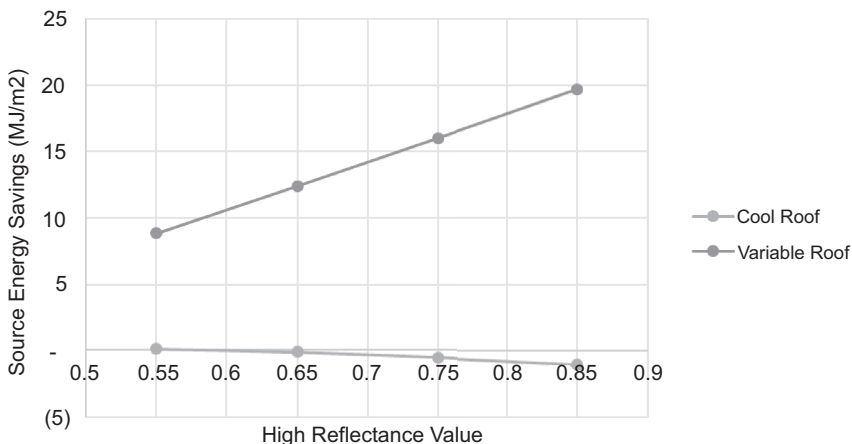


**Figure 2-2** Effect of high reflectance setting on annual energy use savings obtained from DCRs and SCRs compared to standard roofs with a low reflectance value in Chicago, IL.

reflectance roof when compared to a standard roof. The results provided in Figures 2-1 and 2-2 are specific for a light mass residential building with medium insulation, but the trend is the same for all other building configurations and climates. The results show that there is a linear relationship between savings and the difference in roof high-low reflectance values. They also demonstrate that as the high reflectance increases, the annual energy use savings from DCRs increases at a faster rate than those obtained from SCRs. This result is due to the fact that as the reflectance value for SCRs increases, both the cooling savings and the heating penalties increase. Whereas for DCRs with switchable reflectance values, only the cooling savings increase while the heating penalties remain minimal. This behavior is more pronounced for warmer climates when comparing the results obtained Atlanta (i.e., Figure 2-1) with those obtained for Chicago (i.e., Figure 2-2).

#### 2.7.4 Impact of Climate

As part of a comprehensive analysis, the DCR performance has been evaluated for both residential and commercial buildings located in various US climates [52]. Table 2-6 summarizes the results of the analysis using the heating degree-days (HDDs) for a base temperature of 18°C. Specifically, Table 2-6 lists the ranges of annual source energy savings obtained for DCRs with a switchable low/high reflectance

**Table 2-6** Ranges of annual source energy savings from DCRs relative to SCRs for both residential and commercial buildings in various US locations.

Location	HDD	Building prototype			
		Residential building		Office building	
		MJ/m <sup>2</sup>	%	MJ/m <sup>2</sup>	%
New Orleans	787	1.5–5.5	0.9–2.2	0.2–2.0	0.1–0.6
Las Vegas	1264	3.5–12.6	1.6–3.4	1.2–6.8	0.4–2.3
Atlanta	1571	3.5–11.4	2.0–3.8	1.9–7.1	0.8–2.3
Portland	2426	4.5–13.8	3.1–4.9	2.7–9.4	1.7–3.9
Baltimore	2574	5.2–16.4	2.4–4.1	3.9–12.8	1.5–3.4
Chicago	3607	6.2–17.6	2.1–3.3	4.7–14.9	1.4–3.0
St. Paul	4379	6.9–19.4	1.2–3.0	6.1–18.0	15–2.9

of 0.30/0.55 compared to SCRs with a set reflectance of 0.55 for various US locations considered in the analysis. Since the additional energy savings achieved by a switchable roof come from a decrease in heating energy use, the HDDs were used to represent the climatic characteristics for all US locations.

It is clear from Table 2-6 that there is a strong relationship between HDDs and annual source energy savings incurred from DCRs relative to SCRs. Figures 2-3 and 2-4 illustrates the variation of annual source energy savings as a function of HDD for respectively, a light weight residential and an office building with three insulation levels. A similar trend was found for all building configurations. In particular, the results of Table 2-6 and Figures 2-3 and 2-4 show that the annual energy use savings associated with the application of DCRs instead of SCRs increase as HDD increases. Therefore, implementing DCRs would be more beneficial in cold climates.

## 2.8 Economic Analysis of Dynamic Cool Roofs

The cost-effectiveness of DCRs using break-even cost analysis has been investigated for both residential and commercial buildings in various US sites [51–52]. While the life span of variable reflective roofing systems is uncertain from the literature, the average traditional commercial roof

## 64 TECHNOLOGIES FOR SUSTAINABLE LIFE

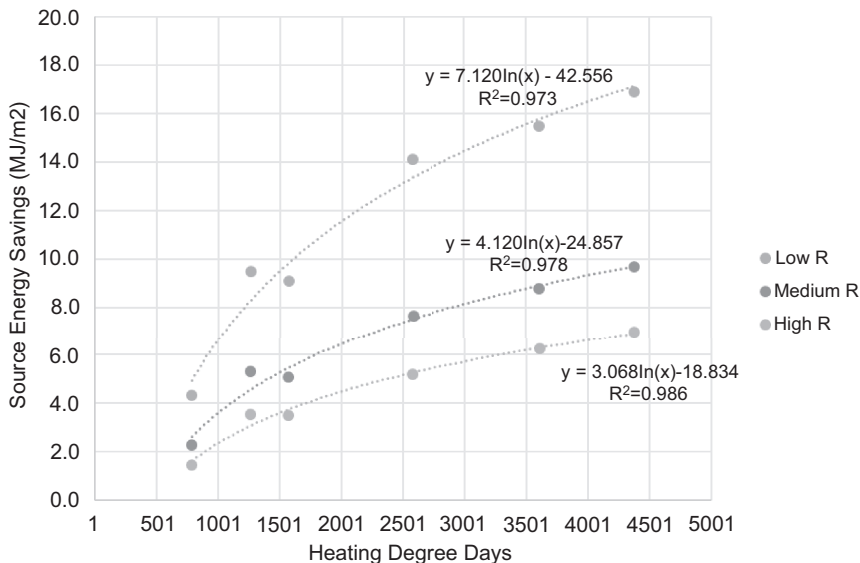


**Figure 2-3** Effect of heating degree days on annual source energy savings obtained from DCRs relative to SCRs for light mass residential buildings.

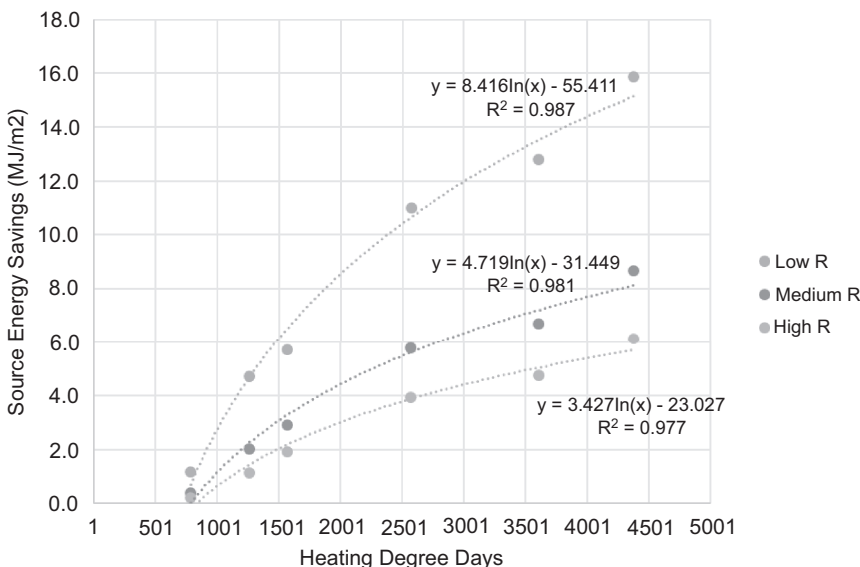


**Figure 2-4** Effect of heating degree days on annual source energy savings obtained from DCRs relative to SCRs for light mass office buildings.

life span is approximately 22 years according to Coffelt and Hendrickson [31]. The economic analysis is based on life cycle cost method using estimated DCR annual energy savings combined with electricity and natural gas rates reported by EIA for all US locations [32, 33].

Table 2-7 shows the break-even costs for DCRs relative to standard roofs (i.e., with a low reflectance value of 0.30) and Table 2-8 shows the break-even costs required when switching from SCRs to DCRs for both residential and commercial buildings.

It is clear from Tables 2-7 and 2-8 that when compared to standard roofs, office buildings with DCRs save more energy cost per m<sup>2</sup> than residential buildings. The opposite, however, is true when comparing the cost savings from SCRs to those obtained from DCRs. This result is most likely associated to the fact that an office building has higher cooling loads due to high internal loads. Therefore, when compared to a residential building, more savings are obtained when the cooling load decreases and less savings are obtained when the heating load decreases.

Another, more obvious general trend is that the highest break-even costs and cost savings are achieved for low insulated building configurations. In particular, the results show that the break-even cost for DCRs for low insulated buildings is more than 1.5 times greater than for high insulated buildings. Therefore, older buildings would be a better target for the application of DCRs.

As noted in the literature review, while some thermochromic (TC) coatings have been developed and tested, their cost is still high [25]. However, the use of DRM roofing system or a mechanically controlled system which only switches reflectance seasonally could be economically feasible based on the benchmark costs listed in Tables 2-7 and 2-8.

## 2.9 Summary and Conclusions

It is clear from the reviewed literature that static cool roofs or SCRs provide cooling energy use savings during hot seasons, but may also cause significant heating penalties during cold seasons. For this reason, SCRs are most beneficial in climates with a long cooling season and a short heating season. Due to higher prices of electricity compared to those of gas, SCRs in several US climates can provide an overall cost savings. As outlined in this Chapter, the specific levels of savings and penalties would be effected by several factors including the roof insulation level, building type, and cool roof reflectance value. Typical

**Table 2-7** Initial cost (\$/m<sup>2</sup>) required to break even if switching from a standard roof with a reflectance of 0.30 to a switchable cool roof with a reflectance of 0.3/0.55.

Location	Residential			Office		
	Low R	Medium R	High R	Low R	Medium R	High R
<b>New Orleans, 2A</b>						
Light mass	2.96	1.76	1.28	2.83	1.65	1.19
Medium mass	3.27	1.82	1.33	3.00	1.66	1.23
Heavy mass	3.08	1.77	1.30	2.78	1.60	1.21
<b>Las Vegas, 2B</b>						
Light mass	4.46	2.60	1.88	4.67	2.76	1.99
Medium mass	4.84	2.67	1.94	4.92	2.80	2.04
Heavy mass	4.59	2.60	1.90	4.57	2.69	1.99
<b>Atlanta, 3A</b>						
Light mass	2.94	1.76	1.27	2.89	1.78	1.30
Medium mass	3.28	1.83	1.33	3.11	1.80	1.34
Heavy mass	3.10	1.77	1.30	2.91	1.73	1.32
<b>Portland, 3C</b>						
Light mass	1.47	0.94	0.72	1.82	1.19	0.89
Medium mass	1.64	0.99	0.75	1.84	1.19	0.91
Heavy mass	1.53	0.96	0.73	1.71	1.14	0.89
<b>Baltimore, 4A</b>						
Light mass	3.06	1.78	1.28	3.17	1.92	1.40
Medium mass	3.33	1.81	1.31	3.31	1.95	1.45
Heavy mass	3.13	1.76	1.28	3.07	1.88	1.43
<b>Chicago, 5A</b>						
Light mass	2.02	1.20	0.88	2.08	1.25	0.91
Medium mass	2.16	1.24	0.92	2.16	1.25	0.93
Heavy mass	2.04	1.20	0.90	1.99	1.20	0.91
<b>St. Paul, 6A</b>						
Light mass	1.81	1.12	0.84	1.98	1.19	0.86
Medium mass	1.98	1.11	0.82	2.07	1.21	0.89
Heavy mass	1.87	1.08	0.80	1.93	1.16	0.87

**Table 2-8** Initial cost (\$/m<sup>2</sup>) required to break even if switching from SCRs with a reflectance of 0.55 to DCRs with a low/high reflectance of 0.3/0.55

Location	Residential			Office		
	Low R	Medium R	High R	Low R	Medium R	High R
<b>New Orleans, 2A</b>						
Light mass	0.54	0.29	0.18	0.17	0.06	0.03
Medium mass	0.68	0.31	0.21	0.28	0.08	0.04
Heavy mass	0.67	0.32	0.21	0.28	0.07	0.04
<b>Las Vegas, 2B</b>						
Light mass	1.36	0.76	0.51	0.68	0.30	0.17
Medium mass	1.79	0.87	0.57	0.97	0.38	0.22
Heavy mass	1.79	0.88	0.58	0.96	0.39	0.22
<b>Atlanta, 3A</b>						
Light mass	1.74	0.97	0.67	1.08	0.56	0.37
Medium mass	2.13	1.07	0.73	1.37	0.61	0.41
Heavy mass	2.08	1.06	0.73	1.33	0.59	0.40
<b>Portland, 3C</b>						
Light mass	1.68	0.92	0.64	1.15	0.58	0.39
Medium mass	1.96	1.00	0.69	1.35	0.64	0.43
Heavy mass	1.91	1.00	0.69	1.29	0.63	0.43
<b>Baltimore, 4A</b>						
Light mass	2.00	1.08	0.74	1.58	0.83	0.56
Medium mass	2.35	1.16	0.80	1.84	0.92	0.63
Heavy mass	2.28	1.15	0.80	1.76	0.90	0.63
<b>Chicago, 5A</b>						
Light mass	1.44	0.82	0.58	1.14	0.60	0.43
Medium mass	1.64	0.87	0.61	1.35	0.65	0.46
Heavy mass	1.59	0.86	0.61	1.31	0.64	0.45
<b>St. Paul, 6A</b>						
Light mass	1.73	1.02	0.73	1.66	0.90	0.64
Medium mass	2.02	1.06	0.75	1.89	0.98	0.68
Heavy mass	1.97	1.06	0.75	1.84	0.96	0.67

reflectance values for standard commercial roofing materials range from 0.05 to 0.36, while typical aged reflectance values of cool roofing materials ranges from 0.55 to 0.65. The thermal emittance for most reported cool roofing materials is typically 0.90. Typical annual electricity savings seen from static cool roofs with reflectance values of 0.3–0.4 for US climates range from 0.1 to 8.6 kWh/m<sup>2</sup> for residential buildings, 1.1 to 8.2 kWh/m<sup>2</sup> for office buildings, and 1.4 to 10.9 kWh/m<sup>2</sup> for retail buildings. Typical reported annual fuel use increases due to application of SCRs range from 0 to 0.22 therm/m<sup>2</sup> for residential buildings, 0 to 0.19 therm/m<sup>2</sup> for commercial buildings, and 0 to 10 therm/m<sup>2</sup> for retail buildings. Additionally, overall annual energy cost savings from SCRs ranges from \$0.16/m<sup>2</sup> to \$0.36/m<sup>2</sup>.

Though SCRs in several climates have been shown to provide overall source energy use savings, there is a potential to provide even more cost and energy use savings by applying switchable reflectance coatings to roof surfaces to achieve what is referred to as dynamic cool roofs or DCRs. A switchable reflectance coating would especially be useful in climates with heating and cooling seasons having a similar length, or in heating dominated climates with a large swing in temperatures between heating and cooling seasons. Though there are currently switchable technologies used for windows (electrochromic and thermochromic coatings), there has been limited reported research on switchable roof coatings. The reviewed available literature indicates that a possible technology would be to apply switchable thermochromic coatings over cool roofs so their overall reflectance changes from 0.3 to 0.55. The major challenge identified for switchable roofing systems is determining their best reflectance settings in order to optimize their performance. Currently, the only applicable switchable technologies have two different control types: manual controlled (electrochromic coating) and temperature controlled (thermochromic coating).

Based on the limited reported analysis results for the performance of DCRs, it is found that seasonal switchable reflectance roofs can avoid heating energy use penalties and achieve additional source energy savings and cost savings when compared to SCRs for both residential and commercial buildings. In particular, the analysis has indicated that DCRs can provide the following annual benefits:

- *Residential Buildings:* For low insulation buildings, the source energy savings range from 4.33 to 19.44 MJ/m<sup>2</sup> (1.6 to 4.9%) and the cost savings range from 0.04 to 0.18 \$/m<sup>2</sup> (1.9 to 5.0%); for medium insulation buildings, the source energy savings range from 2.30 to 10.22 MJ/m<sup>2</sup> (1.3 to 4.0%) and the cost savings range from 0.02 to 0.09 \$/m<sup>2</sup> (1.5 to 4.2%); and for high insulation residential buildings, the source energy savings range from 1.46 to 7.25 MJ/m<sup>2</sup> (0.9 to 3.5%) and the cost savings range from 0.01 to 0.06 \$/m<sup>2</sup> (1.1 to 3.6%).
- *Commercial Buildings:* For low insulation office buildings, the source energy savings range from 1.17 to 18.00 MJ/m<sup>2</sup> (0.3 to 3.9%) and the cost savings range from 0.01 to 0.14 \$/m<sup>2</sup> (0.5 to 4.3%); for medium insulation office buildings, the source energy savings range from 0.42 to 9.35 MJ/m<sup>2</sup> (0.14 to 2.6%) and the cost savings range from 0.0 to 0.07 \$/m<sup>2</sup> (0.2 to 2.8%); and for high insulation office buildings, the source energy savings range from 0.21 to 6.49 MJ/m<sup>2</sup> (0.1 to 1.9%) and the cost savings range from 0.0 to 0.05 \$/m<sup>2</sup> (0.1 to 2.1%).

Moreover, the reported analysis results have indicated that energy savings of DCRs depend largely on the climate, insulation level, and reflectance of the roof. The results also show that energy savings generally increase as thermal insulation level decreases for all building types. Making older buildings with low insulation levels a good target to retrofit with DCRs rather than well insulated new constructions. In addition, the results of a life cycle cost analysis show that for residential buildings the break-even cost using a 22-year life span ranges depending on the climate from 0.80 to 4.84 \$/m<sup>2</sup> for switching to DCRs from standard roofs, and from 0.18 to 2.35 \$/m<sup>2</sup> for switching to DCRs from SCRs. For commercial buildings, the break-even cost for a 22-year life span ranges from 0.86 to 4.92 \$/m<sup>2</sup> for switching to DCRs from standard roofs, and from 0.03 to 1.89 \$/m<sup>2</sup> for switching to DCRs from SCRs.

While more research is needed to improve the performance and lower the cost of switchable reflectance materials like TC coatings, the limited reported analyses indicate that seasonally controlled DCRs such as a mechanically controlled roofs or DRM roofing systems have the potential

to improve the energy efficiency of both residential and commercial buildings and should be further explored and investigated. Moreover, additional savings could be obtained from variable thermal emittance coatings. Indeed, a lower thermal emittance provides additional heating savings since it slows the release of long-wave radiation. The lower the thermal emittance, the slower the roof would cool. This technology could be particularly beneficial in providing additional heating savings during the heating period or even at night during swing months.

## References

- [1] EIA, 2016, United States Energy Information Administration. Energy consumption estimates by sector. <http://www.eia.gov/consumption>. Accessed April 15, 2016.
- [2] D&R International, Ltd. 2012, 2011 *Buildings Energy Data Book*. Washington, D.C.: United States Department of Energy, Washington DC.
- [3] Konopacki, S., Akbari, H., Pomerantz, M., Gabersek, S., and Gartland, L. 1997. Cooling Energy Savings Potential of Light-Colored Roofs for Residential and Commercial Buildings in 11 U.S. Metropolitan Areas. Lawrence Berkeley National Laboratory, Berkeley, CA.
- [4] Levinson, R., and Akbari, H. Potential benefits of cool roofs on commercial buildings: conserving energy, saving money, and reducing emission of greenhouse gases and air pollutants. *Energy Efficiency* 2010; 3:53–109.
- [5] Levinson, R., Akbari, H., and Gartland, L. M. 1996. Impact of the temperature dependency of fiberglass insulation R-value on cooling energy use in buildings. In Proceedings of the 1996 ACEEE Summer Study on Energy Efficiency in Buildings. Pacific Grove, CA: American Council for an Energy-Efficient Economy, 10, 85–94.
- [6] Berdahl, P., and Bretz, S. Preliminary survey of the solar reflectance of cool roofing materials. *Energy and Buildings* 1997; 25:149–158.
- [7] ASHRAE, ANSI/ASHRAE. *Advanced Energy Design Guide for Small to Medium Office Buildings*. 2011, American Society of Heating, Refrigerating, and Air-Conditioning Engineers, Inc. Atlanta, GA.
- [8] Gartland, L. M., Konopacki, S. J., and Akbari, H. 1996. Modeling the effects of reflective roofing. In Proceedings of the 1996

- ACEEE Summer Study on Energy Efficiency in Buildings. Pacific Grove, CA: American Council for an Energy-Efficient Economy, 4, 117–124.
- [9] Akbari, H. Cool roofs save energy. *ASHRAE Transactions* 1998; 104(1B): 783–788.
  - [10] Akbari, H., and Levinson, R., Evolution of cool-roof standards in the US. *Advances in Building Energy Research* 2008; 2: 1–32.
  - [11] Bretz, S., and Akbari, H. Long-term performance of high-albedo roof coatings. *Energy and Buildings* 1997; 25: 159–167.
  - [12] Berdahl, P., Akbari, H., and Rose, L. *Applied Optics* 2002; 41, 2: 2335–2358.
  - [13] Akbari, H., Berhe, A., Levinson, R., Graveline, S., Foley, K., Delgado, A., and Paroli, R. Aging and weathering of cool roofing membranes. Lawrence Berkeley National Laboratory 2005.
  - [14] Parker, D., Huang, J., Konopacki, S., Gartland, L., Sherwin, J., and Gu, L. Measured and simulated performance of reflective roofing systems in residential buildings. *ASHRAE Transactions* 1998; 104: 963–975.
  - [15] Akbari, H., Bretz, S., Kurn, D., and Haniford, J. Peak power and cooling energy savings of high-albedo roofs. *Energy Building* 1997; 25: 117–126.
  - [16] Hildebrandt, E., Bos, W., and Moore, R. Assessing the impacts of white roofs on building energy loads. *ASHRAE Technical Data Bulletin* 1998; 14.
  - [17] Parker, D., Sonne, J., and Sherwin, J. Demonstration of cooling savings of light colored roof surfacing in Florida commercial buildings: Retail strip mall. Florida Solar Energy Center, Cocoa, FL, 1997. Report FSEC-CR-964-97.
  - [18] Konopacki, S., Akbari, H., Gartland, L., and Rainer, L. 1998. Demonstration of energy savings of cool roofs. Lawrence Berkeley National Laboratory, Report number LBNL-40673, Berkeley, CA.
  - [19] Konopacki, S., and Akbari, H. 2001. Measured energy savings and demand reduction from a reflective roof membrane on a large retail store in Austin. Lawrence Berkeley National Laboratory, Report number LBNL-47149, Berkeley, CA.
  - [20] Akbari, H. Measured energy savings from the application of reflective roofs in 2 small non-residential buildings. *Energy*, 2003; 28: 953–967.

- [21] Akbari, H., Levinson, R., and Rainer, L. Monitoring the energy-use effects of cool roofs on California commercial buildings. *Energy and Buildings* 2005; 37: 1007–1101.
- [22] Levinson, R., Berdahl, P., and Akbari, H. Solar spectral optical properties of Pigments—Part II: Survey of common colorants. *Solar Energy Materials and Solar Cells* 2005; 89(4): 351–389.
- [23] Akbari, H., Konopacki, S., and Pomerantz, M. Cooling energy savings potential of reflective roofs for residential and commercial buildings in the United States. *Energy* 1999; 24: 391–407.
- [24] Konopacki, S., and Akbari, H. 1998. Simulated impact of roof surface solar absorptance, attic, and duct insulation on cooling and heating energy use in single-family new residential building. Lawrence Berkeley National Laboratory, Report LBNL-41534, Berkeley, CA.
- [25] Akbari, H., and Konopacki, S. Calculating energy-saving potentials of heat-island reduction strategies. *Energy Policy* 2005; 33: 721–756.
- [26] Levinson, R., Berdahl, P., Akbari, H., Miller, W., Joedicke, I., Reilly, J., Suzuki, Y., and Vondran, M. Methods of creating solar-reflective nonwhite surfaces and their application to residential roofing materials. *Solar Energy Materials and Solar Cells* 2007; 91(4): 304–314.
- [27] Synnefa, A., Santamouris, M., and Akbari, H. Estimating the effect of using cool coatings on energy loads and thermal comfort in residential buildings in various climatic conditions. *Energy and Buildings* 2007; 39: 1167–1174.
- [28] Akbari, H., Pomerantz, M., and Taha, H. Cool surfaces and shade trees to reduce energy use and improve air quality in urban areas. *Solar Energy* 2001; 70: 295–310.
- [29] Akbari, H., and Levinson, R. Evolution of Cool-Roof Standards in the US. *Advances in Building Energy Research* 2008; 2: 1–32.
- [30] ASHRAE, 2013, ANSI/ASHRAE Standard 90.1-2013. Energy Standard for Buildings except Low-Rise Residential Buildings. American Society of Heating, Refrigerating, and Air-Conditioning Engineers, Inc. Atlanta, GA.
- [31] ASHRAE, 2007, ANSI/ASHRAE Standard 90.2-2007. Energy Standard for Low-Rise Residential Buildings. American Society of Heating, Refrigerating, and Air-Conditioning Engineers, Inc. Atlanta, GA.

- [32] California Energy Code. 2013. California Code of Regulations. Title 24, Part 6. California Building Standards Commission. Sacramento, CA.
- [33] US Green Building Council's Leadership in Energy and Environmental Design (LEED). Building Design and Construction rating system, <http://coolroofs.org/resources/leed>.
- [34] Akbari, H., and Matthews, H. Global cooling updates: Reflective roof sand pavements. *Energy and Buildings* 2012; 55: 2–6.
- [35] Hosseini, M., and Akbari, H. Heating energy penalties of cool roofs: The effect of snow accumulation on roofs. *Advances in Building Energy Research* 2014; 8: 1–13.
- [36] Hosseini, M., and Akbari, H. Effect of cool roofs on commercial buildings energy use in cold climates. *Energy and Buildings* 2015.
- [37] Yang, J., Wang, Z., and Kaloush, K. 2013. Unintended Consequences—A research synthesis examining the use of reflective pavements to mitigate the urban heat island effect. Arizona State University, AZ.
- [38] Carter, M., and Stangl, R. 2012. Considerations for building design in cold climates. Whole Building Design Guide, [http://www.wbdg.org/resources/bldgdesigncc.php?r=env\\_roofing](http://www.wbdg.org/resources/bldgdesigncc.php?r=env_roofing).
- [39] Ahrab, M., and Akbari, H. Hygrothermal behavior of flat cool and standard roofs on residential and commercial buildings in North America. *Building and Environment* 2013; 60: 1–11.
- [40] Gray, C. Application of adaptive albedo roofing coatings in the southeastern united states. A Dissertation—The University of Alabama at Birmingham 2015.
- [41] Erdem, C., and Saffa, R. A state-of-the-art review on innovative glazing technologies. *Renewable and Sustainable Energy Reviews* 2015; 41: 695–714.
- [42] Kamalisarvestani, M., Saidur, M., Mekhilef, R., and Javadi, F. S. Performance, materials and coating technologies of thermochromic thin films on smart windows. *Renewable and Sustainable Energy Reviews* 2013; 26: 353–364.
- [43] Baetens, R., Jelle, B. P., and Gustavsen, A. Properties, requirements, and possibilities of smart windows for dynamic daylight and solar energy control in buildings: A state-of-the-art review. *Solar Energy Materials and Solar Cells* 2010; 94(2): 87–105.

- [44] Zinzi, M. Office worker preferences of electrochromic windows: A pilot study. *Building and Environment* 2006; 41(9): 1262–1273.
- [45] Lampert, C. M. Smart switchable glazing for solar energy and daylight control. *Solar Energy Materials and Solar Cells* 1998; 52(4): 207–221.
- [46] Bahaj, A. B. S., James, P. A. B., and Jentsch, M. F. Potential of emerging glazing technologies for highly glazed buildings in hot arid climates. *Energy and Buildings* 2008; 40(5): 720–731.
- [47] Gao, Y. Nanoceramic VO<sub>2</sub> thermochromic smart glass: A review on progress in solution processing. *Nano Energy* 2012; 1(2): 221–246.
- [48] Bamfield, P. 2001. *Chromic Phenomena: Technological Applications of Colour Chemistry*. Cambridge, UK: The Royal Society of Chemistry.
- [49] Lee, E., Fernandes, L., Goudey, C., Jonsson, C., Curcija, D., Pant, X., DiBartolomeo, D., and Hoffmann, S. 2013. A Pilot Demonstration of Electrochromic and Thermochromic Windows in the Denver Federal Center, Building 41, Denver, CO. Lawrence Berkeley National Laboratory, Berkeley, CA.
- [50] Azari, S., and Bierman, J. 2008. System and Method for Energy-Conserving Roofing. US Patent 7,335,419 B2 filed September, 2002 and issued February 2008.
- [51] Park, B., and Krarti, M. Energy performance analysis of variable reflectivity envelope systems for commercial buildings. *Energy and Buildings* 2016; 124: 88–98.
- [52] Testa, J., and Krarti, M. 2016. Evaluation of energy savings potential of variable reflective roofing systems for US buildings, Submitted to Sustainable Cities and Society.
- [53] Hooshangi, H., 2015, Energy Performance Modeling of Buildings with Directional Reflective Roofs. A Thesis – Concordia University.
- [54] Akbari, H., and Touchaei, A. Modeling and labeling heterogeneous directional reflective roofing materials. *Solar Energy Materials and Solar Cells*, 2014; 124: 192–210.

---

### **3. Breathing and living walls**

---

*John Zhai, Saleh Nasser AL Saadi, Mohamed El Mankibi, and Robert Slowinski, Civil, Environmental, and Architectural Engineering Department University of Colorado Boulder, CO 80309 – USA*

**Abstract:** Breathing wall with dynamic insulation properties appears promising in reducing building energy load while providing fresh air to the space. Advanced living wall concept, inspired by biomimetic principles, offer further adaptive nature of envelope systems to changing outdoor conditions. This chapter introduces the principles of both innovative wall systems. Both simulation and experimental approaches are presented to design, evaluate, and optimize the proposed wall systems. Results indicates favorable trends of efficiency for both systems. Recommendations are provided for the wall development.

---

#### **3.1 “Breathing Wall” Concept**

A promising new technology introduces a method of avoiding the efficiency/air quality compromise, yielding better energy efficiency and improved indoor air quality (IAQ). The technology, referred to as a “breathing wall”, draws a steady stream of filtered air through the walls and into the building at all times, providing exceptionally clean ventilation air to the occupants. A schematic breathing wall diagram can be seen in Figure 3-1. Whereas higher ventilation rates traditionally produce higher energy loads in buildings, the “dynamic insulation” used in breathing walls actually works to reduce that load, effectively creating efficient, super-insulated walls.

The projected energy savings and air quality implications associated with breathing wall technology are astounding. Previous studies of the energy and air filtration efficiencies of breathing walls estimated that such technologies can reduce year-round heating and cooling loads between 10 and 40%, while providing a steady stream of fresh ventilation air, filtered to HEPA standards, 365 days per year [1]. Additionally, breathing walls may be able to clean up polluted cities too, as the filtered air exhausted by “breathing wall buildings” will effectively contain lower concentrations of pollutants and particulate matters than the outdoor air. The study also suggests that the filter mechanism of the walls will

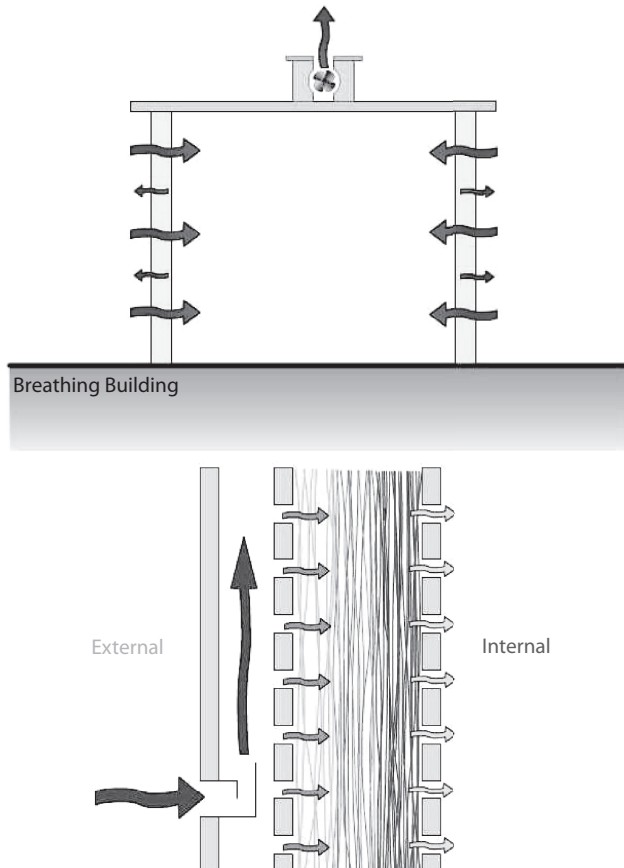


**Figure 3-1** Breathing wall configurations, as proposed by Imbabi and Peacock [1].

last throughout the lifetime of the building, providing the energy savings and air filtration for 60+ years, without requiring replacement.

While a few preliminary reports have projected promising energy and IAQ benefits of breathing walls, much research remains to be done. One major issue at hand pertains to understanding the heat transfer mechanism between the breathing wall media and incoming air, particularly under varied ambient conditions. Some of the previous research provides a simple estimation of the wall's insulative properties (U-value), involving only the conventional U-value and the flow rate of incoming air [2]. Using this method, the insulation of the wall at certain airflow rates is effectively infinite. While this method will suffice to make broad estimations of the

energy savings associated with breathing walls, it may not prove accurate under changing environmental conditions. It is important to understand the behavior of breathing walls under a wide range of conditions, including temperature, humidity, pressure, and air flow rate.

### 3.2 “Living Wall” Concept

Inspired by the breathing wall concept, using biomimetic principles, Zhai et al. [3] proposed a multi-layer living wall concept. Figure 3-2 illustrates the vision of such a climate-adaptive intelligent wall structure with embedded systems of air (respiration in body), water (blood in body), and phase change material (PCM) (fat in body). It shows a potential design of the living wall system for transferring and use of solar heat via a slab water radiation system and a buoyancy-driven overhead air distribution system. Proper design and control of the heat charge/discharge of PCM and circulation of gas and liquid in micro-vascular fluid systems (MVFS) can effectively manage the heat gain and loss through the structure, and maintain a pleasant indoor environment with comfortable temperature/relative humidity and adequate fresh air under dynamic climate conditions. This naturally controlled system will not only significantly reduce the total energy cost required to heat, cool, vent, and light the spaces, but also create attractive architectural

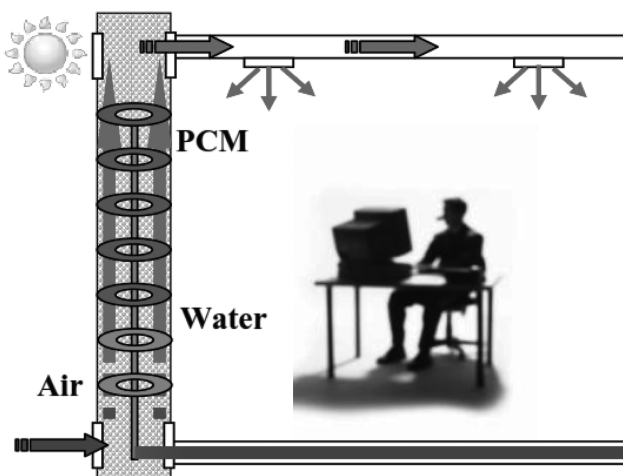


**Figure 3-2** Illustration of a living wall system design; solar energy is harvested via a slab water radiation system and a buoyancy-driven overhead air distribution system.

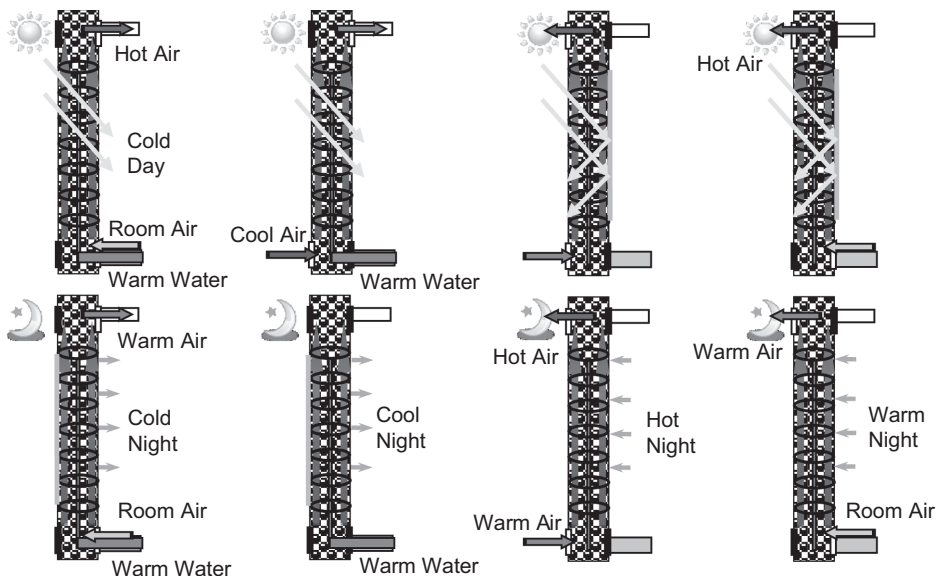


**Figure 3-3** Illustration of different environmental and system operating conditions.

features. Figure 3-3 illustrates different environmental and system operating conditions.

### 3.3 State of the Art

Among the first to conduct experimental studies on the effects of infiltration heat recovery within the building envelope were Bhattacharyya and Claridge [4]. Their one-dimensional model effectively predicted the heat transfer between moving infiltration air and the exterior building envelope. The so-called “heat exchanger” model was then revised and simplified [5], by studying the particular case of a vertical air cavity within a wall. Separate studies [6, 7] added simulation of the airflow within the interior to a model of the heat recovery within the exterior wall element. Further research related to the movement of air throughout the building envelope has investigated the thermal and heat transfer properties of hollow bricks and double-skin façades. Additionally, Chen and Liu [8] studied the airflow through porous media for applications within the solar-collector industry.

Several European studies, including [9, 10], have shown the potential energy saving impacts of dynamic insulation in buildings. Full-scale tests were conducted to study the energy performance of a dynamically

insulated room [11–13]. It was found that dynamic insulation can potentially save up to 14% of the heating load during the wintertime [9].

Krarti [14] developed an analytical model to study the impacts of combined conduction and infiltration/exfiltration upon the thermal performance of dynamic insulation, and demonstrated that the heating load in applications of coupled infiltration and conduction was less than the simple summation of isolated conduction and infiltration. He demonstrates that there is a significant thermal coupling between the leakage and insulation layers that modifies the heat transmission in building thermal envelopes. The correlations developed by Krarti use the Peclet number to indicate the velocity of air moving through the wall. However, the savings is limited due to the fact that the amount of air forced through the dynamic wall must be equal to the air being exhausted. Analysis of the wall temperature profiles shows that the temperature profile within the wall largely depends upon the direction and rate of airflow through the wall. When no air is passing through the wall, the profile is linear, while it takes on a convex shape when air is exfiltrating, and a concave shape when air is infiltrating. The temperature profile throughout the wall is important, as it affects the heat loss due to conduction through the wall. Krarti concludes that the wall as a heat exchanger is capable of reducing the daily heating load due to conduction and infiltration by up to 22%.

Taylor et al. [2] likewise developed a one-dimensional steady-state model of multi-layer breathing wall heat transfer, and proposed to measure the performance through a dynamic U-value. One of Taylor's key findings is that very different types of construction will have the same thermodynamic performance with the same airflow, provided the thermal resistance is equal. Another significant finding of the analytical research is that pro-flux (heat and air flow in the same direction) and contra-flux flow (heat and air flow in opposite directions) exhibit asymmetrical behavior [2]. Imbabi and Peacock [1] conducted physical and analytical experiments on dynamically insulated walls. Their research suggests that a layer of wet-blown cellulose with a static U-value of  $0.168 \text{ W/m}^2\text{K}$ , when subjected to an infiltration airflow rate of  $1 \text{ m/hr}^{-1}$ , can achieve a dynamic U-value of  $0.058 \text{ W/m}^2\text{K}$ , which falls further to  $1.7 \times 10^{-8} \text{ W/m}^2\text{K}$  at an airflow rate of  $10 \text{ m hr}^{-1}$ .

Qiu and Haghigat [15] published research regarding the temperature profile at various depths within a ventilated wall, as well as the concept

of treating the wall as a combination of ventilated and non-ventilated areas. They developed a numerical simulation in order to study the thermal performance of the diffuse building envelope, and conducted physical testing in order to corroborate the numerical results. Their computer simulations indicate that at low airflow rates, the temperature of the air rises very quickly to approximate the temperature of the solid matrix, allowing for a single medium analytical treatment. This research relies heavily upon the Peclet number (closely related to airflow rate) as a determining factor for breathing wall thermal performance. A key finding of the research is that the breathing wall can be broken up into regions affected by the heat transfer of infiltration, and regions that remain unaffected by infiltration, and are therefore dominated by pure conduction heat transfer. Additionally, it was determined that the ratio of these two areas is one of the key indicators of breathing wall performance.

Slowinski [16] conducted both laboratory mock-up experiments and computational fluid dynamics (CFD) simulations to investigate the thermal performance of ventilated breathing walls under varied environmental conditions. His study compared and analyzed the influences of selected design parameters on the wall thermal performance. He found that both the airflow rate through the breathing wall and the temperature difference between indoor and outdoor air will affect the wall efficiency [17].

Zhai et al. [3] first presented the concept of “Living Wall” with a research plan ranging from micro-scale holding material studies to system-scale whole building system designs. A series of research articles were published as a result of the project, which demonstrate the progress of the research and major outcomes. This chapter will present some of the key findings from these studies.

### 3.4 Prototypes and Products

Among the earliest applications of dynamic insulation within buildings were the ceilings of agricultural buildings in Norway in the 1960s [18]. Improvements in dynamic insulation technology led to the application of breathing walls within traditional barns, and then in the 1980s, inside a small number of traditional residential dwellings. Among the more contemporary installations of breathing wall technologies is the first major building in the United Kingdom to incorporate such a strategy, the McLaren Community Leisure Center, in Callendar, Scotland.

There are several products currently on the market that incorporate dynamic insulation or some of the properties of breathing walls. A start-up company in the United Kingdom and associated with the research team of Imbabai and Peacock markets “innovative modular breathing wall systems to provide clean, pre-heated, filtered ventilation air to the building”. This project has received substantial funding from the Scottish Executive SMART Program, in order to facilitate development. The specific product sold by EBP is called an Energyflo™ Cell (Figure 3-4), and it can be easily integrated into a building structure to incorporate the benefits of dynamic insulation (Figure 3-5). Additionally, Gaia Research Group included dynamically-insulated squash courts, bowling hall, sports hall, and swimming pool rooms in the McLaren Community Leisure Centre, which was finished in 1998 in Callander, Scotland. This building was the first major building in the United Kingdom to use dynamic insulation, and was undergoing a detailed monitoring program. Several other companies market “breathing wall” technologies as well, but many of these deal with breathability as it relates to building moisture and mold, rather than the energy saving performance of dynamic insulation.



Figure 3-4 A single Energyflo cell.



**Figure 3-5** Various Energyflo cell installations.

As a part of the Zhai's research team, Andreas developed an Interstitial (IS) Wall/Living Wall prototype model in 2016 for commercial and residential building types, consisting of a  $0.1 \text{ m}^2$  slice from a full scale wall utilizing off the shelf building and modeling materials (Figure 3-6). The goal was to mimic as closely as possible the performance of the Living Wall assembly and materials as well as develop construction details at full scale. Figure 3-6 is the commercial living wall assembly. The right figure details, from left to right: high U value acetate panel, layered copper sheet, copper tubing intersected by heat pipe ends connected to a centralized antifreeze remote storage system, single temperature tuned encapsulated phase change materials (ePCM) sheet, two low-e film layers with airspaces, and Kalwall surface to the right.

This current prototype model made of typical building materials is designed to test the heat flow performance capacity of the living wall structures and concepts, namely testing insolation heat gains within the IS walls, distribution within the walls, heat migration capacities within the wall, insulation within the wall from conductive/convective heat transfer to the interior, radiative heat transfer within the wall's interior surfaces while (mostly) maintaining translucency for daylighting. This model will facilitate the analysis of heat transfer, heat migration, heat resistance, regulation and transport of heat through the living wall's micro structures, effectivity of phase change material, heat collection/exchanger efficiency and insulation layer resistance to heat flow.

### 3.5 Modeling Advanced Façade Systems

Modeling heat transfer processes of the air, liquid and PCM systems in the living wall and exploring the thermal coupling fundamentals between various heat sources and sinks are the most important but challenging

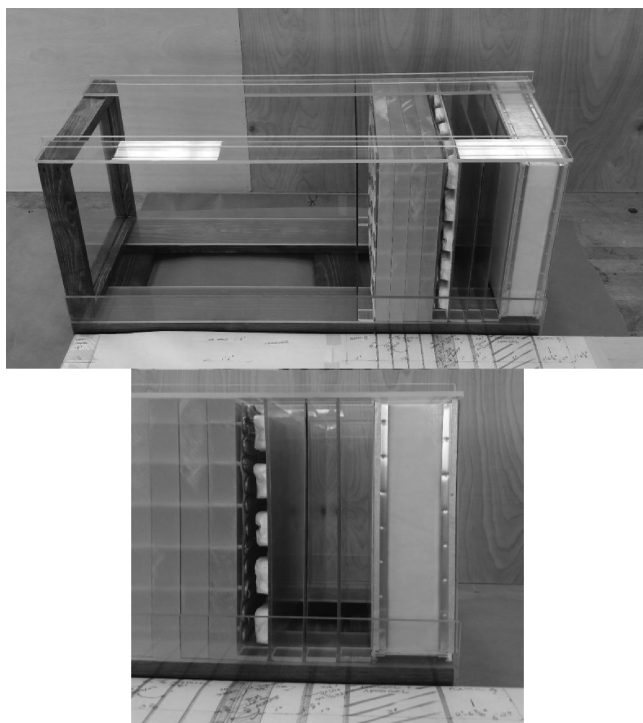


**Figure 3-6** Full scale interstitial (IS) wall/living wall model.

work. This requires establishing more sophisticated fluid dynamics and heat transfer models that can account for the coupled multi-physics and multi-phase fluid flow and heat transfer processes with connection to both indoor and outdoor environments. Saadi and Zhai [19] developed a generic program for studying advanced façade systems (named “AdvFacSy”) using SIMULINK environment. The program includes (1) weather data reader; (2) solar radiation model; (3) models for different wall layers (e.g., solid, cavity, glass, PCM etc.) that can be used to form different wall configurations (Figure 3-7).

Using “AdvFacSy”, a variety of wall designs can be easily generated and assessed under different climatic conditions (as seen in Figure 3-8). In addition to envelope designs, the program can be used to evaluate different operational strategies such as to charge and discharge energy stored in PCMs using the air in the cavity as a heat transfer medium. The air is driven by thermal buoyancy or mechanical fan. The air can be induced from the outdoor or indoor environment via air vents located at top and

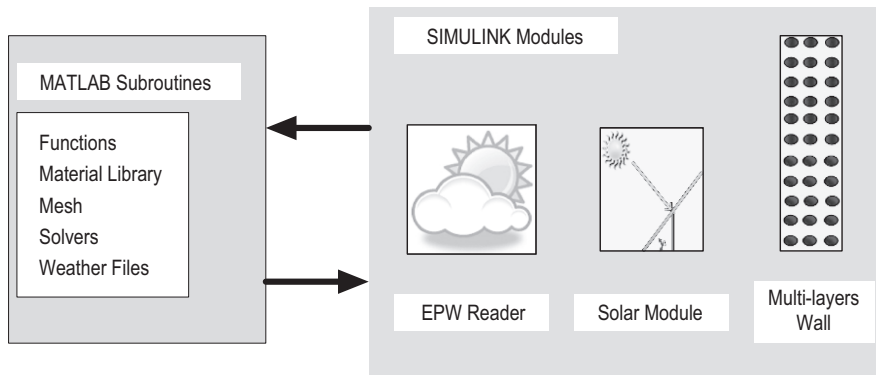


**Figure 3-7** AdvFacSy toolbox concept in SIMULINK.

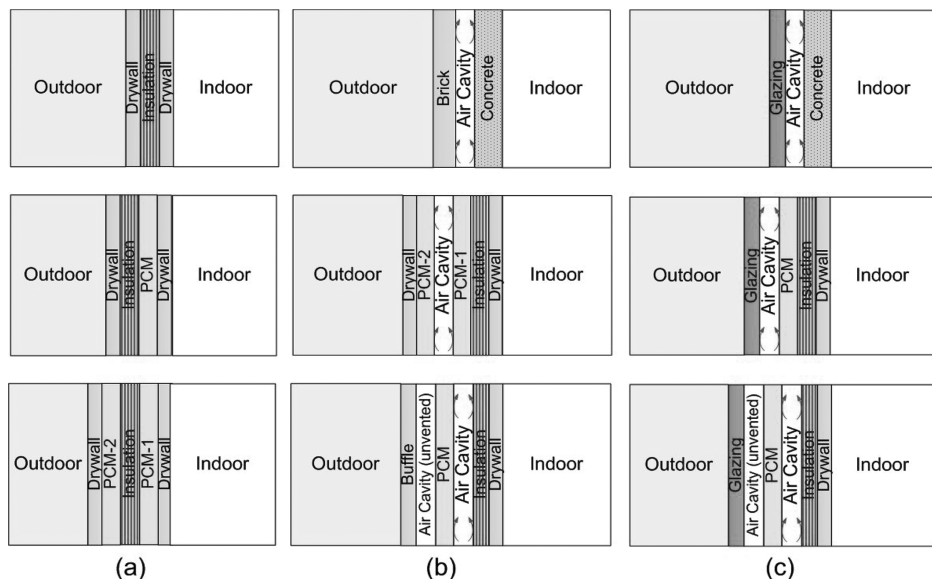


**Figure 3-8** Classical and advanced façade designs with and without PCM and ventilated cavity in “AdvFacSy” Toolbox  
 (a) Multi-layer wall; (b) Ventilated opaque multi-layer wall;  
 (c) Ventilated transparent multi-layer walls.

bottom of the façade system. The controlling mechanism facilitates the charging and discharging of PCMs in the wall unit. The recovered heat can then be directly used to meet the heat demand, or used to preheat fresh air before treated centrally in air conditioning system, or transported to other heat storage medium for later usage. The program has been well validated against experiments and other simulation tools for both conventional multi-layer walls and ventilated cavity walls [20].

### 3.6 Testing Advanced Façade Systems

Full scale or mock-up experimental chambers are critical and inevitable for investigating the principles and comparing the performance of breathing/living wall prototypes, and for evaluating simulation models. Small-scale test chambers were built for developing new building envelope systems [17]. Figure 3-9 shows one of the test chambers developed for controlled experimentation. In order to simulate a wide variety of exterior and interior environmental conditions, separate test chambers of  $1.1176\text{ m} \times 1.1176\text{ m} \times 1.1176\text{ m}$  each, simulating interior and exterior environmental conditions, are built with  $U = 0.437\text{ W/m}^2\text{-}^\circ\text{C}$  polystyrene panels and can be heated to varying degrees by a system of dimming incandescent lamps. Allowing the temperatures to reach a steady state, this system facilitates breathing wall simulations at winter conditions with a temperature differential of up to  $38^\circ\text{C}$ . The test chambers also possess the capability to vary pressure differentials and therefore airflow rates by means of an exhaust fan and a variable outlet damper, in order to develop a pressure drop – flow rate curve for each type of breathing wall construction. Pressures are varied from 2 Pa to 12 Pa and the corresponding air volume flow rates are measured. A small fan is located within the interior space, to encourage even mixing of the interior air.

One example of the tested breathing walls was constructed with outside dimensions of  $1.1176\text{ m}$  by  $1.1176\text{ m}$ , and featured interior and exterior cladding, made of  $6.35\text{ mm}$  thick plywood. The exterior façade featured an inlet grille located in the center of the wall,  $0.767\text{ m}$  up from the bottom. The interior façade featured a similar exhaust grille located  $0.2\text{ m}$  from the bottom. An air gap was created between the cladding element and the porous breathing wall material, such that air was allowed to freely flow away from the inlet vent and penetrate the porous material in a relatively even fashion. The prototype breathing wall was constructed using commercially-available un-faced fiberglass

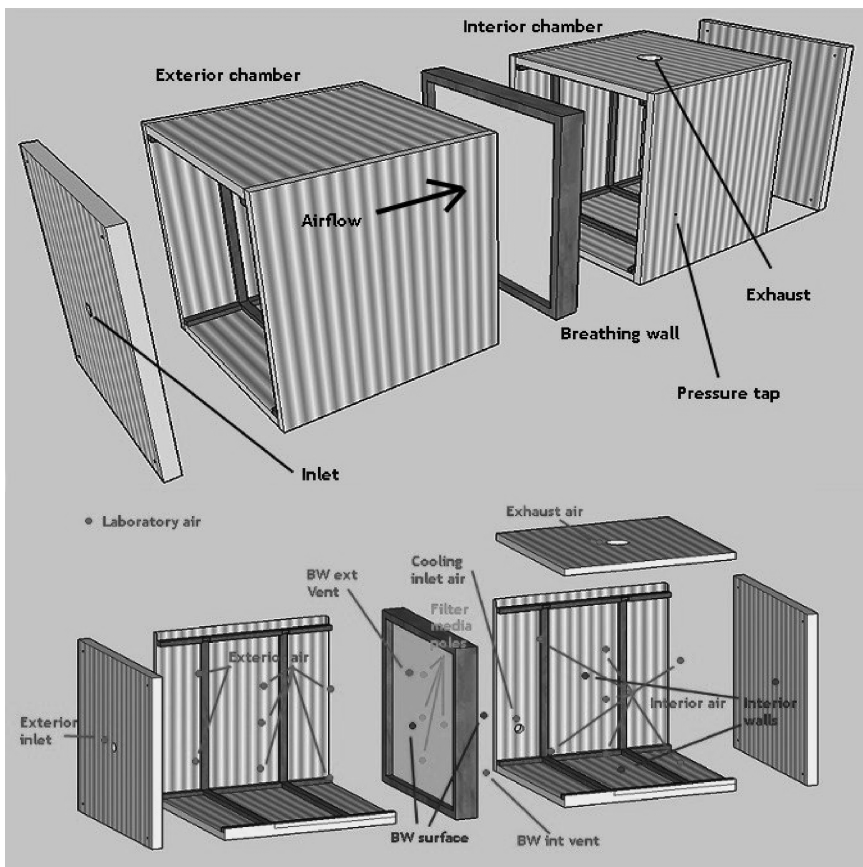


**Figure 3-9** Experimental test chamber setup and thermo-couple locations.

batt insulation, which were spread out across a fiberglass window screen and secured within the wood plane of the wall.

In the experiment, temperature is measured by thermocouples at 44 different locations, both inside and outside of the test chamber (shown in Figure 3-9). The selected locations allow for the determination of average interior and exterior temperatures, average interior wall temperatures, exhaust air temperature, laboratory ambient temperatures, breathing wall vent temperatures, as well as simple wall temperature profiles at 4 poles throughout the breathing wall media. Thermocouples are embedded at various depths (25%, 50%, and 75%) throughout the breathing wall, to form four different “poles” so as to

obtain simple temperature profiles throughout the wall in desired locations. Additional thermocouples are located in both the interior and exterior air gaps of the poles. One thermocouple is located within the exterior vent and another within the interior vent, in order to measure both the inlet and exhaust breathing wall air temperatures. Experiments continue as long as necessary to achieve average temperature changes less than 0.5°C per hour. In some cases, steady state conditions can be achieved within two hours, while in others, it may take more than 24 hours. Various experimental parameters, including temperature, pressure, airflow rate, and auxiliary heating load are continuously measured and analyzed. The measurement accuracy meets or exceeds all relevant ASHRAE/ASTM standards.

Another experiment test chamber was built that can test various developed living wall prototypes under actual weather conditions (Figure 3-10). The test box of 1.65 m<sup>3</sup>, representing a mock-up building, is fully sealed with well insulated envelopes expect one side that can be replaced by various living wall prototypes to be tested. The inside conditions of the box can be controlled with a heating/cooling system. The box can be placed in either a controlled "outdoor" environment or a true outdoor climate for different test conditions. The outdoor weather



**Figure 3-10** Picture of the experimental chamber in outdoor environment.

data is collected and used as inputs to the computer models, such as the vertical and horizontal solar irradiation (global and diffuse radiation), the outdoor air temperature and the wind speed. The indoor air and surface temperatures are extensively recorded including the temperatures throughout the depth of the living wall to be tested. Figure 3-11 illustrates one PCM-embedded storage-focused living wall with air cavity that was tested outdoors. The wall is composed, from the inside to the outside, of: an insulating multilayer panel, an air gap of 15 cm and a glazing. The insulating multilayer panel has two layers of 6.35 mm of cement board and the middle PCM with 2.54 cm thickness (with the melting point of 23°C and the heat storage of 165–200 J/g). The air cavity allows the flow and collection of the heated air. In this example test, the air comes from the indoor space and moves through two vents of 51 cm<sup>2</sup> each at the top and bottom, respectively. The air movement can be either natural or forced.

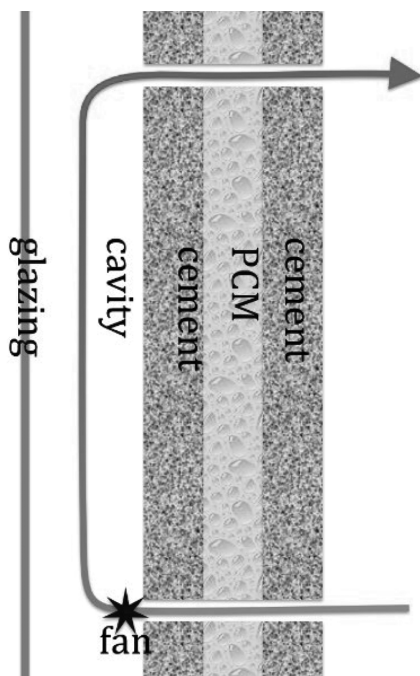


**Figure 3-11** Illustration of one PCM-embedded living wall tested.

### 3.7 Thermal Performance of Single-Layer Breathing Wall

#### 3.7.1 Measured Results and Analysis

In order to properly document the energy savings of the ventilated breathing wall assembly over a static wall construction, a base case is defined, from which the static wall heat loads can be calculated. The base case consists of a conditioned stream of ventilation air entering through a simple vent on one of the test chamber walls, rather than passing through the breathing wall. Winter conditions are simulated by heating the interior test chamber up to temperatures as high as 60°C, to provide contrast with the “outdoor” environmental conditions found in the exterior chamber, at 22°C. In each of the 13 base case runs, temperature, pressure, and airflow measurements were taken in the same fashion as in the dynamic breathing wall cases. Twenty experiments were performed with varying “outdoor” conditions simulated in the exterior chamber and with ventilation air flowing through the breathing wall. The twenty dynamic runs consist of permutations of four different airflow rates across the breathing wall and five different temperature differentials, with a temperature range similar to that of the base case runs.

It is important to quantify the thermal performance and potential energy saving of breathing walls, such that the benefits of breathing wall technology can easily and effectively be incorporated into whole building energy simulations. Efficiency values that allow for interpretation of the breathing wall’s performance can be developed from the energy balance equation. The control volume is defined as the interior surfaces of the interior chamber walls, extending out to the exterior surface of the breathing wall. The energy balance equation accounts for HVAC energy supply within the interior space, as well as the air being exhausted by the exhaust fan and heat loss through chamber walls. A conceptual model of the experimental model energy balance can be seen in Figure 3-12.

The experimental model energy balance equation includes the exhaust energy flow,  $\dot{Q}_{\text{exhaust}}$ , as seen in Eq. (3.1), and the enthalpy being introduced into the space as ventilation air through the breathing wall,  $\dot{Q}_{\text{cool}}$ , seen in Eq. (3.2). Note that in the dynamic cases,  $T_{\text{cooling-inlet}}$  represents the temperature at the breathing wall exterior vent, while in the base cases it represents the temperature at the supply inlet on one of the chamber walls.

$$\dot{Q}_{\text{exhaust}} = \dot{m} \times C_p \times T_{\text{exhaust}} \quad (3.1)$$

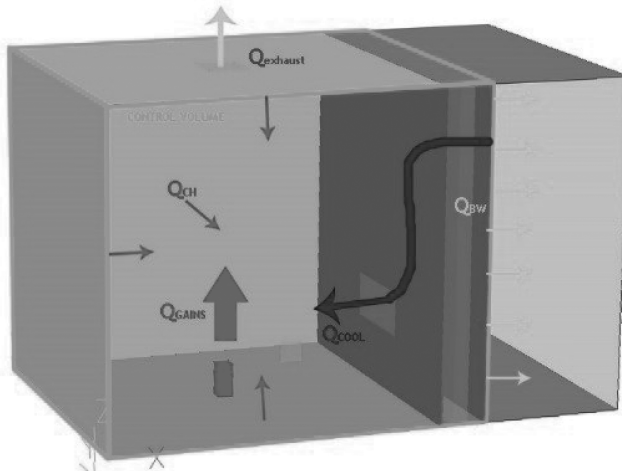


**Figure 3-12** Energy balance model for the test chamber.

$$\dot{Q}_{cool} = \dot{m} \times C_p \times T_{cooling-inlet} \quad (3.2)$$

Equation (3.3) shows the heat flow through the test chamber walls. The UA-value of the test chamber is derived from the tests.

$$\dot{Q}_{ch} = UA_{ch} \times (T_{interior-walls} - T_{lab}) \quad (3.3)$$

$\dot{Q}_{gains}$  is the combination of the heat inputs from the light bulb and from the mixing fan. The final energy balance equation for the test chamber provides an analytical solution for  $\dot{Q}_{BW}$ , shown in Eq. (3.4).

$$\dot{Q}_{BW} = \dot{Q}_{cool} + \dot{Q}_{gains} - \dot{Q}_{ch} - \dot{Q}_{exhaust} \quad (3.4)$$

Krarti [14] defined the efficiency of breathing walls (referred to as  $\eta_1$ ) as a function of the total energy needed by a case with breathing walls,  $\dot{Q}_{dynamic}$ , and that used in a similar scenario with dedicated vents,  $\dot{Q}_{static}$ , as in Eq. (3.5):

$$\eta_1 = 1 - \frac{\dot{Q}_{dynamic}}{\dot{Q}_{static}} \quad (3.5)$$

Taylor et al. [2] defined efficiency (referred to as  $\eta_2$ ) as a function of breathing wall conduction heat exchange (excluding the heat being

carried by airflow) and static breathing wall heat exchange, as seen in Eq. (3.6):

$$\eta_2 = 1 - \frac{\dot{Q}_{BW,dynamic}}{\dot{Q}_{BW,static}} \quad (3.6)$$

In order to account for any increase or decrease in conduction heat transfer through the breathing wall, our study defined the term  $U_{dynamic}$  in Eq. (3.7) simply as the heat flow through the non-vent portion of the breathing wall, divided by the product of wall area and temperature differential across the wall surfaces.

$$U_{dynamic} = \frac{\dot{Q}_{BW,dynamic}}{A_{BW} \times (T_{inside-surface} - T_{outside-surface})} \quad (3.7)$$

A third definition of efficiency, referred to as  $\eta_3$ , is defined as in Eq. (3.8) [17].

$$\eta_3 = 1 - \frac{U_{dynamic}}{U_{static}} \quad (3.8)$$

Many building energy simulation programs, such as DOE-2 or EnergyPlus, calculate the amount of energy load dedicated to conduction losses through building walls and the amount of energy heating outside air for ventilation purposes. If  $U_{dynamic}$  for a dynamic wall can be determined and used to replace the corresponding  $U_{static}$  in the input file of a building energy simulation program, the potential energy savings on an hourly basis using the dynamic wall can then be predicted with these energy simulation programs.

Multiple regression analyses were conducted on the experimental data points, and correlations were developed, respectively, for  $\dot{Q}_{static}$ ,  $\dot{Q}_{dynamic}$ ,  $\dot{Q}_{BW,static}$ ,  $\dot{Q}_{BW,dynamic}$ ,  $U_{static}$ , and  $U_{dynamic}$ . The developed correlation between interior-exterior temperature differential, airflow rate, and dynamic case  $\dot{Q}_{dynamic}$  can be seen in Eq. (3.9). The calculated  $R^2$  value for this correlation is 93.15%, indicating a fairly close match. In particular, the correlation predicts values with lower values of  $\dot{Q}_{dynamic}$  very accurately, while the data points with higher  $\dot{Q}_{dynamic}$  values appear more scattered.

$$\dot{Q}_{dynamic,exp} = (6.176 \times \ln(1.249 \times \dot{V}) - 5.556) \times \Delta T_{(avg,inside-avg,outside)} \quad (3.9)$$

where  $\dot{V}$  is the average “breathing” air velocity over the entire wall surface in  $CFM/m^2$ . The applicable mass flow and temperature differential ranges are 5.9 to 16 CFM and 9 to 38°C, respectively. In contrast to the dynamic case values, the  $\dot{Q}_{static}$  base case values conform much more closely to the determined correlation, shown in Eq. (3.10). This correlation has an  $R^2$  value of 99.53%, indicating a very close match. Consequently, there is no trend of over or under-prediction from the correlation.

$$\dot{Q}_{static,exp} = 1.108 \times \dot{V} \times \Delta T_{(avg,inside-avg,outside)} \quad (3.10)$$

Similarly,  $\dot{Q}_{BW,static}$ ,  $\dot{Q}_{BW,dynamic}$ ,  $U_{static}$  and  $U_{dynamic}$  are obtained below:

$$\dot{Q}_{BW,dynamic,exp} = 1.781 \times \dot{V} + 3.658 \times \Delta T_{(avg,inside-avg,outside)} - 15.483 \quad (3.11)$$

$$\dot{Q}_{BW,static,exp} = (0.241 \times \dot{V} + 1.866)(\Delta T_{(avg,inside-avg,outside)} \times 0.821 + 2.739) \quad (3.12)$$

$$U_{dynamic,exp} = 0.103 \times \dot{V} + 2.165 \quad (3.13)$$

$$U_{static,exp} = 0.211 \times \dot{V} - 0.097 \times \Delta T_{(avg,inside-avg,outside)} + 2.883 \quad (3.14)$$

Now that trends in the base and dynamic case indicators have been obtained, they can be compared to examine the measures of efficiency. Previous research has suggested that efficiency measures, at least for one-dimensional cases and for breathing walls with no internal air cavities, depend only upon the airflow rate and not upon the temperature differential. The developed correlations certainly suggest that flow rate plays more of a role, as the coefficients of flow rate in the equations are generally larger. However, the experimental results suggest that temperature differential does have some impact upon efficiency trends. Figure 3.13 shows the  $\eta_3$  contour (defined in terms of  $U_{dynamic}$ ). The experimental results show a clear positive correlation between airflow rate and efficiency, as well as a clear negative correlation between temperature differential and efficiency. Efficiencies range from –10 to 30%.

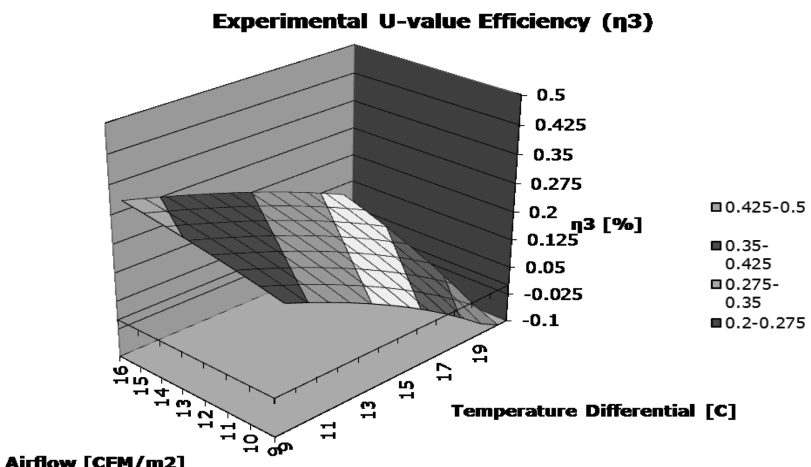


**Figure 3-13** Experimental efficiency ( $\eta_3$ ) for varying temperature gradients and airflow rates.

### 3.7.2 Predicted Results with Analytical Formula and CFD Simulation

The study compared the calculated efficiency of the tested wall to the analytical solutions obtained by Krarti [14] and Taylor et al. [2]. Both analytical solutions were developed for ideal and uniform flow through one-dimensional porous walls. The three-dimensional experiment has small inlet and outlet vents on the walls as well as interior wall cavities, which will introduce different heat transfer behaviors. Figure 3-14 demonstrates that the efficiency  $\eta_1$  and  $\eta_2$  do not vary with temperature differential. Experimental efficiencies have similar trends to the analytical solutions, although the efficiencies are much lower, with negative efficiencies below certain airflow rates.

A Computational Fluid Dynamics (CFD) model was created to explore the flow details in and out of the breathing wall that could not be revealed in the physical experiment. A Reynolds-Averaged Navier–Stokes (RANS) equations based CFD solver (with the KERNG turbulence model) was used to simulate various tested chamber conditions with a 500 K non-uniform grid (identified via a rigorous grid-independence study). Figure 3-15 illustrates that free convection circulation loops are formed at both the interior and exterior air gaps within the breathing wall. These circulation loops may play a part in increasing convection heat transfer within the wall and decreasing the efficiency as

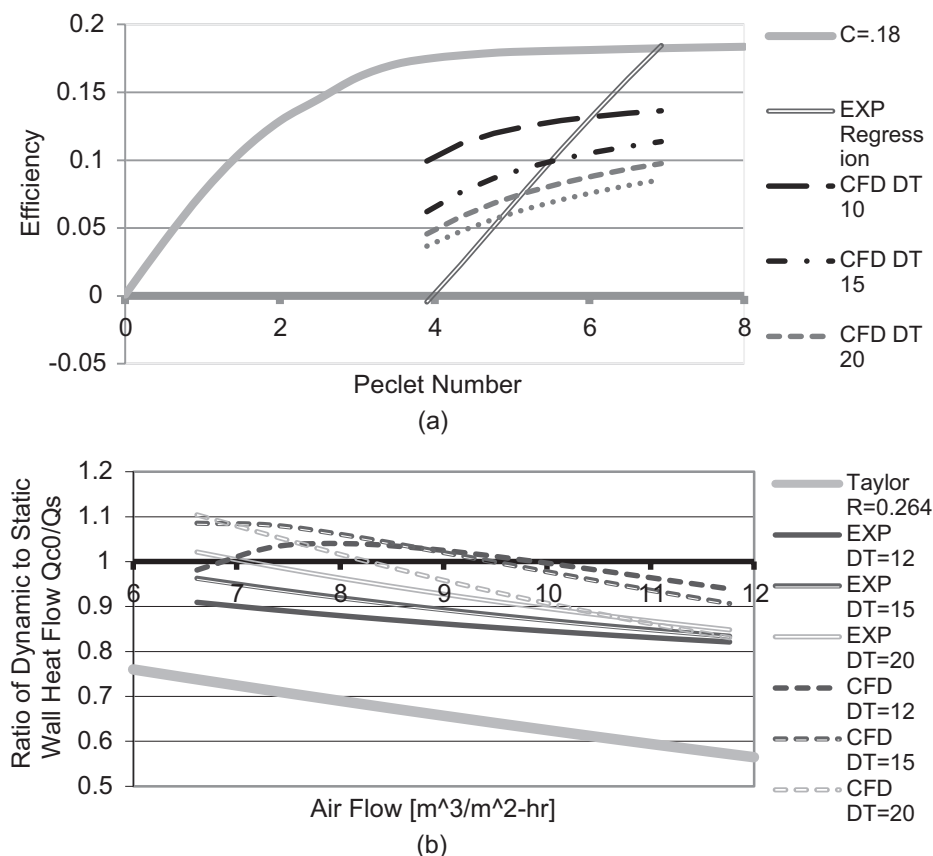


**Figure 3-14** Comparison of analytical efficiency of Krarti (a) and Taylor (b) and CFD results with tested efficiency.

temperature differential across the wall increases. CFD provides similar efficiency results and trends as the experiments as qualitatively illustrated in Figure 3-14.

### 3.8 Thermal Performance of Advanced Multi-Layer Walls

#### 3.8.1 Validation of Simulation Tools

Simulation tools are useful and critical for evaluating and optimizing advanced wall systems and designs such as breathing and living walls – innovative yet often unavailable for physical testing. A thorough validation of modeling tools is a must before the tools can be utilized with confidence. Our newly developed simulation tools for modeling

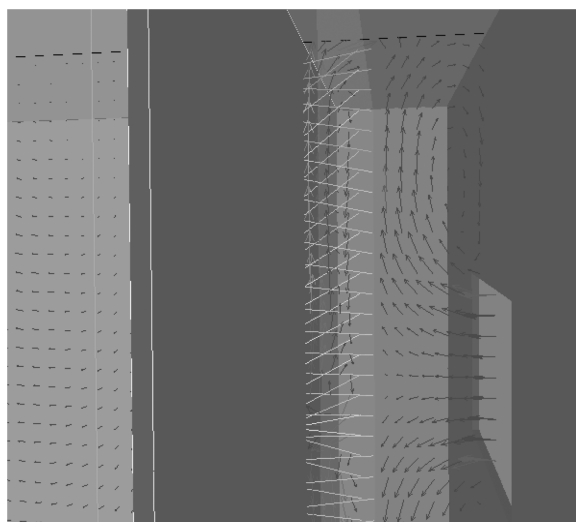


**Figure 3-15** Airflow vectors within the breathing wall, indicating circulation loops. Color profiles are based upon air velocity.

advanced façade systems have undergone a series of rigorous validations against experiment and peer simulation programs. As one example, Figure 3-16 shows a comparison of the measured and predicted indoor air temperature under actual dynamic weather conditions, using the test chamber in Figure 3-10 and the living wall setting in Figure 3-11. The results reveal a fair agreement. Figure 3-17 presents the predicted and measured temperatures inside the multilayer wall panel, and a reasonable match is observed.

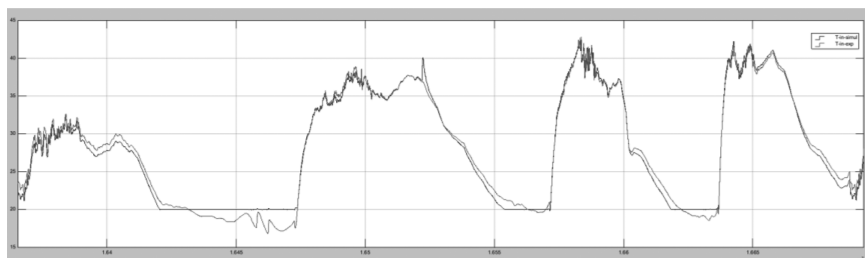


**Figure 3-16** Measured and predicted indoor air temperatures for the  $2.5 \text{ m}^3/\text{h}$  force convection case with indoor heater in place.

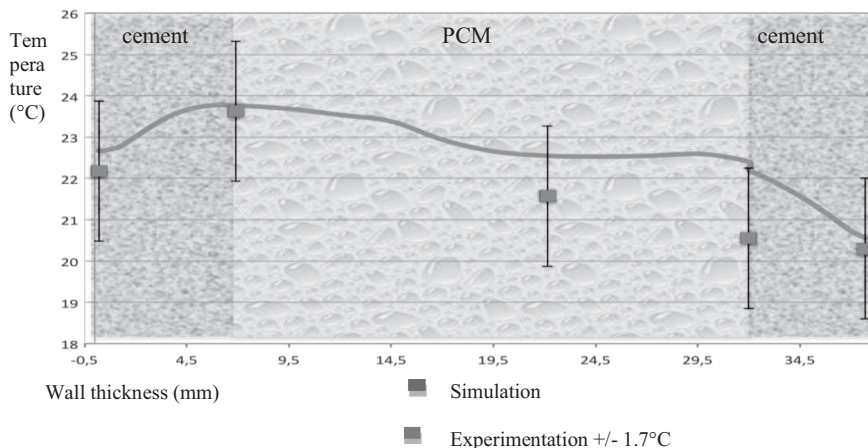


**Figure 3-17** Measured and predicted temperatures inside the multilayer wall panel at 8am of the test day.

### 3.8.2 Parametric Simulation Studies

The validated simulation tools can be used to study and optimize the performance of a standalone exterior envelope with a predefined interior air temperature representing prescribed indoor conditions. As a demonstration, the heating season from January to the end of April and again from October to the end of December is modeled below. During this period the indoor air temperature is set at 22°C. The cooling season is from May to the end of September where the cooling set-point is constant at 24°C. The outdoor conditions are provided using the weather file in EnergyPlus format (EPW) for Golden, CO, USA. The inside and outside convective heat transfer coefficients are important factors that may influence the thermal performance of the walls. For this analysis, the internal convective heat transfer coefficient is assumed to be 4.43 W/m<sup>2</sup>.K based on experimental results [21]. The outside convective heat transfer coefficient is based on ASHRAE winter design conditions [22]. Table 3-1 provides the summary of the boundary conditions used in the simulations.

A ventilated living wall design is proposed and tested as schematically shown in Figure 3-18, where the PCM is placed to the interior side of the wall (the most efficient location as proved) to enhance the performance. The ventilated living wall design consists of several components: the main multi-layer wall, a cavity and a glazing, whereas the

**Table 3-1** Parameters used for modeling advanced multi-layer walls.

Parameter	Values	Units
Indoor Air Temperature		
Heating season:	Jan-April & Oct-Dec	22
		°C
Cooling season:	May-Sept	24
External Convective Heat transfer Coefficient	29.30	W/m <sup>2</sup> .K
Internal Convective Heat transfer Coefficient	4.43	W/m <sup>2</sup> .K
Solar Absorption	0.6	[−]
Weather File	EPW for Golden, CO.	
Simulation Time	Annual simulation at sub-hourly time step of 5 minutes	

cavity and glazing characteristics are of top design interest. The cavity depth of 0.15 m and vent area of 1.05 m<sup>2</sup> are adopted. A typical double-pane glazing is used and the air is naturally induced from the indoor environment in this design. The rationale behind this design has been thoroughly investigated [23]. Upon the same design of the ventilated cavity, a reference model without the PCM layer is simulated as a comparison. A series of simulations are performed for various PCM characteristics including the latent heat between 50–300 kJ/kg at an

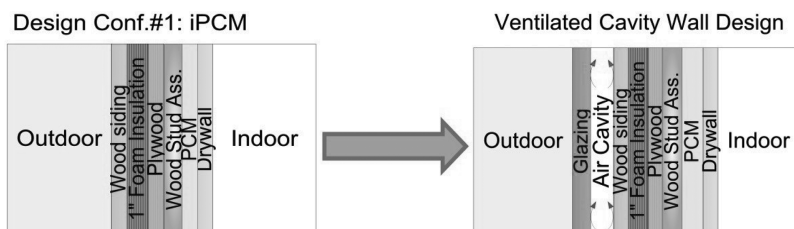


**Figure 3-18** Multi-layer wall configuration and the ventilated living wall design for harvesting solar for heating purpose.

increment of 50 kJ/kg, the melting temperature of 20–25°C at an increment of 1°C, and the melting range of 0.1°C, 1°C, 2°C, 4°C, and 6°C.

For all the cases, the PCMs are assumed to be concentrated as a separate layer with an overall thickness of 12.5 mm. Such systems have been proved to offer higher potential for heating and cooling application when compared to the randomly distributed mixed system [24]. Lightweight wall system for residential building is selected. The reference wall has been developed for Golden, Colorado climate based on the Building America House Simulation Protocols [25, 26]. The analysis is applicable for both new design and retrofitting projects.

The objective of this analysis is to investigate the general behaviors and identify the overall trends of thermal performance of the PCM-enhanced ventilated walls under typical meteorological weather data. Four performance indicators have been selected for comparison: peak heating load, annual heating load, peak cooling load, and annual cooling load. The peak heating load is the maximum instantaneous heat flux from indoor environment to the wall surface. The peak heating load is used for sizing heating systems. The annual heating load is the yearly summation of the instantaneous heat flux from the indoor to the wall surface. The peak cooling load, on the other hand, is the maximum instantaneous heat flux from interior wall surface to the indoor. The peak cooling load is used for sizing cooling systems. The annual cooling load is the yearly summation of the instantaneous heat flux from the wall surface to the indoor environment.

### 3.8.3 Simulated Results and Analysis

Figure 3-19 shows the simulated results of all orientations across all the PCM parameters as described above. The dotted line below all curves represents the contribution of the cavity when no PCM is used. It is apparent that the performance of thermal storage has been improved by introducing the cavity. There is clear distinction in PCM's performance as the melting temperature varies. When no cavity is used, the maximum savings in annual heating load was found ~3%. When a cavity is introduced in the south wall, the maximum savings in annual heating loads reaches above 95% as shown in Figure 3-19 (a) for the south wall case. Cavity contributes 65% of the saving in the annual heating load, and the rest (i.e., of more than 30%) is due to the PCM layer.

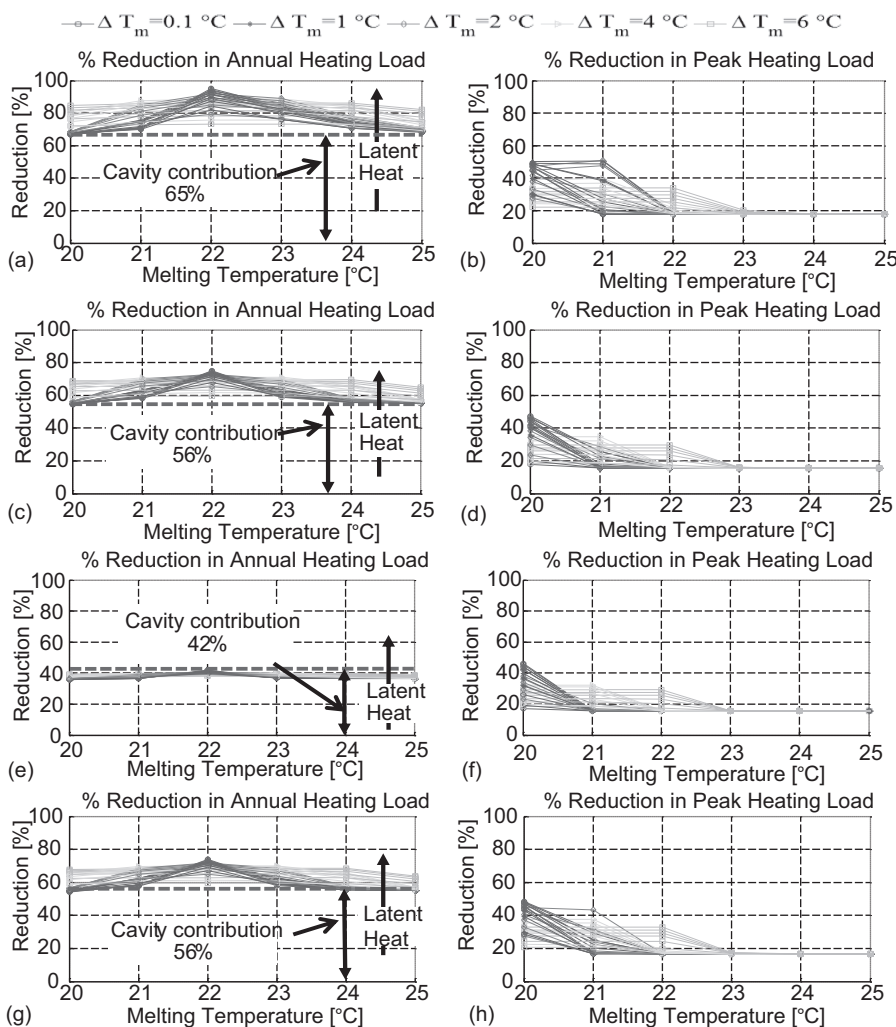


**Figure 3-19** Percentage reduction in heating loads across all PCM's thermal parameters for ventilated cavity PCM-enhanced wall under Golden CO (a) % reduction in annual heating load for south wall, (b) % reduction in peak heating load for south wall, (c) % reduction in annual heating load for west wall, (d) % reduction in peak heating load for west wall, (e) % reduction in annual heating load for north wall, (f) % reduction in peak heating load for north wall, (g) % reduction in annual heating load for east wall, (h) % reduction in peak heating load for east wall.

The PCM contributions in west and east are lower than the south wall as shown in Figure 3-19 (c) and (g). The saving in the annual heating load due to PCM is around 20%, if the cavity contribution due to conduction is subtracted. The cavity in the north wall is not effective in improving the performance of PCM as shown in Figure 3-19 (e). When PCM is used, the saving in the annual heating load is less than the case when no PCM is used. This is likely due to the storage of PCM, which is not utilized internally to reduce heating demand. In all the cases, the optimal melting temperature is close to the heating set-point of 22°C with a narrow melting range of 0.1°C. At the melting temperature moves away from the heating set-point, the PCMs with wide melting range provide more savings.

The saving in the peak heating load has improved comparing the cavity design to the non-cavity design. For all the orientations, the savings in the peak heating load are similar as shown in Figure 3-19 (b), (d), (f) and (h). For the south multi-layer PCM wall, a maximum saving in the peak load achieved by the non-cavity case is 20%. For the cavity design, the maximum saving in the peak heating load is around 50%. When cavity contributions are ignored (i.e., 15.40%), 34.5% saving in the peak heating load is due to the PCM layer only. This is a 14.5% improvement over the non-cavity design. The savings in the other orientations are similar to that in the south wall. In all these cases, the optimal melting temperature is below 20°C with a narrow melting range of 0.1°C.

Clear distinctions among the PCMs with different melting temperature ranges are observed. Those with narrow melting ranges achieve their maximum savings in the annual heating load at a melting temperature close to the heating set-point, following a triangular shape. The cases then tend to provide low savings as the melting temperature moves away from the set-point. The savings of the cases with wide melting ranges are flat and therefore are less sensitive to the heating set-point. This group can be considered conservative. When the cavity contributions are subtracted, the cavity enhances the performance of interior PCM from 3% with no cavity to 30% for south and 20% for east and west, respectively. The cavity on the north do not improve the performance of PCM. In all the cases, the optimal melting temperature is close to the heating set-point of 22°C with a narrow melting range of 0.1°C.

### 3.9 Thermal Performance of Buildings with PCM-Enhanced Walls

#### 3.9.1 Prototype House Model

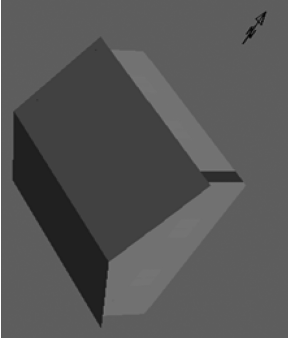
Skin-load or envelope dominated buildings such as residential types are constructed with thin thermal inertia structure making them ideal candidates for integrating thermal storage materials such as PCM. This building typology has thus been selected to evaluate the thermal performance of PCM-enhanced envelope. Building America House Simulation Protocols published by US National Renewable Energy Laboratory (NREL) have been used as the main source to create a base residential building [26]. Other resources have also been utilized to set other assumptions [27, 28]. The building is modeled as a single story, detached house with a total floor area of 167 m<sup>2</sup>. As a simplification, the house is modeled with two thermal zones: main conditioned zone and unconditioned attic zone. To simplify the inputs of internal heat gain in the model, the schedule and the maximum load wattage are determined from the peak consumption load profile and the total electricity consumption estimate [26]. The tool can model the HVAC systems in a building at two different levels: energy rate control and temperature level control [29]. In this work, the energy rate control modeling approach is adopted to evaluate the impact of PCM on the heating and cooling loads at the zone level. This approach assumes a simple HVAC system with an ideal control of thermal zones [29]. The energy is added or extracted at the zone level to meet the heating or cooling load as needed so as to manage the indoor air temperature within desirable heating and cooling set-points. For this analysis, the housing model is also simulated using the TMY3 weather file of Golden CO. As per the code requirement for this climate, the basic characteristics of the house's model are summarized in Table 3-2.

#### 3.9.2 Thermal Performance of Houses with PCM-Enhanced Lightweight Walls

##### 3.9.2.1 Influence of PCM Locations within the Wall Assembly

The external wall in the base case is modified by placing a PCM layer with a 12.5 mm thickness at three locations: to the interior side (iPCM), in the middle of the wood assembly (midPCM), and to the exterior side of the wall (ePCM) as shown in Figure 3-20. A PCM layer with a latent heat of 200 kJ/kg is selected with varying melting temperatures and

**Table 3-2** Characteristics of the base model of a residential building.

Parameter	Description	Remarks
Shape/Dimensions	<p>One story (3 bedrooms, 3 baths) Front of house faces north Aspect ratio: 1:1 Roof slope: 4:12 Conditioned floor Area = 167.29 m<sup>2</sup> Walls width = 12.93 m Floor to ceiling height = 2.4 m</p> 	Vented attic
Modeling Zones	Two thermal zones: main zone and attic zone	
Foundation	As per Building America benchmark [26]	
Exterior Walls	As per Building America benchmark [26]	
Ceiling R-Value	As per Building America benchmark [26]	
Solar absorptivity	Roof = 0.9, Wall = 0.6	
Window Area/ Distribution	15% of exterior wall area, uniformly distributed in all orientations	
Window Type	<p>Double glazing: <math>U = 1.98 \text{ W/m}^2\text{K}</math> <math>\text{SHGC} = 0.35</math></p>	The model doesn't use SHGC but an equivalent window is selected [28]

Infiltration Model	Room zone: ASHRAE K1, K2, K3 model Attic Zone: $10^*$ infiltration of room zone	As per [28]
Internal Loads		As per Building America benchmark [26]
Max lighting power	553.6 W	
	radiative power = 0.4 convective power = 0.6	
Max equipment power	Sensible = 733.3 W Latent = 89.3 W	
Max occupancy load (3 people)	Sensible = 225 W Latent = 225 W	
Operation set-points	Cooling set-point = 24°C Heating set-point = 22°C	
Weather file	TMY3	
Simulation Time step	5 minutes	
Notes: 1 [Btu/(hr.F $\cdot$ ft $^2$ )] = 5.6745 [Watt/(m $^2$ .K)], SHGC: solar heat gain coefficient.		

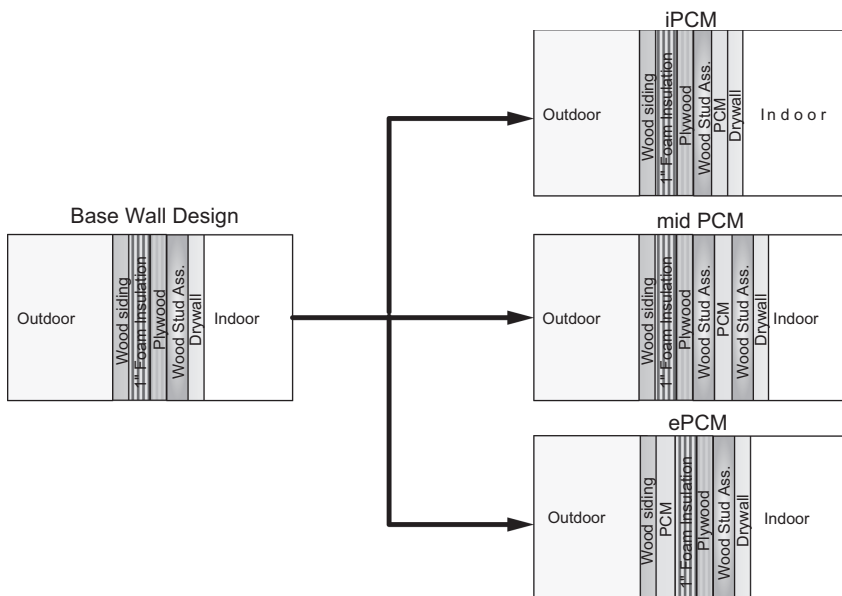


**Figure 3-20** PCM locations in the base wall design for Golden, CO.

melting ranges. For this analysis, the annual cooling and heating loads are adopted as performance indicators.

Figure 3-21 shows the impact of PCM location on the annual zone loads. When PCM is located to the interior side, a maximum cooling saving of 6% occurs at 1°C below the cooling set-point with 1°C melting temperature range being the best. The saving in the annual heating load is 2.4% and occurs at the heating set-point with a 2°C melting temperature range. As the PCM location moves away from the indoor environment, the saving becomes less significant. The lowest savings are observed when the PCM is located on the exterior side. For the PCM to the middle, the saving in the cooling load drops by almost half and optimal properties move to the wide melting range side of 4°C. The maximum saving in the annual heating load is in the range of 1.8% which is not significantly different from the iPCM case but the melting range covers a wider range (2–8°C) at an optimal melting temperature of 20°C. When the PCM layer is located to the exterior side, the optimal melting temperature for maximum savings in both cooling and heating loads is shifted to the cold range. This is an expected result for the cold climate of Colorado.

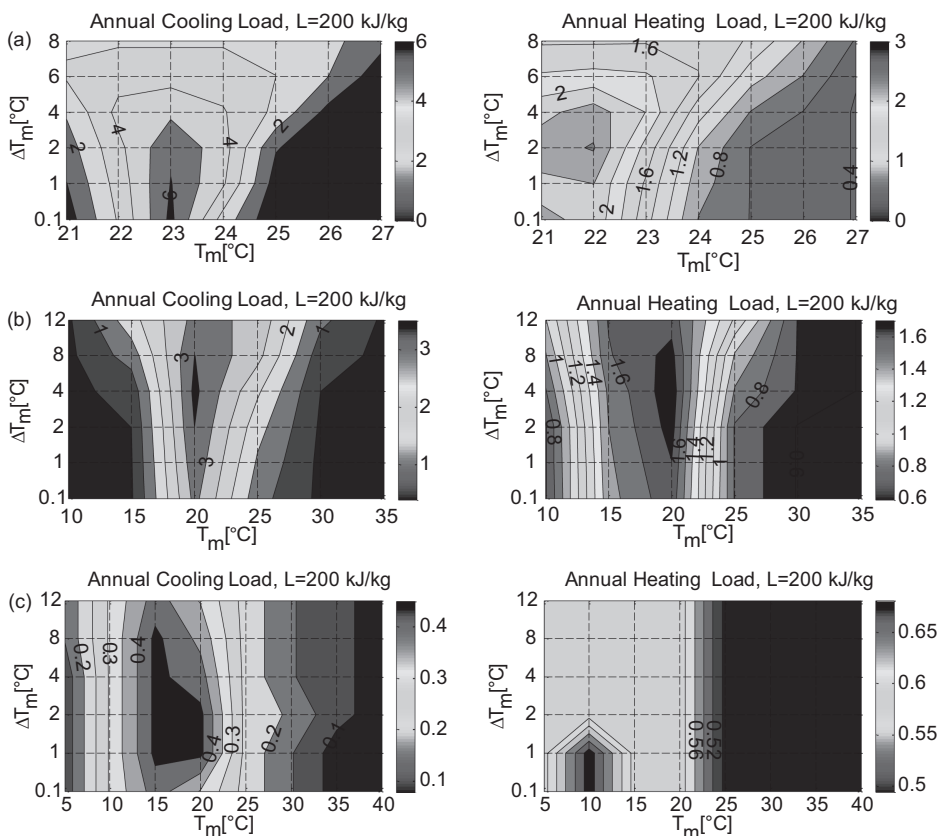


**Figure 3-21** Impact of PCM location on the annual zone loads.

### 3.9.1.2 Influence of PCM at Different Orientations

The previous section considers the use of a PCM layer equally in all orientations at different locations within the wall assembly. The best PCM location is found to be the interior side of the wall. Therefore, the iPCM case (i.e., PCM to the interior side) is selected to investigate the impact of PCM installed at individual orientations on annual loads. The latent heat of 200 kJ/kg is selected with a melting temperature of 22–23°C and a melting range of 1–2°C. This range provides maximum savings in annual heating and cooling load as shown previously in Figure 3-21(a). The predicted result at every orientation is shown in Table 3-3. Although the savings in the annual loads for using PCM at specific orientations are insignificant, the table shows that the maximum savings

**Table 3.3** Impact of internal PCM on annual loads when placed at different orientations.

Orientation	$T_m$ [°C]	$\Delta T_m$ [°C]	Heating reduction [%]	Cooling reduction [%]
East Wall	22	1	0.62	1.03
	22	2	0.65	1.14
	23	1	0.50	1.80
	23	2	0.52	1.77
South Wall	22	1	0.68	0.96
	22	2	0.74	1.07
	23	1	0.55	1.84
	23	2	0.59	1.69
West Wall	22	1	0.67	0.99
	22	2	0.74	1.07
	23	1	0.53	1.69
	23	2	0.58	1.58
North Wall	22	1	0.62	0.99
	22	2	0.67	1.10
	23	1	0.48	1.66
	23	2	0.52	1.55
All Walls	22	1	2.20	3.43
	22	2	2.42	3.74
	23	1	1.57	6.05
	23	2	1.73	5.82

Maximum savings in annual heating loads

Maximum savings in annual cooling loads

are achieved in south, west and east, and finally north. When PCM is utilized in all orientations, the savings for both annual cooling and heating loads are manifested.

### 3.9.1.3 Influence of Hybrid PCM Layers Placed to the Interior Side of a Wall

According to Table 3-3, the maximum savings in annual cooling and heating loads occur at different PCM thermal properties. Therefore, it is interesting to test the concept of hybrid PCM layers with different thermal properties: one dedicated for reducing cooling load and another for reducing heating load. The design configurations and thermal properties are listed in Table 3-4.

The results for these four cases are shown in Figure 3-22. The concept of hybrid PCM layers performs slightly better than a single PCM layer (i.e., 1% better) as to save the annual heating load. The saving in the cooling load, however, does not improve. In addition, the order of PCM layers is not important in the hybrid PCM design. Manipulating the distribution of the latent heat beyond an equal 50%–50% share does not improve the overall thermal performance of PCM.

**Table 3-4** Design configurations for single and hybrid PCM layers.

Wall design sketch*	PCM layer	Latent heat [kJ/kg]	T <sub>m</sub> [°C]	ΔT <sub>m</sub> [°C]
WD#1: One PCM layer	PCM	200	23	2
WD#2: Two PCM layers (Latent heat distribution: 50%clg_50%htg)**	PCM-1 PCM-2 PCM-1(for Cooling) PCM-2 (for Heating)	100 100	23 22	1 2

(Continued)

**Table 3-4** Design configurations for single and hybrid PCM layers. (*Continued*)

Wall design sketch*	PCM layer	Latent heat [kJ/kg]	T <sub>m</sub> [°C]	ΔT <sub>m</sub> [°C]
WD#3: Two PCM layers (Latent heat distribution: 50% htg_50%clg)**				
PCM-1(for Cooling)	100	23	1	
PCM-2(for Heating)	100	22	2	
Indoor				
Outdoor				
WD#4: Two PCM layers (Latent heat distribution: 25%clg_75%htg)***				
PCM-1(for Cooling)	50	23	1	
PCM-2(for Heating)	150	22	2	
Indoor				
Outdoor				

**Notes:**

\* properties of other layers are as per Building America benchmark [26]; \*\* latent heat of 200 kJ/kg is equally distributed for heating and cooling; and \*\*\* 75% of 200 kJ/kg latent heat is for heating and 25% for cooling.

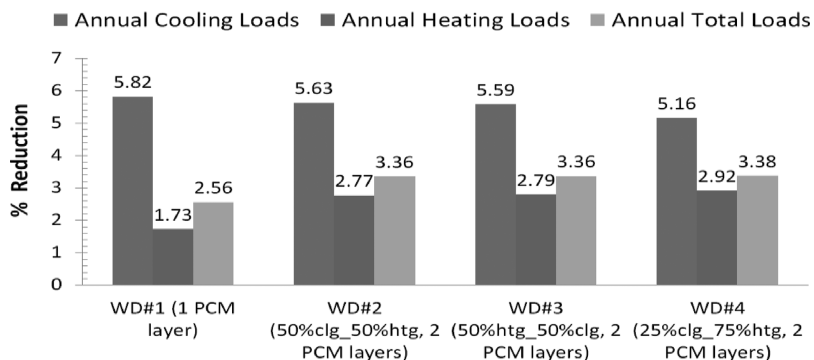


**Figure 3-22** Impact of hybrid PCM layers on percentage savings in annual loads when PCM placed to the interior side.

### 3.9.1.4 Seasonal Performance of PCM Placed to the Interior Side of a Wall

It is valuable to compare and analyze the seasonal energy performance of thermal storage walls, as the materials may work better in one season than the other. A case is built with PCM placed to the interior side of all exterior walls. A medium latent heat of 200 kJ/kg with a melting temperature of 23°C and a melting range of 2°C is employed for this seasonal analysis. Figure 3-23 presents the predicted results of the case. For the climate of Colorado, PCM performs the best in the transition months. In particular, the saving in the heating load starts to increase in March (1%) and reach a maximum saving of 10% in May. The maximum

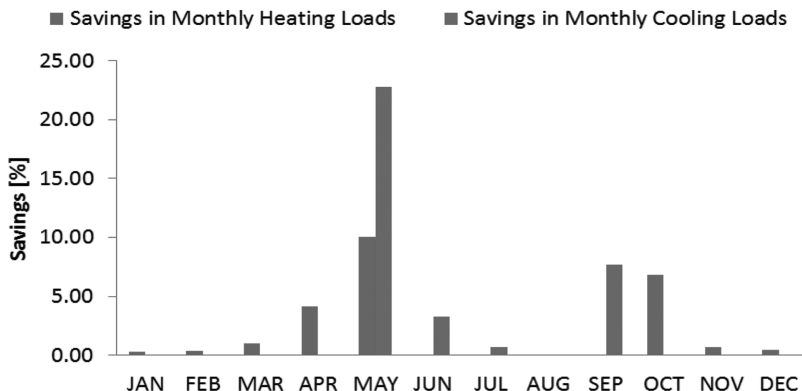


**Figure 3-23** Seasonal performance of PCM when placed to the interior of all exterior walls.

saving in the cooling load occur in May too at almost 23% but reduce significantly during the summer months.

### 3.9.1.5 Influence of Space Set-Point on PCM Performance

Defining proper environmental control schemes may be as important as defining optimal PCM properties. It is highly likely that one set of optimal PCM thermal properties developed for one environment may not be optimal or even suitable for another environment. The cooling and heating set-points are, respectively, 24°C and 22°C in the base model. For the comparison, the set-points are varied for both the base case and the south-PCM case, while the PCM thermal properties remain the same (i.e., latent heat of 200 kJ/kg, melting temperature of 23°C, and melting range of 2°C). Figure 3-24 illustrates the impact of varying the cooling and heating set-points on the annual loads. First, the cooling set-point is varied between 22–27°C while the heating set-point is kept constant at 22°C. Then, the heating set-point is varied from 18 to 24°C while the cooling set-point is kept unchanged at 24°C. It is clearly shown that the PCM performance is sensitive to both cooling and heating set-points. It is interesting to note that the maximum savings in the annual total load are achieved when the cooling set-point is decreased by 1°C (i.e., a new set-point at 23°C) or when heating set-point is increased by 1°C (i.e., the new heating set-point at 23°C). Increasing or decreasing the set-points beyond this makes PCM less effective. No saving in the annual cooling load is observed when the cooling set-point is changed to 26°C or above. This confirms that the optimal PCM thermal properties derived for the base case will not work for environments with distinct cooling and heating set-points.

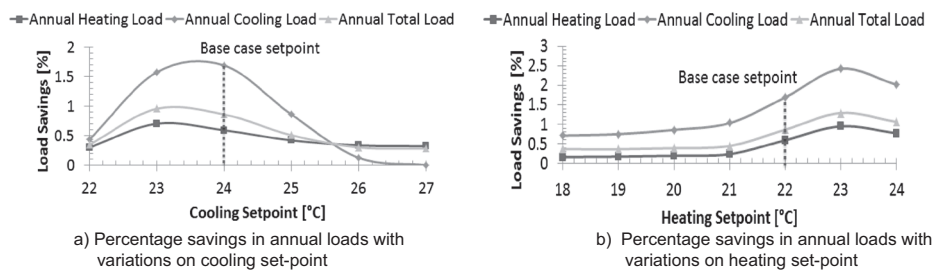


**Figure 3-24** Impact of varying the zone cooling and heating set-points on annual loads.

### 3.9.3 Thermal Performance of Houses with PCM-Enhanced Heavy Massive Walls

The previous study focuses on the application of PCM for lightweight structures in a typical residential building. One may argue that PCM's performance may be enhanced when integrated into sensible heat storage materials such as concrete. This section evaluates this particular design concept. Table 3-5 provides the thermo-physical properties for the design options tested to evaluate the PCM performance. For a fair comparison to the lightweight wall design considered previously for the residential building, the base wall is designed with a similar thermal resistance (i.e., R-18) but with a thermally massive material: a concrete block instead of wood assembly. Two designs are considered: (1) PCM is located to the interior side of the wall, and (2) PCM is concentrated in the middle of the concrete block. The PCM latent heat is fixed at 200 kJ/kg but the melting temperatures and melting range are varied as listed in Table 3.5.

The percentage reductions in annual heating and cooling loads for both designs are shown in Figure 3-25. When the figure is compared to the lightweight wall results presented early in Figure 3-21, it is clear that PCM performs better when integrated into lightweight wall rather than with heavy massive wall. The optimal PCM thermal properties are not significantly different for both designs except for the maximum savings in the heating load. For the maximum saving in the heating load, the heavy massive structure favors tight melting range compared to lightweight structures regardless of PCM location. Since sensible storage can absorb the heat energy at wide operational regime compared to PCM that only works at a narrow operational condition, PCM's energy storage becomes weak and secondary. Additionally, the high level of insulation may also contribute to the low performance of PCM, hindering its discharging process especially in summer for reducing the cooling load.

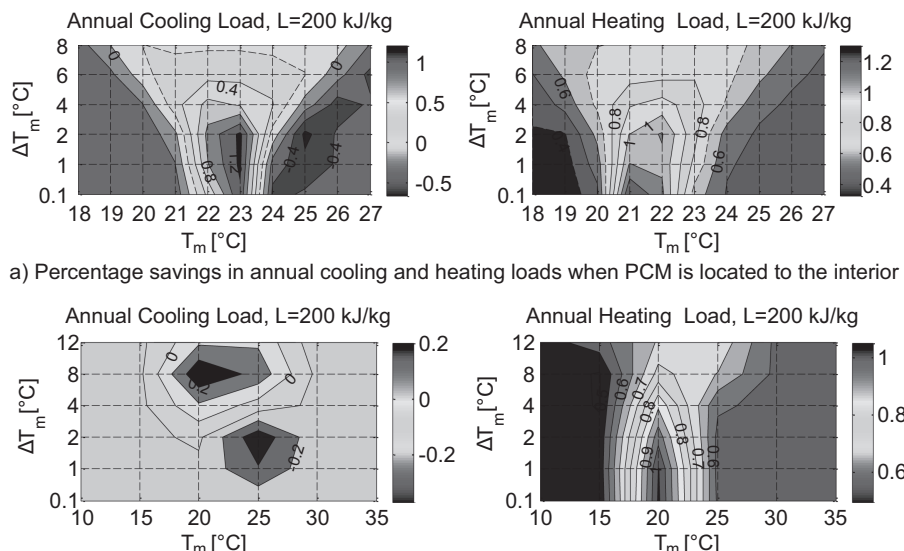
The performance of thermally massive and insulated PCM-enhanced walls is not better than the lightweight PCM-enhanced walls due to many reasons including the high level of insulation. Therefore, the insulation layer is eliminated from all thermally massive walls, for further tests. Note that this design concept might not comply with local or national energy codes but rather to evaluate the PCM performance when insulation is eliminated. Two PCM locations are considered: (1) one

**Table 3-5** Thermo-physical properties of thermally insulated massive wall designs enhanced with PCM layer.

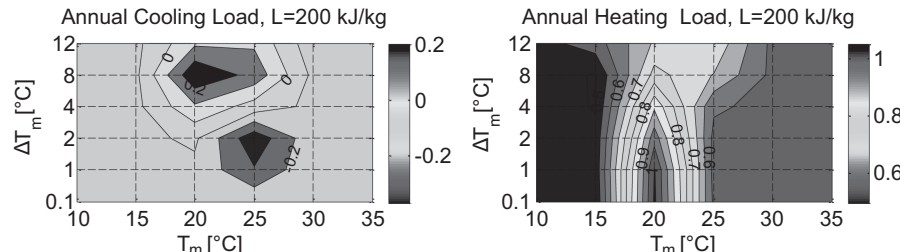
Sketch	Material	Thickness [mm]	Thermal conductivity [W/(m.K)]	Density [kg/m <sup>3</sup> ]	Heat capacity [J/(kg.K)]	Latent heat [kJ/kg]	Melting temp. [°C]	Melting range [°C]
Base Case Wall Design (thermally insulated massive wall)*								
Outdoor	Plaster	12.5	0.72	840	1860			
Indoor	Expanded Polystyrene	100	0.034	24	1250			
Outdoor	Concrete Block	200	1.02	2020	920			
Indoor	Gypsum	12.5	0.21	1200	1000			
Wall Design#1 (PCM to interior)								
Outdoor	Plaster	12.5	0.72	840	1860			
Indoor	Expanded Polystyrene	100	0.034	24	1250			
Outdoor	Concrete Blk	200	1.02	2020	920			
Indoor	PCM	12.5	0.2	235	1970	200	(18–27)	(0.1,1,2,4,6,8)
Indoor	Gypsum	12.5	0.21	1200	1000			

Wall Design#2 (PCM in the middle)		Plaster	12.5	0.72	840	1860
Outdoor	Indoor	Plaster	100	0.034	24	1250
Expaned Polystyrene	Drywall	Polystyrene	Concrete Blk	1.02	2020	920
PCM	PCM	PCM	Concrete Blk	0.2	235	1970
Concrete Blk	Concrete Blk	Gypsum	Concrete Blk	1.02	2020	920
Gypsum	Gypsum	Gypsum	Gypsum	0.21	1200	1000

Notes: \*this design has a similar R-value (R-18) as the lightweight wall used in the previous residential building case.



a) Percentage savings in annual cooling and heating loads when PCM is located to the interior



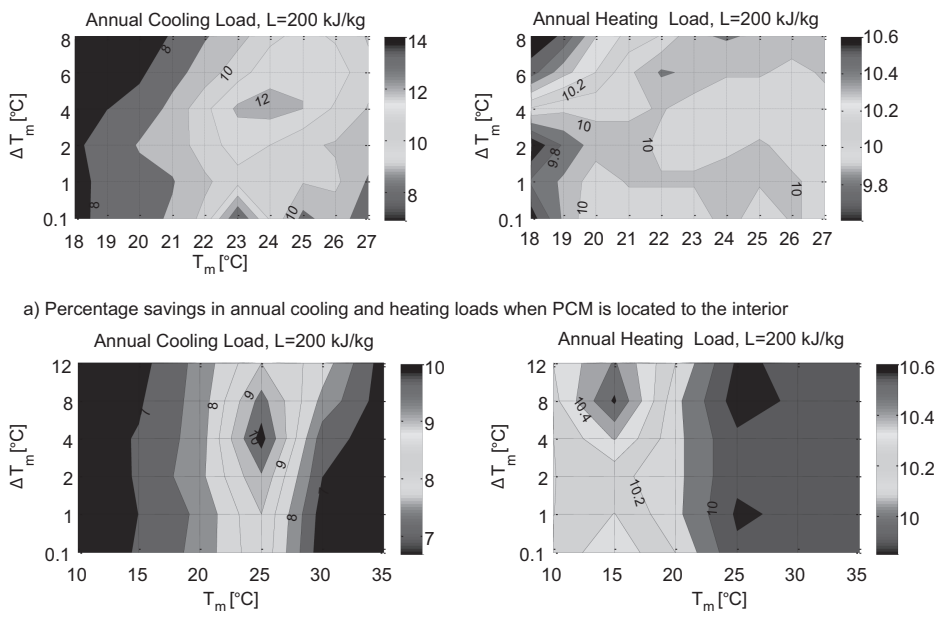
b) Percentage savings in annual cooling and heating loads when PCM is located to the middle

**Figure 3-25** Percentage savings in annual loads for the case of 200 kJ/kg for thermally massive insulated PCM-enhanced walls with different PCM locations.

to the interior side and (2) another in the middle as previously tested. Figure 3-26 shows the results for these two designs when the insulation layer is removed. It is clearly shown that the performance of non-insulated massive wall has been enhanced compared to the insulated wall design when PCM is utilized.

When PCM is placed to the interior side, the saving in the annual cooling load is at least 4% more than when it is placed in the middle. The optimal melting temperature is 1°C below the cooling set-point (i.e., 23°C) at melting range of 0.1°C. When PCM is placed to the middle, the optimal melting temperature is 1°C above the cooling set-point (i.e., 25°C) at a wider melting range of 4°C. The saving in the annual heating loads is similar for both designs. Both PCM locations favor a wide melting range of 8°C for the maximum savings in the annual heating load. The melting temperature is 15°C for the middle PCM compared to 18°C for the interior PCM.

In summary, the PCM performance is enhanced when used with non-insulated thermally massive wall designs than when used with insulated designs. In summer, the charging and discharging process is



a) Percentage savings in annual cooling and heating loads when PCM is located to the interior

b) Percentage savings in annual cooling and heating loads when PCM is located in the middle

**Figure 3-26** Percentage savings in annual loads for the case of 200 kJ/kg for thermally massive non-insulated PCM-enhanced walls with different PCM locations.

improved since the daily diurnal cycles are naturally provided by the local climate. In winter and when insulation is not used, the heat losses are increased. However, through its journey to the sink (i.e., the outside cold environment), PCM stores the lost heat and utilizes the stored energy for heating purposes when possible. It can be concluded that the mechanism of the charging and discharging process of PCM has been enhanced by the absent of thermal insulation.

### 3.10 Thermal Performance of Buildings with Advanced Multi-Layer Walls

The developed and validated envelope “AdvFacSy” model as described earlier was integrated into a full-scale building simulation model, the HYBCELL 1.2 [31]. HYBCELL 1.2 was developed under Matlab/Simulink® environment by coupling a thermal model and a pressure air flow model. The building thermal model can be divided in three parts: the envelope model based on the finite volume method, the short wavelength radiation model based on an accurate description of the

sunspot inside the simulated building, and the long wavelength radiation model using the radiosity method. The air flow model is a pressure model that takes into account the effect of the wind and the thermal buoyancy of air to calculate the airflow through the openings of the building. Indoor air temperature is calculated considering several thermal evolution phenomena, such as heat transfer through the walls, air infiltration and ventilation, internal heat gains and auxiliary heating or cooling. Schedule and occupation patterns can also be integrated in the model.

The tested building is a 80 m<sup>2</sup> single zone dwelling having a rectangular shape (10 m long, 8 m wide and 3 m high). The studied multi-layer wall represents the south facade. The properties of the walls (refer to Table 3-6) and the windows (illustrated by Figure 3-27) are defined to represent several configurations (i.e., high and low inertia, large and small glazing area). Table 3-6 presents the material layer thicknesses adopted in the case of a building envelop with high inertia. In order to simulate the building envelop with low inertia, the internal layer (Layer 1) of vertical walls and Layer 2 of roof and floor has been divided by 10 (0.02 m instead of 0.2 m). The building configurations with large glazing has two windows in each façade except north façade (Figure 3-27) with 26.39% glazed area, and the building configuration with less glazed area (13.19%) has only one window per façade except north façade.

The tested multi-layer wall is composed of three layers (external sensible storage layer, intermediate latent heat storage layer – PCM, and

**Table 3-6** Building material properties in multi-layer walls.

Wall	Thickness (m)				
	Less Inertia	Density (kg/m <sup>3</sup> )	Specific heat (J/kg.K)	Conductivity (W/m.K)	
Vertical walls (except south)	0.2	2500	800	1.5	
	0.2	30	700	0.04	
	0.1	1500	800	0.2	
Floor and roof	0.01	1500	700	1	
	0.2	2500	700	1.5	
South wall	Studied Multi-layer wall				

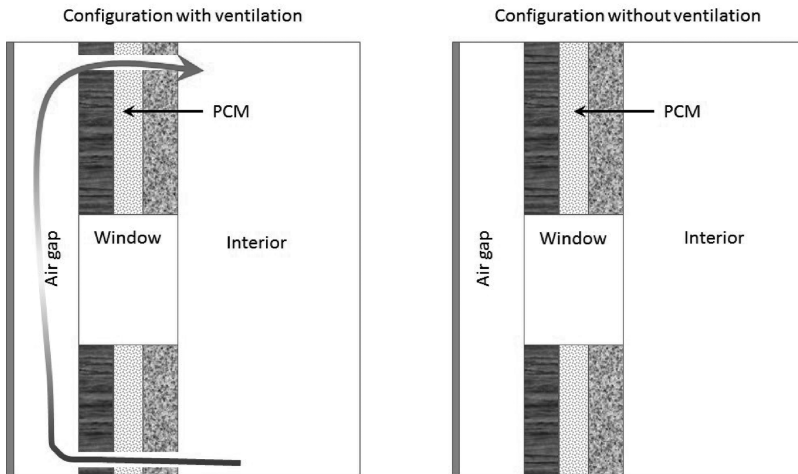


**Figure 3-27** Multi-layer wall configurations coupled to a full-scale building.

internal sensible storage layer). The goal is to investigate and optimize the thickness, density and conductivity of the three layers and the melting temperature range and the latent heat of the PCM layer. To perform the optimization, NSGA-II [32], a non-dominated sorting genetic algorithm (NSGA) tool coupled to Simulink model has been used. The ranking criteria (to minimize) are: heating energy consumption (kWh) and thermal discomfort risk ( $^{\circ}\text{C}$ -hours) related to the number of hours when indoor air temperature is above  $25^{\circ}\text{C}$ . The energy consumption is evaluated calculating the injected heat (convective heating) at each step time in order to keep indoor air temperature above the set-point. A PID controller maintains the indoor air temperature above  $18^{\circ}\text{C}$  and a shading system is activated to keep indoor air temperature under  $26^{\circ}\text{C}$ . Thermal discomfort risk is calculated using Equation (3.15):

$$\text{Discomfort risk} = \int_0^{\text{Simulation time}} \left( \frac{\max(0; (T_{in}(t) - 26)) \cdot dt}{3600} \right) \quad (3.15)$$

Where,  $T_{in}(t)$  is the indoor air temperature at step time  $t$  [ $^{\circ}\text{C}$ ], and  $dt$  is the step time [s]. Discomfort risk is related to the inertia and greenhouse effect of the multi-layer wall cavity. Thus, there is a risk to overheat the building even if the heating system is switched off. If this risk exists in the winter conditions it will be higher in the summer conditions.

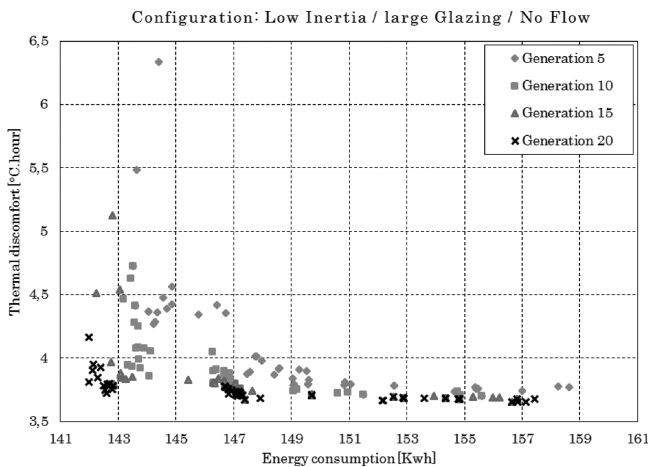


**Figure 3-28** The 5th, 10th, 15th and 20th generations from GA based optimization results for low inertia building configuration.

The number of NSGA generations considered is 20 generations with 50 as the size of population. The simulated period is the first week of January. Figures 3-28 and 3-29 show the examples of optimization results for the building with high inertia configurations. Each configuration optimization results are shown at the 5th, 10th, 15th and 20th generations.

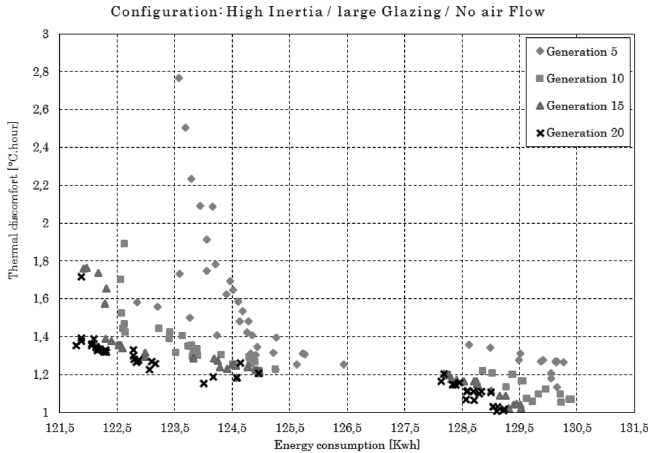


**Figure 3-29** The 5th, 10th, 15th and 20th generations from GA based optimization results for high inertia building configuration.

**Table 3-7** Identified best configurations (Inputs).

Building configuration	Living wall layers thickness (cm)			Sensible storage			Phase change layer			3,15 27607 1,00 89705 2,31 37695 3,09 51661 1,00 89766 1,00 70223 1,94 56357 1,51 88046	20,84 21,00 21,01 18,73 21,01 21,92 20,03 1,94 20,52 1,51 88046
	Inertia	Glazing	Air flow	External	PCM	Internal	External	Internal	Internal		
				layer	layer	layer	layer	layer	layer		
Low	Small	No	6	1	10	1,47	1,46	2500	2500	3,15	27607
Low	Small	Yes	6	3	12	1,07	1,40	985	2167	21,00	1,00
Low	Large	No	7	4	3	1,50	1,43	2406	2398	19,46	2,31
Low	Large	Yes	11	2	6	1,50	0,96	2419	2033	18,73	3,09
High	Small	No	1	4	2	0,92	1,05	1288	1935	21,01	1,00
High	Small	Yes	18	16	2	0,07	1,14	30	2092	21,92	1,00
High	Large	No	9	2	1	1,45	1,05	2162	1648	20,03	1,94
High	Large	Yes	1	3	13	0,81	1,26	1576	1761	20,52	1,51

Table 3-7 summarizes the optimal multi-layer wall materials and thicknesses for each tested configuration. Table 3-8 shows the energy and thermal discomfort reduction related to the selected optimal multi-layer wall configurations shown in Table 3-8. The optimal solutions (multi-layer wall configurations) are compared to the reference case results. The reference case is a building that has the same characteristics except the fact that the south façade is constituted by a classical wall like all other vertical walls. There are four reference case studies (with/without inertia and with/without large glazing).

The results show that the performance of multi-layer wall system enhances the performance of the reference case by 28% (for the building with less inertia configuration) and up to 38% (for the building with high inertia configuration) in energy saving. The multi-layer configuration without cavity ventilation is thermally more efficient but induces high risk of thermal discomfort. Hence, control strategies of shading and outdoor air circulation should be provided to avoid this risk.

It is found that the PCM layer thickness varies between 1 and 4 cm depending on the whole building inertia. The external and internal layers should be conductive with high thermal inertia. The thickness depends on the ventilation configuration and the whole building inertia. The internal layer is found to be more sensitive to these two parameters. The same conclusion applies to the glazing ratio and ventilation rate.

**Table 3-8** Predicted best configurations (Outputs).

Building configuration			Building with living wall performances		Reference without living wall	
Inertia	Glazing	Cavity air flow	Energy (kWh)	Discomfort (°C-hours)	Energy (kWh)	Discomfort (°C-hours)
Low	Small	No	99,09	5,01	138,50	0
Low	Small	Yes	98,47	5,36		
Low	Large	No	141,97	3,81	203,80	3,16
Low	Large	Yes	142,92	4,50		
High	Small	No	87,21	3,87	134,00	0
High	Small	Yes	83,21	4,81		
High	Large	No	121,78	1,35	176,30	0
High	Large	Yes	121,87	4,40		

### 3.11 Summary on Single-Layer Breathing Wall

Breathing wall with dynamic insulation properties appears promising in reducing building energy load. Both the simulation and experimental results generally indicate trends of efficiency – as defined in three different forms – increasing with airflow rates. These findings tend to conform to the previous research conducted by both Krarti and Taylor. In addition, the experimental and CFD data both tend to indicate a slight negative correlation between efficiency and temperature differential across the breathing wall. Applying all three definitions of efficiency, slight but consistent trends showing decreased efficiency with increased temperature differential are apparent. Analysis of the airflow vectors within the breathing wall seem to confirm that circulation loops within the breathing wall cavities work to increase convection heat transfer within the wall and decrease overall efficiencies. This phenomenon may account for the observation that analytical breathing wall efficiency estimates, as defined by Krarti and Taylor, tend to overestimate the amount of savings in the case of a breathing wall constructed with cavities, despite the fact that the savings trends are similar.

The observed saving trends and magnitudes with the three different definitions of efficiency are similar for each.  $\eta_1$  relates the energy input required to maintain a constant set-point temperature, comparing the dynamic and static breathing wall cases. Depending upon the temperature differential and air flowrate, this efficiency value may range from -10% to +20%.  $\eta_2$  relates the amount of conduction heat transfer at the outer surface of the breathing wall in the static and dynamic cases, which also ranges from -10% to +20%, depending upon temperature differential and air flowrate.  $\eta_3$  is defined in terms of breathing wall U-value, in both the dynamic and static cases. This term can be used to provide a quick estimate of the amount of potential saving to expect from a breathing wall installation. It is also most easily integrated into an existing piece of building energy simulation software.  $\eta_3$ , has been shown to range between -10% and +30%, depending upon the air flowrate and temperature differential.

Breathing wall systems appear to be particularly promising in applications that require large amounts of ventilation air. Such applications include laboratories, healthcare facilities, office buildings, and many other commercial buildings. It has been suggested that breathing walls, when implemented on a large scale, may be able to impact the air quality

within large cities, by filtering particulates and other pollution out of building ventilation air, effectively exhausting cleaner air than ambient. This yields yet another potential application of breathings walls – projects with stringent indoor air quality requirements.

It is possible and desired to conduct a simplistic analysis of the saving potential of breathing walls using the degree-day method. Assume the application is a hospital, located in Boulder, Colorado (a climate with 6911 heating degree-days). The hospital has 7432 m<sup>2</sup> of perimeter patient rooms (with 3-m ceilings) that require 8 air changes per hour (ACH) to ensure adequate interior air quality. An assumption of a 9-m room depth yields 2477 m<sup>2</sup> of exterior wall area. In a static condition, the walls have an overall U-value of 0.64 W/m<sup>2</sup>·°C. If the percentage of wall area suitable for installation of breathing walls is 35%, the overall area of breathing wall is therefore 867 m<sup>2</sup>.

The airflow through the walls can then be calculated to be 11.43 CFM/m<sup>2</sup>. From Figures 3-13 and 3-14, one can see that the average breathing wall U-value efficiency ( $\eta_3$ ) is estimated to be 17.5% from the experimental regression. The calculation of heating energy saving then follows, using Eq. (3.16).

$$\text{FuelSavings} = \frac{\Delta BL C_{\text{wall}} \times \text{DegreeDays} \times 24[\text{hr/day}]}{\eta_{\text{heating}}} \quad (3.16)$$

The predicted energy saving from the breathing wall, assuming a heating efficiency of 90%, is 378 therms, according to the experimental regression. Assuming a fuel cost of \$1.20 per therm, this amounts to a cost savings of roughly \$453 per year. It would be straightforward for breathing wall efficiency equations to be programmed into an hourly building energy simulation software program. While the Degree-Day method serves to provide a rough estimate of the annual savings, an hourly program will provide much more detailed feedback, and further indicate the seasonal performance of a breathing wall assembly.

### 3.12 Summary on Advanced Multi-Layer Living Wall

Multi-layer living walls can offer adaptive envelope systems to changing outdoor conditions. Analysis results indicate that thermal performance of living walls is enhanced with a PCM as part of the interior layer. For the multi-layer PCM-enhanced wall design, a narrow melting

range coupled with optimal melting temperature close to the heating and cooling set-points achieve maximum savings in annual and peak heating and cooling loads. The full-scale building model results show that when optimized, the living wall system can allow 27% to 38% of reduced heating energy consumption while avoiding thermal discomfort.

Thermal storage is crucial for living wall featured with ventilated cavity and exterior glazing. Despite its sensitivity to the thermostat set-points, the study shows that PCM performs relatively better when it is located in direct contact with the controlled indoor environment. PCM shows improved performance during transition season when compared to winter or summer seasons. A closer look at PCM layer level indicates that the diurnal cycle during the transition months is the main reason for the improved performance. As the result, the charging and discharging cycles occur on a daily base, driven mainly by the climate. Multiple PCM layers – one for cooling and another for heating is found to provide slightly better performance. The order of PCM layers relative to the indoor environment is not sensitive. The optimal melting temperature is found to hover around the thermostat set-points: 1°C below the cooling set-point for maximum savings in annual cooling load while at the heating set-point for maximum savings in annual heating load. The corresponding melting range should be 0.1–1°C and 2°C for maximum savings in annual cooling and heating loads, respectively.

Studies reveal that utilization of thermal storage such as PCM without proper passive design strategies such as night ventilation presents relatively low energy performance. Integration of optimal passive design strategies with living wall designs will be necessary to improve the performance. Ideally, the charging and discharging process should occur on a daily base for maximum benefits. In mild climates, PCM can be flushed with outside cool air via natural ventilation during night to prepare PCM for the next hot day cycle. In cold winter climates, solar harvesting techniques should be fully exploited to store the solar heat for later night use. The parametric study reveals that among the important parameters, affecting the wall performance, are the solar radiation and zone set-points. Optimum thermal properties tuned for one environment may not be optimal or suitable for other environments. Integrating PCM with insulated and heavy massive concrete wall does not enhance the PCM thermal performance, which however can be improved by eliminating insulation.

As demonstrations, in addition to Golden CO (cold climate), three other representative US climates are tested: Phoenix, AZ (hot dry climate); Atlanta, GA (temperate climate); and Seattle, WA (marine climate). The same houses are built but using the local energy codes for envelope configurations. For all these climates, the PCM layer is placed to the interior side. No passive heating, cooling and ventilation strategies are implemented for these cases. The performance of PCM is found to behave in a similar fashion across the climates. Table 3-9 provides the summary results of relative savings in annual and peak loads for the two extreme latent heat cases (50 and 300 kJ/kg) with corresponding optimal PCM thermal properties and potential savings for the four US cities. Table 3.10 shows the absolute savings in annual heating and cooling loads.

The results in this table are comparable to those found in literature. For instance, Medina et al. [33–35] reported an average reduction of 9–11% in space cooling load and a reduction of 5.7–15% in peak heating load in Lawrence, Kansas. Based on simulation under Dayton climate, Kissock found that the peak and annual cooling loads were reduced by 19% and 13%, respectively [36]. Using EnergyPlus, Tabares reported a peak cooling reduction of 4% in the peak month of July in Phoenix [37].

In all the climates, the optimal melting temperature for maximum savings in cooling load is 1°C below the cooling set-point and at the heating set-point for maximum savings in heating load, with some exceptions for extreme cases. For a heavy latent heat case of 300 kJ/kg, the maximum percentage savings in annual cooling load range from 0.8–15.8% with low in Phoenix and high in Seattle. The maximum percentage savings in annual heating load range from 2.8–55.8% with low in Golden and high in Phoenix. In terms of absolute values, maximum savings in cooling load range from 0.83–1.2 kWh/m<sup>2</sup> with low in Atlanta and high achieved in Phoenix. The maximum absolute savings in annual heating load range from 0.49–1.79 kWh/m<sup>2</sup>, low in Phoenix and high in Seattle. Despite the high heating degree day of Golden when compared to Seattle, PCM achieves marginal savings in annual heating load (Table 3-10). The enhanced performance in Seattle is found due to the different insulation level requirements for both climates; and an extra R5 is mandated for Colorado climate.

**Table 3-9** Summary of simulation results for four US cities.

Latent heat case [kJ/kg]		Annual heating loads*			Annual cooling loads*		
	Cities	T <sub>m</sub> [°C]	ΔT <sub>m</sub> [°C]	Savings [%]	T <sub>m</sub> [°C]	ΔT <sub>m</sub> [°C]	Savings [%]
50	Phoenix, AZ.	21	0.1	22.59	23	0.1	0.24
	Atlanta, GA.	22		1.95		1	0.79
	Seattle, WA.	21		1.88		2	3.64
	Golden, CO.	22	1	1.28			1.54
	Phoenix, AZ.	22	0.1	55.82		0.1	0.79
	Atlanta, GA.			4.17		1	2.60
	Seattle, WA.		2	3.59		0.1	15.80
	Golden, CO.		4	2.80		1	7.32
Latent heat case [kJ/kg]		Peak heating loads			Peak cooling loads		
	Cities	T <sub>m</sub> [°C]	ΔT <sub>m</sub> [°C]	Savings [%]	T <sub>m</sub> [°C]	ΔT <sub>m</sub> [°C]	Savings [%]
50	Phoenix, AZ.	20	1	4.68	27	0.1	1.60
	Atlanta, GA.	19	0.1	2.31	26	1	2.83
	Seattle, WA.	20	1	1.74	25	0.1	4.43
	Golden, CO.	19	0.1	2.59			5.43
	Phoenix, AZ.	21	0.1	23.39	26	0.1-1	6.76
	Atlanta, GA.	20		10.45	25		11.33
	Seattle, WA.			8.93	24	2	13.29
	Golden, CO.			6.95	25	1	10.29

Notes: \* Heating set-point is 22°C and cooling set-point is 24°C.

**Table 3-10** Annual heating and cooling load comparison for the two extreme cases in four US cities.

	Base case (no PCM)	PCM case of 50 kJ/kg	PCM case of 300 kJ/kg	Savings for PCM case of 50 kJ/kg*	Savings for PCM case of 300 kJ/kg**
Annual heating loads [kWh]					
Phoenix	143.4	111	63.35	32.4	80.05
Atlanta	6468	6342	6198	126	270
Seattle	8329	8172	8030	157	299
Golden	10130	10000	9846	130	284
Annual cooling loads [kWh]					
Phoenix	25170	25110	24970	60	200
Atlanta	5341	5299	5202	42	137
Seattle	1044	1006	879.1	98	164.9
Golden	2595	2545	2405	50	190

Notes: \*: minimum savings case, \*\*: maximum savings case.

## References

- [1] Imbabi, M.S. and Peacock, A.D. Smart breathing walls for integrated ventilation, heat exchange, energy efficiency and air filtration. ASHRAE/CIBSE Conference, Sept 2003.
- [2] Taylor, B.J., Cawthorne, D.A., and Imbabi, M.S. Analytical investigation of the steady-state behavior of dynamic and diffusive building envelopes. *Building and Environment* 1996;31(6):519–525.
- [3] Zhai, Z. et al. 2010. <http://grantome.com/grant/NSF/EFRI-1038305>.
- [4] Bhattacharyya, S. and Claridge, D.E. Energy impact of air leakage through insulated walls. *Journal of Solar Energy Engineering* 1995;117(3):167–172.
- [5] Barhoun, H. and Guerracino, G. Evaluating the energy impact of air infiltration through walls with a coupled heat and mass transfer method. Proceedings of the CIB Conference, Toronto, Canada, 2004.
- [6] Buchanan, C.R. and Sherman, M.H. A mathematical model for infiltration heat recovery." Lawrence Berkeley Laboratory Report. LBL-44294. 2000.
- [7] Abadie, M.O., Finlayson, E.U., and Gadgil, A.J. Infiltration heat recovery in building walls: computational fluid dynamics investigations results. Lawrence Berkeley Laboratory Report. LBNL-51324. August 2002.
- [8] Chen, W. and Liu, W. Numerical analysis of heat transfer in a composite wall solar-collector system with a porous absorber. *Applied Energy* 2004;78(2):137–149.
- [9] Bailly, N.R. Dynamic insulation systems and energy conservation in buildings. *ASHRAE Transactions* 1985;91(1):447–466.
- [10] Kohonen, R. and Ojanen, T. Non-steady state coupled diffusion and convection heat and mass transfer in porous media, 5th International Conference on Numerical Methods in Thermal Problems, Montreal, Canada (1987).
- [11] Baker, P.H. The thermal performance of a prototype dynamically insulated wall. *Building Services Engineering Research and Technology* 2003;24(1):25–34.

- [12] Dimoudi, A., Androutsopoloulus, A., and Lykoulis, S. Experimental work on a linked, dynamic and ventilated wall component. *Energy and Buildings* 2004;36(5):443–453.
- [13] Morrison, I.D. and Karagiozis, A.N. Energy impact of dynamic wall ventilation. Proceedings of the 18th Annual Energy Society of Canada. Edmonton, Alberta. 1992.
- [14] Krarti, M. Effect of airflow on heat transfer in walls. *Journal of Solar Energy Engineering* 1994;116(1):35–42.
- [15] Qiu, K. and Haghight, F. Modeling the combined conduction-air infiltration through diffusive building envelope. *Energy and Buildings* 2007;39:1140–1150.
- [16] Slowinski, R. Thermal Performance of Ventilated Breathing Walls under Varied Environmental Conditions. MS thesis, University of Colorado at Boulder (2009).
- [17] Zhai, Z. and Slowinski, R. Investigation on thermal performance of ventilated wall in winter conditions. International Symposium on Green Manufacturing and Applications (ISGMA 2013), June 25–29, (2013) Honolulu, HI, US.
- [18] Græe, T. Breathing Building Construction. Oklahoma: ASEA Stillwater, 1974.
- [19] AlSaadi, S.N. and Zhai, Z. Systematic evaluation of mathematical methods and numerical schemes for modeling pcm-enhanced building enclosure. *Energy and Buildings* 2015;92:374–388.
- [20] El Mankibi, M., Zhai, Z., Al-Saadi, S.N., and Zoubir, A. Numerical modeling of thermal behaviors of active multi-layer living wall. *Energy and Buildings*, 2015;106:96–110.
- [21] Liu, H. and Awbi, H.B. Performance of phase change material boards under natural convection, *Building and Environment*. 2009;44(9):1788–1793.
- [22] ANSI/ASHRAE Standard 140-2011, Standard method of test for the evaluation of building energy analysis computer programs, Atlanta, GA: ASHRAE, 2011.
- [23] Al-Saadi, S.N. Modeling and simulation of PCM-enhanced facade systems, Ph.D. Dissertation, University of Colorado at Boulder, 2014.
- [24] Kim, J.S. and Darkwa, K. Simulation of an integrated PCM-wallboard system. *International Journal of Energy Research*. 2003;27(3):215–223.

- [25] Engebrecht-Metzger, C., Wilson, E., and Horowitz, S. Addendum to the building america house simulation protocols, in, 2012, pp. Medium: ED; Size: 36 pp.
- [26] Hendron, R. and Engebrecht, C. Building America house simulation protocols (Revised), in: Related Information: Supercedes September 2010 version, 2010, pp. Medium: ED; Size: 88 pp.
- [27] Kneifel, J. NIST TN-1765: Prototype Residential Building Designs for Energy and Sustainability Assessment. 2012.
- [28] Armin Rudd, Hugh I. Henderson J, Daniel Bergey, and Don B. Shirey, ASHRAE. Energy Efficiency and Cost Assessment of Humidity Control Options for Residential Buildings: ASHRAE 1449-RP Final Report: Building Science Corp., CDH Energy Corp., and University of Central Florida/Florida Solar Energy Center, 2013.
- [29] TRANSSOLAR Energietechnik GmbH. TRNSYS 16: A TRAnsient SYstem Simulation program, Volume 6: Multizone Building modeling with Type56 and TRNBuild. 2007.
- [30] Kosny, J., Kossecka, E., Brzezinski, A., Tleoubaev, A., and Yarbrough, D. Dynamic thermal performance analysis of fiber insulations containing bio-based phase change materials (PCMs). *Energy and Buildings*. 2012;52:122–131.
- [31] El Mankibi, M., Cron, F., Michel, P., and Inard, C. Prediction of hybrid ventilation performance using two simulation tools. *Solar Energy*. 2006;80(8):908–926.
- [32] Deb, K. Kanpur Genetic Algorithms Laboratory. NSGA-II source code, URL: <http://www.iitk.ac.in/kangal/codes.shtml>, [Accessed: June/06/2015].
- [33] Zhang, M., Medina, M.A., and King, J.B. Development of a thermally enhanced frame wall with phase-change materials for on-peak air conditioning demand reduction and energy savings in residential buildings. *International Journal of Energy Research*. 2005;29:795–809.
- [34] Medina, M.A., King, J.B., and Zhang, M. On the heat transfer rate reduction of structural insulated panels (SIPs) outfitted with phase change materials (PCMs). *Energy*. 2008;33:667–678.
- [35] Evers, A.C., Medina, M.A., and Fang, Y. Evaluation of the thermal performance of frame walls enhanced with paraffin and hydrated salt phase change materials using a dynamic wall simulator. *Building and Environment*. 2010;45:1762–1768.

- [36] Kelly Kissock, J., Michael Hannig, J., Whitney, T.I., and Drake, M.L. Testing and simulation of phase change wallboard for thermal storage in buildings. In: Morehouse JM, Hogan RE, editors. International Solar Energy Conference. Albuquerque: American Society of Mechanical Engineers; 1998.
- [37] Tabares-Velasco, P.C., Christensen, C., and Bianchi, M. Verification and validation of EnergyPlus phase change material model for opaque wall assemblies. *Building and Environment*. 2012;54:186–196.

---

## Authors biography

---

**Dr. Moncef Krarti**, Professor, Building Systems Program, Civil, Environmental, and Architectural Engineering Department at the University of Colorado, has been very active in ASME from the last 25 years, especially in the ASME Solar Energy Division (SED). He has served both as Technical and Conference Chairs, and is a past president. He has been elected ASME Fellow in 2015 as testament of his leadership qualities within SED and ASME and also to his great research contributions in solar energy, energy efficiency in buildings and renewable energy systems modeling and analysis. He is the co-founder and the co-chair of the ASME Emergency Technologies Committee on Integrated Sustainable Building Equipment and Systems (ISBES) which initiated several activities including workshops, monographs, and handbooks. Prof. Krarti is considered a world expert in building energy management and has helped establish energy efficiency programs in several countries. He has been able to attract over \$15 million in sponsored research and has contributed enormously in the fields of energy efficiency and renewable energy through his publications, research supervision of graduate students and undergraduate teaching. In particular, Prof. Krarti has published over 250 technical journals in wide of fields related to sustainable energy technologies. He authored three textbooks on building energy management and has been an invited keynote speaker in several national and international forums and conferences.

**Dr. Zhiqiang (John) Zhai** is a Professor in the Department of Civil, Environmental and Architectural Engineering (CEAE) at the University of Colorado at Boulder (UCB). He has a unique and integrated background in both Mechanical and Architectural Engineering with a Doctor degree in Fluid Mechanics (Tsinghua University) and a Ph.D. in Building Technology (MIT). Dr. Zhai has been actively engaged in research activities in the field of fluid/thermal science and building/energy/environment technology since 1994. His particular research interests and expertise include: experimental and numerical study of building thermal and environmental systems; indoor/outdoor environmental quality; immune and sustainable building design and technology development. Dr. Zhai is an Associate Editor for Energy



and Buildings Journal and an Editorial Board Member of Building Simulation International Journal, Journal of Building Physics, Indoor and Built Environment Journal, Journal of Energy, Journal AIMS Energy, as well as invited guest editors for several international journals. Dr. Zhai received the Young Researcher Award (2007) and the Research Development Award (2010) from UCB-CEAE, as well as the University Sustainability Award of Green Faculty (2008). Dr. Zhai was granted the Best Paper Award of International Journal of Building Simulation (2008) and the William Mong Visiting Research Fellowship in Engineering from The University of Hong Kong (2009). He also received the Charles A. and Anne Morrow Lindbergh Foundation Project Award (2007) and the Distinguished Service Award of ASHRAE (2010) and was named Distinguished Lecturer by ASHRAE (2014). He was named the Distinguished "Changjiang Scholar" Professor by the Ministry of Education, China in 2016.

**Dr. Benjamin Park** is an analyst at Noresco, a part of United Technologies Corp.'s UTX UTC Building & Industrial Systems, Boulder, CO USA. He obtained a Ph.D. degree in Architectural Engineering from the University of Colorado Boulder in 2016. Dr. Park has an extensive experience and has published several peer-reviewed technical papers on his research. His expertise includes building physics, thermodynamics, numerical analysis, and thermally activated systems such as radiant heating/cooling slabs and hollow core ventilated slabs. He is passionate about the integration of HVAC system with building envelopes not only to improve building energy efficiency but also thermal comfort. His research interests include dynamic building envelope, adaptive optimal control strategies, and the integration of IoT with HVAC system.

**Kathleen Menhart** recently graduated from the Building Systems Program of the Civil, Environmental, and Architectural Engineering Department at the University of Colorado Boulder with an M.S. degree. As part of her Master's research work, she investigated the energy savings potential of Dynamic Insulation Materials in US residential buildings and has published a peer-reviewed technical paper on this topic. She also holds a B.S. degree in Physics from the University of Michigan.

@Seismicisolation

**Vinay Shekar** is currently working as a Mechanical Engineer with the Buildings & Infrastructure division at Jacobs. He has obtained an MS degree from the Building Systems program of the Civil, Environmental, and Architectural Engineering Department at the University of Colorado at Boulder. As part of his Masters Project and research, he has been actively involved in the research of advanced and energy efficient buildings envelop technologies.

**Jenna L. Testa** is currently a practicing engineer in the Building Technology department at Simpson Gumpertz & Heger Inc. (SGH). She has been involved in a variety of projects involving investigation and design of historic building envelopes, new construction building enclosure design, and building science (hygrothermal and thermal analyses). She obtained a M.S. degree from the University of Colorado Boulder in 2016 in Architectural Engineering with an emphasis on building systems and sustainable design. As part of her M.S. research work, Ms. Testa evaluated the energy savings potential of dynamic cool roofing systems for various building types and climates.

**Dr. Saleh Al-Saadi** is an assistant professor and the program coordinator of the Architectural Engineering program at Sultan Qaboos University (SQU), Oman. He holds a Ph.D. in Architectural Engineering (Specialization: Building systems engineering) from the University of Colorado at Boulder (USA), a M.Sc in Architectural Engineering (Specialization: Building environmental control systems) from King Fahd University of Petroleum and Minerals (Saudi Arabia) and a Bachelor of Civil Engineering from Sultan Qaboos University (Oman). Dr. Saleh has a diversified work experience in industry and academia. His current research interests include modeling, design and analysis of building energy systems, energy conservation, energy auditing and retrofitting opportunities in existing buildings, renewable and sustainable energy applications for buildings. His research on PCM walls was selected by the U.S. National Academies and The Research Council of Oman among top Young Arab Engineers and Scientists to participate in the 2nd Arab-American Frontiers of Science, Engineering, and Medicine Symposium.

**Dr. Mohamed El Mankibi** is Research Director at Tribology and System Dynamics Laboratory (French CNRS joint research center).

@Seismicisolation

He is also professor at ENTPE/university of Lyon (France). He is qualified as international expert by the French ministry of environment, energy and sea. He has a PhD degree (Hybrid ventilation control strategies design and assessment) and the accreditation to direct and manage research (equ Tenure). He is the manager and supervisor of building related courses of ENTPE and co-creator and co-manager of a "Green Building" Master degree. Highly evolved in ENTPE Green and Low Impact Buildings design and optimization program, El Mankibi has two major fields of research: one is related to the dynamic simulation of thermal and aeraulic phenomena in buildings; the other is related to the development multi-objective optimization. El Mankibi has also spent one year as invited researcher at the University of Colorado at Boulder and been involved in 6 tasks of the International Energy Agency (ECES and ECBCS programs). He has taken part to 8 national research projects as coordinator or partner and 3 European/International projects. He has developed several original models and experimental apparatus and initiated and led partnerships with the building industry. He has received grants from French Energy Agency, French research agency and European Union.

**Robert Slowinski** has worked professionally in buildings and energy since 2005. His expertise is in sustainable design, measurement and verification of Utility-level energy efficiency programs, renewable energy and the integrated design process. Robert earned a Master's Degree from the Building Systems Program and an MBA from the Leeds School of Business, both at the University of Colorado at Boulder.